POWER REACTOR TECHNOLOGY

A Quarterly Technical Progress Review

Prepared for U. S. ATOMIC ENERGY COMMISSION by GENERAL NUCLEAR ENGINEERING CORP.

June 1960

● VOLUME 3

● NUMBER 3

TECHNICAL PROGRESS REVIEWS

To meet the needs of industry for concise summaries of current atomic developments, the Atomic Energy Commission is publishing this series, Technical Progress Reviews. Issued quarterly, each of the reviews digests and evaluates the latest findings in a specific area of nuclear technology and science.

The four journals published in this series are:

Nuclear Safety, W. B. Cottrell, editor, R. A. Charpie, advisory editor, and associates, Oak Ridge National Laboratory

Power Reactor Technology, Walter H. Zinn and associates, General Nuclear Engineering Corporation

Reactor Core Materials (covering solid material developments), R. W. Dayton, E. M. Simons, and associates, Battelle Memorial Institute

Reactor Fuel Processing, Stephen Lawroski and associates, Chemical Engineering Division, Argonne National Laboratory

Each journal may be purchased ($2.00 per year for subscription and individual issues $0.55) from the Superintendent of Documents, U. S. Government Printing Office, Washington 25, D. C. See back cover for remittance instructions and foreign postage requirements.

●

Availability of Reports Cited in This Review

Unclassified AEC reports are available for inspection at AEC depository libraries and are sold by the Office of Technical Services, Department of Commerce, Washington 25, D. C. Some of the reports cited are not available owing to their preliminary nature; however, the information contained in them will eventually be made available in formal progress or topical reports.

Unclassified reports issued by other Government agencies or private organizations should be requested from the originator.

Unclassified British and Canadian reports may be inspected at AEC depository libraries. British reports are sold by the British Information Service, 45 Rockefeller Plaza, New York, N. Y.; Canadian reports (AECL series) are sold by the Scientific Document Distribution Office, Atomic Energy of Canada, Ltd., Chalk River, Ontario, Canada.

Classified U. S. and foreign reports identified in this journal as Classified may be purchased by properly cleared Access Permit Holders from the Technical Information Service Extension, U. S. Atomic Energy Commission, P. O. Box 1001, Oak Ridge, Tenn. Such reports may be inspected at classified AEC depository libraries.

POWER REACTOR TECHNOLOGY

A REVIEW OF RECENT DEVELOPMENTS

Prepared for U. S. ATOMIC ENERGY COMMISSION
by GENERAL NUCLEAR ENGINEERING CORP.

● JUNE 1960

● VOLUME 3

● NUMBER 3

foreword

This quarterly review of reactor development has been prepared at the request of the Division of Information Services of the U. S. Atomic Energy Commission. Its purpose is to assist interested organizations in the task of keeping abreast of new results in reactor technology for civilian application.

The report is a concise discussion of selected phases of research and development for which there have been significant advances or a heightened interest in the past few months. It is not meant to be a comprehensive abstract of all material published during the quarter, nor is it meant to be a treatise on any part of the subject. The intention is to cover the various areas of reactor development from the general viewpoint of the reactor designer rather than from the more detailed points of view of specialists in the individual areas. However, papers which are thought to be of particular significance or particular usefulness in specialized fields will be mentioned in short notes. In the over-all plan of the report, it is intended that various subjects will be treated from time to time and will be brought up to date at that time.

Any interpretation of results which is given represents only the opinion of the editors of the report, who are General Nuclear Engineering Corporation personnel. Readers are urged to consult the original references in order to obtain all the background of the work reported and to obtain the interpretation of the results given by the original authors.

W. H. ZINN
General Nuclear Engineering Corporation

contents

contents (continued)

Issued quarterly by the U. S. Atomic Energy Commission. Use of funds for printing this publication approved by the Director of the Bureau of the Budget on November 1, 1957.

Thermal-neutron Distributions Near Temperature Discontinuities

For some time Hanford has been investigating, both theoretically and experimentally, the distributions of thermal neutrons, in space and energy, near a temperature discontinuity in a moderating medium. These investigations are interesting for the additional insight they give into the process of neutron thermalization, and they have practical implications for some power reactors, for example, those employing solid moderators in which there may be sizable variations of temperature with position.

The theoretical problem has been treated by Kottwitz, in a number of Hanford quarterly reports,[1–5] and, more recently, by Whitehead.[6] The results of an experimental investigation have been reported by Bennett.[5,6] These results will be summarized briefly.

A column of graphite, about 2 ft square in cross section, was installed in a closely fitting, vacuum tank; the tank was inserted horizontally into a closely fitting square hole in the Physical Constants Testing Reactor (PCTR), where it was surrounded by the reactor fuel rods. The square graphite column was divided longitudinally into three rectangular columns which lay side by side, separated by gaps. The central column of the three could be either heated or cooled. The evacuated gaps insulated the central column from the two adjacent columns, and moderator temperature discontinuities were established at the gaps. Fission neutrons from surrounding fuel elements were thermalized in the graphite columns, and a current of thermal neutrons flowed from the columns to the walls of the vacuum tank and its surroundings. The spatial variation of thermal-neutron spectrum produced by the temperature discontinuity was inferred from the spatial distribution of activation produced in $1/v$ detector foils (copper).

Figure 1 shows traverses of the subcadmium activation of the copper foils, along a line from the center of the central (heated or cooled) graphite column, across the insulating gap, and to the outer edge of one of the outer columns. In the second curve from the top, all three graphite columns are at one temperature, and the activation curve follows the normal distribution of thermal-neutron flux, as established by the production of thermal neutrons in the graphite and their leakage to the wall. When the temperature of the central graphite column is raised or lowered, respectively, the activation of the foils in the central region becomes lower or higher relative to that of the foils in the outer graphite, because of the $1/v$ variation of the activation cross section.

In analysis of the experiment, a representation proposed by Selengut[3] was applied to fit the observed activation distributions. For the case of two regions at two different uniform temperatures T_1 and T_2 (as in the experiment), it is assumed that all thermal neutrons lie in one or the other of two energy groups and that the two energy groups are Maxwellian distributions of neutrons, with characteristic temperatures T_1 and T_2. All thermal neutrons born, by slowing down, in region 1 are considered to be born into the group characterized by T_1, whereas all neutrons born in region 2 are considered to be born into the group characterized by T_2. Any neutrons crossing the boundary between the two regions are considered to be subject to transfer into the energy group characteristic of the new region, with a probability specified by a rethermalization cross section which is analogous to the intergroup slowing down cross section of the conventional multigroup formulation.

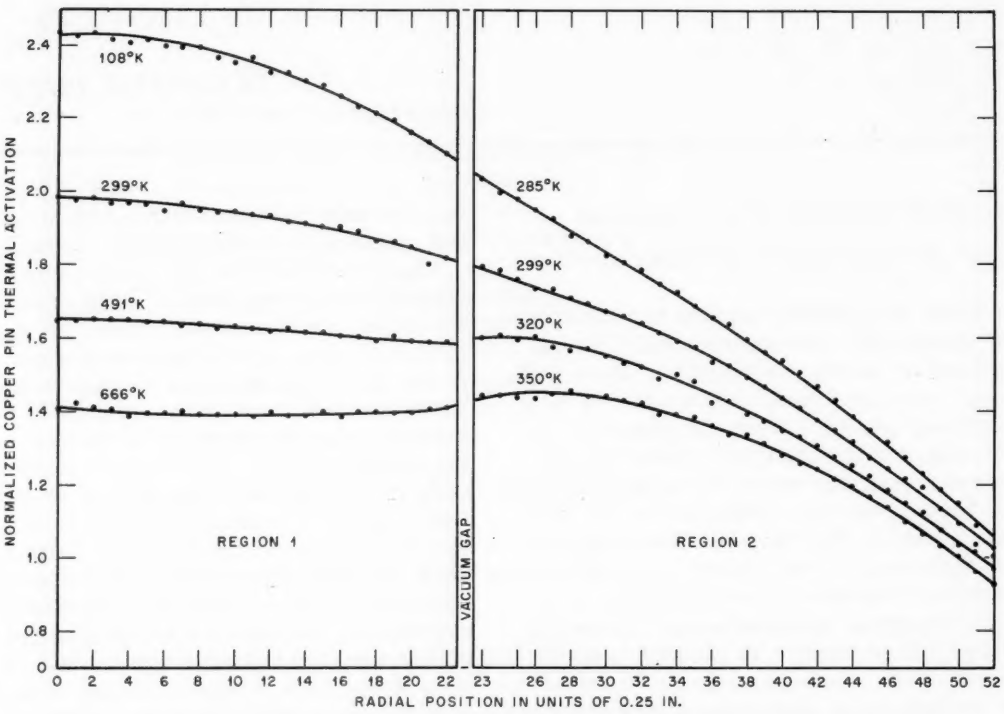

Figure 1—Experimental thermal-activation traverses in graphite with a temperature discontinuity.[5]

Thus, mathematically, the distribution of neutron flux in space and energy can be expressed as a sum of two fluxes, $\phi_1(x)$ and $\phi_2(x)$, having the Maxwellian energy distributions $M(E,T_1)$ and $M(E,T_2)$

$$\phi(E,x) = \phi_1(x)\, M(E,T_1) + \phi_2(x)\, M(E,T_2)$$

The distribution of ϕ_1 and ϕ_2 in space can be determined by solving the two-group equations for the appropriate source distribution and geometry. In region 1, for example, the two-group equations would be

$$-D_1 \nabla^2 \phi_1 + \Sigma_{a_1}\, \phi_1 = \Sigma_{12}\, \phi_2 + q$$
$$-D_2 \nabla^2 \phi_2 + (\Sigma_{a_2} + \Sigma_{12})\, \phi_2 = 0$$

where D is the diffusion constant, Σ_a is the (macroscopic) absorption cross section, Σ_{12} is the rethermalization cross section for transfer of neutrons from group 2 to group 1, and q is the source density of thermal neutrons.

For a foil with a $1/v$ activation cross section, the effective activation cross section in a neutron flux having a Maxwellian energy distribution characterized by the temperature T will be proportional to $T^{-1/2}$. The spatial distribution of foil activation, $A(x)$, arbitrarily normalized, will then be given in terms of ϕ_1 and ϕ_2 as

$$A(x) = \sqrt{T_2/T_1}\ \phi_1(x) + \phi_2(x)$$

In analyzing the experimental results, the thermal source distribution, q, was first determined by finding a source distribution which would fit the activation distribution measured when all the graphite was at the same temperature. Using this source distribution, each of the cases involving a temperature discontinuity was analyzed, and a value of the rethermalization cross section was sought that would give flux distributions, $\phi_1(x)$ and $\phi_2(x)$, consistent with the observed activation distribution. In each case it was assumed that the rethermalization cross section Σ_{12} for transfer from group 2 to group 1 was equal to the cross section Σ_{21}, for the reverse transfer, although the reference points out that this equality is not necessarily true.

It was found that the apparent value of the rethermalization cross section varied from experiment to experiment. Theoretically, the rethermalization cross section can be expressed in terms of the scattering cross section, Σ_s, and the ratio, μ, of the neutron mass to the effective mass of the moderator atom:[3]

$$\Sigma_{ret} = 2\mu\Sigma_s$$

In Table I-1 are listed, for four cases measured, the values of the rethermalization cross section, Σ_{ret}; the values of the rethermalization relaxation length, $L_{ret} = \sqrt{D/\Sigma_{ret}}$; and the corresponding values of the effective mass of the graphite "atom" as a scatterer.

Table I-1 RETHERMALIZATION PROPERTIES OF GRAPHITE[6]

Experiment No.	Temp., °K Region 1 (T_1)	Region 2 (T_2)	Macroscopic cross section (Σ_{ret}), 10^{-3} cm^{-1}	Relaxation length (L_{ret}), cm	Effective mass (M_{eff}), amu
1A	108 ± 2	285 ± 2	1.9 ± 0.5	21.0 ± 2.8	420 ± 110
2A	491 ± 2	320 ± 2	6.4 ± 1.5	11.4 ± 1.4	125 ± 30
2B	491 ± 2	320 ± 2	3.8 ± 0.9	14.8 ± 1.7	208 ± 47
3A	666 ± 2	350 ± 2	14.5 ± 2.6	7.5 ± 0.7	55 ± 10

$\Sigma_a = 2.822 \times 10^{-4}$ cm^{-1} (macroscopic absorption cross section of graphite).
D = 0.8086 cm (graphite diffusion coefficient).
$\rho = 1.66$ g/cm^3 (graphite density).

Temperature Coefficients of Reactivity

Although the temperature coefficient of reactivity in the temperature range near room temperature is not of the greatest importance for power reactors, a comparison of theoretical and experimental values for these coefficients constitutes a test of theory and is, therefore, of considerable interest. Reference 7 reports comparisons of this kind for a highly enriched assembly made up of plate type uranium-Zircaloy elements in a slab geometry, 7.4 by 29.7 by 54 in. high. The slab was controlled by a centrally located row of four cruciform control rods operated as a bank. The critical position of the bank of rods was approximately 32 in. withdrawn.

The temperature coefficient was measured over the temperature range from about 20 to 90°C. The variation of the coefficient with temperature was nearly linear over this range, $\Delta\rho/\Delta T$ varying from about 1.4×10^{-4}/°C at 20°C to about -0.5×10^{-4}/°C at 90°C. The temperature at which the coefficient reached zero and changed sign from positive to negative was about 72°C.

The major difficulty in the theoretical calculation was considered to be the geometrical complexity of the assembly. Calculations based on three different geometrical models were compared with the measured values. One of these models could be handled by one-dimensional calculations, whereas the other two required two-dimensional calculations. Reasonable agreement was obtained with all three, but a two-dimensional calculation in the x-z directions (x being the direction of the thin dimension of the slab and z being the direction of the control-rod axes) was considered best. The two-group approximation was used in all cases, with Maxwell-averaged thermal constants.

Although the reference describes the calculation methods in some detail, it does not attempt to account for the results in terms of the various physical processes involved. Such an analysis would be interesting, since it seems rather surprising that an assembly of such high neutron leakage would demonstrate a positive temperature coefficient of reactivity at temperatures up to 72°C. The assembly did contain a rather large fraction of its water in the control-rod channels, and it is possible that a high thermal-flux peaking in the channels may account for much of the positive component of the temperature coefficient.

Measurements of the temperature coefficients of reactivity in several highly enriched water-moderated assemblies at elevated temperatures (up to about 540°F) are reported in reference

8. The measurements were made in the Pressurized Test Reactor (PTR) at Knolls Atomic Power Laboratory (KAPL). The assemblies were relatively uncomplicated, and a simplified analysis was applied in which it was assumed that the temperature dependence of reactivity arises only from changes in L^2 and τ, the thermal-diffusion area and the Fermi age. It was found that this approximation was good enough to support predictions of the reactivity variation for a given assembly over a range of temperatures, based on measurements of the temperature coefficient of reactivity at two different temperatures. However, neglect of the change of geometrical buckling of reflected reactors when the temperature is changed appears to be questionable.

Measurements Related to Thermal Breeding

In the last issue of *Power Reactor Technology*, 3(2): 21 (March 1960), a summary was given of the Conference on the Physics of Breeding, at Argonne National Laboratory, Oct. 19–21, 1959. Two recent reports from Oak Ridge National Laboratory (ORNL) give more detailed accounts of two of the investigations discussed at the Conference.

Reference 9 reports the measurements of η (neutrons produced per neutron absorbed) for thermal-neutron irradiation of U^{235} and U^{233} by the manganese-bath method. In concept, the method is simple and direct. A beam of thermal neutrons is directed through a tube to the center of a large spherical tank filled with an aqueous solution of $MnSO_4$. After a sufficient time the neutron beam is stopped, the $MnSO_4$ solution is thoroughly mixed, and the manganese activity is determined by counting a sample of the solution. A target of U^{233} or U^{235} is then installed at the center of the sphere where the neutron beam will impinge upon it. The sample is sufficiently thick to absorb very nearly all the incident neutrons, and the spherical tank is so large that very nearly all the fission neutrons produced in the uranium are slowed down and absorbed in the $MnSO_4$ solution. For equal neutron beam strengths (as determined by monitors) and equal irradiation times, η is obtained (except for small corrections) from the ratio: (manganese activity produced when the uranium is present)/(manganese activity produced when the uranium is absent).

The experimental technique and the corrections are discussed in the reference in considerable detail. The results, corrected to 2200 m/sec values, are given in Table I-2.

Table I-2 THERMAL η VALUES DERIVED FROM MANGANESE BATH MEASUREMENTS[9] (2200 M/SEC VALUES)

Material	η
U^{233}	2.296 ± 0.010
U^{235}	2.077 ± 0.010
Natural uranium	1.329 ± 0.009

Also given is η for natural uranium, based on the measured value of η for U^{235} and on recent determinations of the absorption cross sections of U^{235} and U^{238} (681 ± 7 barns[10] and 2.71 ± 0.02 barns,[11] respectively).

The status of critical experiments with aqueous solutions of fissionable isotopes, for the determination of η of U^{233}, is reported in reference 12. Analyses of the data were not finished at the time of publication of the reference. The measurement judged to give the best measurement in spherical geometry gave $\eta = 2.295 \pm 0.036$ for U^{233}, whereas measurements in cylindrical geometry gave values from 2.281 ± 0.016 to 2.290 ± 0.025. These are evidently the effective η values for the neutron spectra in the critical assemblies.

Reference 13 gives the details of the calculation of the "fast effect" in beryllium oxide, which was reported at the Physics of Breeding Conference. The net fast effect, ϵ, analogous, in the neutron balance, to the fast fission effect in U^{238}, is calculated to be between 1.027 and 1.046. This net effect includes the neutron production by the $(n,2n)$ reaction and the neutron loss by the (n,α) reaction but does not include the neutron loss to Li^6 manufactured in the BeO by the (n,α) reaction. The latter effect is discussed also in the reference.

Power Flattening by Variation of Moderator Properties

The results of a calculational study of power flattening in a Sodium Graphite Reactor (SGR) by means of spatial variation of the moderator properties is reported in reference 14. It is

proposed that the properties of the moderator might be varied, as a function of position, either by varying the density of the graphite or by replacing some of the graphite by BeO. It is considered that the latter alternative might be accomplished either by mixing the BeO with the graphite at some stage in the manufacture or by placing solid BeO inserts in holes in the graphite.

To flatten the normal power distribution in the sodium graphite reactor, the effective moderator-to-fuel ratio should be increased progressively from the center of the core to the edges. This could be done either by decreasing the graphite density progressively toward the center or by increasing the BeO addition progressively toward the edges, or by a combination of the two variations.

Table I-3 gives the characteristics of the sodium graphite reactor investigated. The reference gives calculated results for a number of different moderator distributions. An improvement of 22 per cent in average specific power was shown for the case in which the power was flattened radially by incorporating 40 vol.% of BeO in the peripheral annulus described by the outer 20 per cent of the core radius. An increase in average specific power of about 27 per cent was shown for the case in which the graphite density was varied radially from 80 per cent at the center to 100 per cent of normal density in the outer annulus. Increases of up to 44 per cent in average specific power were shown for combinations of radial variations of graphite density and BeO content. Substantial improvements were also shown for axial variations of the moderator properties. The changes in moderator properties resulted in changes of reactivity of magnitude up to about 3 or 4 per cent k_{eff}. As would be expected, the addition of BeO increased reactivity, whereas the reduction of graphite density decreased reactivity.

Table I-3 CHARACTERISTICS OF SGR CORE FOR POWER FLATTENING STUDY[14]

Dimensions	
Core height, ft	12.5
Core diameter, ft	12.5
Reflector thickness, in.:	
Axial	24
Radial	17
Moderator can size, in.	16.75
Fuel Element	
Fuel rods per element	37
Fuel rod diameter, in.	0.434 (10 g UO_2/cm^3)
Fuel enrichment	3.5 at.% U^{235}
Process tube inside diameter, in.	4.00
Unit Cell Volume Fractions	
Uranium dioxide	0.0466
Sodium	0.0835
Graphite	0.8510
Stainless steel	0.0080
Zirconium	0.0106
Void	0.0003

Two-group Constants

	Core	Reflector	
		Axial	Radial
Σ_{a_1}, cm^{-1}	0.000617		
Σ_{R_1}, cm^{-1}	0.002368	0.00308	0.00322
D_1, cm	0.986	1.044	0.958
Σ_{a_2}, cm^{-1}	0.005728	0.002764	0.001277
$\epsilon\nu\Sigma_{f_2}$, cm^{-1}	0.008521		
D_2, cm	0.887	0.949	0.879

Analogue for Three-dimensional Reactor

It has been reported[15] that an analogue method was used for some of the three-dimensional flux-distribution determinations in connection with the design of the British Trawfynydd reactor. The analogue is a thermal one which simulates the one-group reactor equation. The instantaneous temperature distribution in a cooling solid obeys a diffusion equation identical to the one-group critical equation for the neutron flux. In the analogue the reactor core is represented by a hot solid of similar shape which loses heat to the boundaries, and the temperature distribution in the solid is observed. The model is made of a suitable wax. Spatial variations in the material buckling $B^2 [= (k-1)/M^2]$ are simulated by the use of waxes of different thermal diffusivities, whereas control rods and other lumped absorbers are simulated by cooled holes drilled in the wax.

References

1. Nuclear Physics Research Quarterly Report for April–June 1957, USAEC Report HW-51983, Hanford Atomic Products Operation, Aug. 14, 1957.
2. Nuclear Physics Research Quarterly Report for July–September 1957, USAEC Report HW-53492, Hanford Atomic Products Operation, Nov. 6, 1957.

3. Nuclear Physics Research Quarterly Report for April–June 1958, USAEC Report HW-56919, Hanford Atomic Products Operation, July 21, 1958.
4. Nuclear Physics Research Quarterly Report for July–September 1958, USAEC Report HW-57861, Hanford Atomic Products Operation, Oct. 20, 1958.
5. Nuclear Physics Research Quarterly Report for October–December 1958, USAEC Report HW-59126, Hanford Atomic Products Operation, Jan. 20, 1959.
6. Nuclear Physics Research Quarterly Report for April, May, and June 1959, USAEC Report HW-61181, Hanford Atomic Products Operation, July 20, 1959.
7. S. L. Shufler et al., Temperature Coefficients of a Highly Enriched Core in Slab Geometry, USAEC Report WAPD-TM-128, Bettis Atomic Power Division, Westinghouse Electric Corporation, October 1959.
8. Reactor Technology Report No. 11, Physics, USAEC Report KAPL-2000-8, Knolls Atomic Power Laboratory, December 1959.
9. Oak Ridge National Laboratory, Mar. 15, 1960. (Unpublished)
10. G. J. Safford and W. H. Havens, Fission Parameters for U^{235}, Nucleonics, 17(11): 134 (November 1959).
11. D. J. Hughes and R. B. Schwartz, Neutron Cross Sections, USAEC Report BNL-325(2nd. Ed.), Brookhaven National Laboratory, July 1, 1958.
12. Neutron Physics Annual Progress Report for Period Ending Sept. 1, 1959, USAEC Report ORNL-2842, Oak Ridge National Laboratory, Nov. 16, 1959.
13. The Fast Multiplication Effect of Beryllium Oxide in Reactors, USAEC Report ORNL-2849, Oak Ridge National Laboratory, Dec. 14, 1959.
14. T. J. Connolly, Power Flattening in Sodium Graphite Reactors by Spatial Variation of Moderator Properties, USAEC Report NAA-SR-4180, Atomics International, Dec. 15, 1959.
15. S. A. Young, Trawsfynydd Nuclear Power Station: 2—Technical Calculations, *Nuclear Power*, 4(43): 95–97 (November 1959).

Hot-channel Factors

The concept of hot-channel factors has been discussed in the September 1959 and March 1960 issues of *Power Reactor Technology*. In reference 1 the application of hot-channel hot-spot factors to the Engineering Test Reactor (ETR) was demonstrated, and the hot-channel calculations indicated a wall temperature at the hot spot of 395° F, some 30° above saturation. Reference 2 presents another method of taking into account the hot-channel factors and investigates the calculations presented in reference 1.

The statistical method presented in reference 2 is similar to that shown by Bonilla,[3] in that the hot-spot wall temperature is written as the sum of two terms

$$T_{wHC} = T_w + N\sigma \qquad (1)$$

where T_{wHC} = hot-spot wall temperature associated with N number of sigmas
T_w = the "nominal" wall temperature
σ = variance (standard deviation)

If $N = 1$, the probability that the actual hot-spot wall temperature exceeds T_{wHC} is 0.16; if $N = 2$, the probability is 0.023, etc. In reference 3, T_w is the wall temperature calculated without the application of any hot-channel factors. Sigma is calculated as the square root of the sum of the squares of the product of the individual fractional root-mean-square variation and the corresponding temperature rise. Although it is assumed that all hot-channel factors correspond to two fractional root-mean-square variations, this would, of course, be modified by actual experience. For example, a recent reactor design report lists hot-channel factors that are three standard deviations from the design values.[4]

The methods used in calculating T_w and σ_{T_w} in reference 2 are somewhat different. The usual calculation for T_w is defined by

$$T_w = T_b + \frac{q/A}{h} \qquad (2)$$

where q/A is the heat flux and h is the heat-transfer coefficient at film temperature as calculated by some appropriate relation, e.g., the modified Colburn equation ($h = bB$ of that equation). This form is neither explicit in T_w (since h is a function of T_f and T_f is a function of T_w) nor does it lend itself to a statistical error analysis. To circumvent this difficulty, utilizing the modified Colburn equation, triples of numbers T_w, T_b, and $K^* = (q/A)/B$ which solve Eq. 2 were determined, and by statistical regression analysis the equation

$$T_w = 46.68 + 0.87T_b + 16.99 \times 10^{-4}K^* \qquad (3)$$

was derived which approximates to Eq. 2 within 10° F in the range $250° F \leq T_w \leq 550° F$. The application of this equation to hot-spot temperature and associated uncertainty estimation is accomplished by defining T_b and K^* in terms of the basic components entering into their evaluation and through factors applied to the components where appropriate to translate them from the normal condition to the hot-channel or hot-spot condition. Gaussian distributions with known means and variances are postulated for each of the components and factors entering into the computation, and, by means of Eqs. 2 and 3 and the propagation-of-errors formula, the estimate and the associated standard deviation in T_w (σ_{T_w}) are determined. Inferences can then be made relative to the true hot-spot wall temperature exceeding any given value.

A typical ETR calculation serves as an example of the procedure. Using the data of reference 1, risks of exceeding various temperatures are determined. For 395° F, the maximum value determined in reference 1, the risk was found to be 0.02.

The procedure has application to any calculation of this same general type.

Another paper on the statistical analysis technique is presented in reference 5. The section on the analysis of individual factors

points out that the engineering hot-channel factors arise from distributions which are often normal distributions of mechanical data; and, if such is the case, the hot-channel factors can be calculated by the use of tolerance limits for a specified confidence level, the number of observations or measurements of the particular parameter of a fuel element being considered. The fuel-density hot-channel factor is illustrated and defined as

$$F_{\text{density}} = \frac{\rho + \bar{\rho}}{\rho}$$

where ρ is nominal density and $\bar{\rho}$ is variation from nominal.

Table II-1 shows the probability for F_{density} being exceeded, with a confidence level of 99 per cent, assuming 500 observations are recorded. The figures in Table II-1 illustrate that, as $\bar{\rho}$ increases, the probability of exceeding $\rho + \bar{\rho}$ decreases.

Table II-1 PROBABILITY FOR FUEL-DENSITY HOT-CHANNEL FACTOR BEING EXCEEDED

F_{density}	Probability of being exceeded
1.0022	0.10
1.0027	0.05
1.0038	0.01
1.0051	0.001

Other hot-channel factors can be calculated in much the same way, and the problem becomes one of how to combine the various factors in a meaningful manner. Consideration must be given as to whether any of the factors are related, e.g., eccentricity and fuel meat thickness. Reference 5 illustrates both a graphical and a numerical technique for combining two independent factors and briefly discusses how to combine related factors, and the combination of more than two factors, some of which are related. The results of the multiplication of several independent factors yield a table similar to Table II-1. The "probability of being exceeded" column may then be multiplied by the number of coolant channels in the reactor to obtain the expected number of hot channels, that is, the number of channels whose temperature exceeds that specified by the overall hot-channel factor. Presumably, for a conservative design, one would make this number considerably less than unity. It is to be remembered, of course, that hot channels and hot-spot factors are used only to take account of those deviations whose occurrence and location in the reactor cannot be predicted. Any predictable deviation from the average thermal situation, such as the deviations due to predictable neutron-flux distributions or to preferential orificing of coolant flow, must be accounted for in an appropriate manner. The approximate result will be, for most reactors, that the probability of being exceeded will not be multiplied by the total number of coolant channels but by some considerably smaller number made up of those channels computed to be the "hottest" on the basis of the predictable quantities. An alternative, and perhaps preferable, approach would be to decide on some acceptable probability of exceeding the design condition somewhere in the reactor. The ETR, for example, apparently has been successfully operated with about a 2 per cent probability of the wall temperature exceeding 395°F. The corresponding probability for the wall temperature exceeding saturation is about 10 per cent.

Geometrical Complications

Reference 6 contains recent information on the analysis of turbulent flow and heat transfer in noncircular passages. The introduction contains several references to papers dealing with heat transfer and flow wherein turbulent axial flow between rods and in eccentric annuli was studied. The particular geometries studied were a triangular duct and square duct, for Reynolds number 10^4 to 10^6. The analytical investigation proceeded by integrating the differential equations for shear stress and heat transfer for fully developed flow, using appropriate functions for the momentum eddy diffusivity and assuming the heat-transfer eddy diffusivity to be equal to the momentum diffusivity. The results were compared with a limited number of experimental data and were found to be "in reasonably good agreement." The following results are quoted from the reference:

1. The velocities and shear stresses in the region near the corner were lower than the average values and went to zero at the corner.

2. When the passages were heated, the heat transfer to the fluid in the region near the corner was lower than the average value and went to zero at the corner.

3. The friction factors for the noncircular passages were somewhat lower than those for a circular tube.

4. When uniform heat sources in the passage wall and uniform heat transfer at the surface were assumed to occur, the difference between the maximum and average wall temperatures was directly proportional to the heat flux.

5. The average Nusselt numbers for the noncircular passages were somewhat lower than those for a circular tube. The average Nusselt number was also found to be a function of wall temperature distribution and of Prandtl number.

It was pointed out in the reference that, if secondary flows were present in the corner regions, the velocity distribution might be different. Secondary flows, peripheral conduction, and turbulent transport in the fluid were neglected in the analysis and have not been extensively investigated experimentally.

Reference 7 presents an analytical treatment of a fairly common problem in reactor design, that of determining the temperature of a UO_2 fuel pellet encased in a cylindrical rod. The solution to Fourier's equation was accomplished with some interesting modifications, however. The heat source was described by the following equation (cylindrical coordinates):

$$S(r,\theta) = C_1 + C_2 r \cos\theta$$

The cosine distribution was taken as an approximation to the physical fact that part of the fuel rod "saw" the moderator and the remainder saw other fuel rods. The net neutron current would then be greater on the moderator side than on the other side. Because of this same geometry, the coolant-gas temperature was represented by the following function:

$$T_{\text{coolant}} = C_3 + C_4 \cos\theta$$

Circumferential conduction in the metal wall of the tube was included, and two cases were studied: (1) the pellet is centered in the tube, and (2) the pellet is located off-center in the tube. The detailed numerical results of the study are restricted to the fuel-element sizes and specific powers used in the calculations and will not be repeated here. In general, however, circumferential temperature differences of the clad wall and pellet surface (i.e., maximum wall temperature − minimum wall temperature) up to several hundred degrees were calculated. The equations given in the report should enable a hot-channel factor for this effect to be calculated with reasonably good assurance.

Burnout

The September 1959 issue of *Power Reactor Technology* contained a section presenting various correlations for burnout heat flux. To these correlations can be added several others recently proposed by Bell.[8] A statistical analysis was performed on available burnout heat-flux data from various sources for water flowing vertically upward in uniformly heated rectangular channels at 2000 psia. The range of variables studied are: burnout enthalpy from 540 to 1000 Btu/lb and mass velocity from 0.2×10^6 to 5×10^6 lb/(hr)(sq ft). Two correlations were determined, one for "best fit" of all the data and one for best fit in the quality region ($672 \le H_b \le 1000$ Btu/lb) only. The form of the correlation equations is

$$\frac{\phi_{BO}}{10^6} = a\left(b + \frac{G}{10^6}\right)^c \left(\frac{H_g - H_b}{10^3}\right)^{d(G/10^6)^e}$$

where ϕ_{BO} = burnout heat flux, Btu/(hr)(sq ft)
a,b,c,d,e = correlation constants
G = mass velocity, lb/(hr)(sq ft)
H_g = enthalpy of saturated vapor, Btu/lb
H_b = bulk enthalpy at burnout location, Btu/lb

The values for the correlation constants for the two correlations are presented in Table II-2, along with other pertinent data.

A frequency distribution graph for the two correlations showed that nearly all the data fell within $\pm 2\sigma$ from the mean, so a conserva-

Table II-2 RESULTS OF STATISTICAL ANALYSIS
$0.2 \le G/10^6 \le 5$ lb/(hr)(sq ft)

	Correlation 1*	Correlation 2†
Correlation constants:		
a	0.427	1.37
b	2.59	1.19
c	1.81	1.44
d	1.77	1.67
e	0.406	0.474
No. of data points	238	186
Log mean standard deviation	0.100	0.0947

*$540 \le H_b \le 1000$ Btu/lb.
†$672 \le H_b \le 1000$ Btu/lb.

tive estimate of ϕ_{BO} for design purposes would be 65 per cent of the value obtained from either calculation. A somewhat disquieting note was added, however, when a comparison of the correlations was made with 25 runs with a rectangular channel having an axial heat-flux distribution in the form of a chopped cosine (Bettis data). It was shown that the burnout data (presumably the burnout heat flux was taken as the heat flux at the point of burnout) for the cosine shape fell an average of 30 per cent below ϕ_{BO} calculated by the correlations, and four of the points fell below the correlation by factors ranging from about 2 to 2.9. The chopped cosine used had a maximum-to-average ratio of 1.38 and a maximum-to-minimum ratio of 4.0. In all cases burnout occurred between the halfway point, where the heat flux was highest, and the end of the channel. This chopped cosine peak-to-average ratio is not particularly high; the Dresden reactor, for example, has an axial peak-to-average ratio of about 2. The detailed conclusions of Bell are quoted below:

> Based upon this study, the following conclusions can be made for vertical upflow of water in rectangular channels at 2000 psia:
>
> 1. The burnout heat flux is primarily dependent on the fluid enthalpy at the burnout point with a varying dependency of the fluid mass velocity.
>
> 2. The burnout flux decreases as the mass velocity increases, for a constant burnout enthalpy in the quality range. This inverse effect occurs for both uniform and cosine shaped axial heat-flux distributions. The higher the quality, the stronger is this inverse effect. The opposite is true for subcooled burnout, with the crossover point occurring near the saturated liquid point where mass velocity has a minimum effect on the burnout heat flux.
>
> 3. Channel length and length-to-thickness ratio (L/S) appear to have no effect on the burnout heat flux. Since the range of channel thickness was narrow, no conclusions regarding the effect of this variable alone can be made.
>
> 4. For the same conditions at the burnout point, the burnout heat flux for a channel having a cosine-shaped axial heat-flux distribution is significantly lower than for a uniformly heated channel. One must take this effect into consideration, then, in applying any correlations based upon uniform-heating burnout data to reactor design.

Short Notes

Present boiling-water reactor designs are primarily fuel temperature limited because of the economics of fuel-element design. As fuel-element technology improves, however, the limiting design condition could be burnout. The September 1959 issue of *Power Reactor Technology* presents several empirical correlations of the critical heat flux in water at high pressure. Reference 9, recently published, presents an extensive analytical approach to the subject of pool boiling. The table of contents is quoted below:

Chapter I. A Review of Nucleate Boiling
II. The Problem of Bubble Growth
III. Hydrodynamic Aspects of Nucleate Boiling
IV. Hydrodynamic Aspects of Transitional Boiling
V. The Minimum Heat Flux in Transitional Boiling from a Horizontal Surface
VI. The Critical Heat Flux Density from a Horizontal Surface

Since the condition of pool boiling from a horizontal surface occurs infrequently in reactor problems, the work is of general, rather than specific, interest.

Compilations of physical properties of reactor materials are of continuing interest. References 10 and 11 are such publications. The former reference contains papers presented at the Symposium on Thermal Properties held in February 1959, under the sponsorship of the American Society of Mechanical Engineers. The latter reference investigates thermodynamic and transport properties of water and water vapor in the critical region.

References

1. V. A. Walker, Heat Transfer in ETR Fuel Assemblies for Cycle 13, USAEC Report IDO-16562, Phillips Petroleum Company, November 1959.
2. F. H. Tingey, Error Propagation in Hot Channel–Hot Spot Analysis, USAEC Report IDO-16558, Phillips Petroleum Company, October 1959.
3. C. F. Bonilla, *Nuclear Engineering*, p. 445, McGraw-Hill Book Company, Inc., New York, 1957.
4. Experimental Gas-cooled Reactor: Preliminary Hazards Summary Report, USAEC Report ORO-196, Kaiser Engineers Division, Henry J. Kaiser Company, and Allis-Chalmers Manufacturing Company, Atomic Energy Division, May 1959.
5. P. A. Rude and A. C. Nelson, Statistical Analysis of Hot-channel Factors, *Nuclear Sci. and Eng.*, 7(2): 156–161 (February 1960).
6. R. G. Deissler and M. F. Taylor, Analysis of

Turbulent Flow and Heat Transfer in Noncircular Passages, Report NASA-TR-R-31, National Aeronautics and Space Administration, 1959.

7. J. L. Routbort, Temperature Distribution in a UO_2 Fuel Pellet and Surrounding Metal Wall, USAEC Report AGN-TM-364, Aeroject-General Nucleonics, October 1959.
8. D. W. Bell, Correlation of Burnout Heat Flux Data at 2000 Psia, *Nuclear Sci. and Eng.*, 7(3): 245–251 (March 1960).
9. N. Zuber, Hydrodynamic Aspects of Boiling Heat Transfer, USAEC Report AECU-4439, June 1959.
10. *Thermodynamic and Transport Properties of Gases, Liquids, and Solids*, McGraw-Hill Book Company, Inc., New York, 1959.
11. E. S. Nowak and R. J. Grosh, An Investigation of Certain Thermodynamic and Transport Properties of Water and Water Vapor in the Critical Region, USAEC Report ANL-6064, Argonne National Laboratory, October 1958.

In the design of secondary containment shells for water-cooled power reactors, current practice* is to provide sufficient strength in the shell to withstand the pressure rise due to the escape of steam and water through the maximum credible rupture in the primary coolant system. Although credit may be taken for some condensation of steam on walls and other surfaces if the magnitude of the effect can be predicted, no deliberate attempt has been made to increase the condensation effect in previous containment-building designs.

In recent months, however, a new concept of containment has been under investigation[1] and has been considered for use on the Humboldt Bay reactor of the Pacific Gas and Electric Company. This concept can best be described by the schematic drawing shown in Fig. 2. The reactor is suspended in an air-filled cylindrical tank called the dry well. The dry well is connected to a pool of water by vent pipes. Over the pool of water is a vaportight container. Should a leak or rupture occur in the reactor vessel, the steam-water mixture would flow out of the vessel and into the dry well, displacing the air in the vent pipes. As pressure increased in the dry well, the air-steam-water mixture would flow into the pool of water wherein the steam would condense. If this condensation were rapid and complete, the pressure buildup within the vaportight enclosure would be small, and the water in the pool would act as a heat sink for the steam-water mixture. Ideally, the water would also scrub solid fission products from the vent pipe effluent, should any be present due to the nature of the accident.

Reference 1 describes the development program conducted to investigate the containment system. After analytical investigation of the concept, two test facilities were constructed. The first facility, the condensing test facility, was designed to investigate the behavior of the vent units. The facility consisted of water enclosed in a test tank; steam could be injected into the water through various experimental vents at rates up to about 100,000 lb/hr. The first series of experiments was done with a test tank 20 ft in diameter by 24 ft high. The following range of parameters was tested:

Vents	4-, 6-, 8-, and 14-in.-diameter single straight pipes and a set of three parallel 4-in.-diameter pipes
Depth of submergence	1 in. to 6 ft
Direction of discharge	Vertically downward and horizontal
Steam flow	10,000 to 93,000 lb/hr, 100 psig steam at near saturation
Tank water temperature	50 to 150°F

In all but a few cases, the steam was completely condensed; the few exceptions were for the vent pipe discharge within a few inches of the surface of the water. Difficulty with tank vibration was experienced when the water pool temperature was hotter than 120 to 130°F, but this should not be a serious restriction in an actual plant design. A second series of tests was done to investigate the vent discharge when a small volume of water was used. Into the large tank was placed a small compartment containing water; the compartment volume was varied but was under 100 cu ft. Ninety-one tests were run to investigate the effect of steam flow rate, vent diameter, and compartment geometry. Complete condensation was obtained, and mixing of the water in the compartment was said to be excellent.

The second test facility utilized was the transient test facility. Basically, the facility is a model of the arrangement shown in Fig. 2. The volumetric size was $1/1000$ that of the Humboldt Bay (California) Power Plant reactor. Discharge of the "reactor" water to the dry well was accomplished by breaking a rupture disk by

*A general review of reactor containment was given in the June 1959 issue of this journal (Vol. 2, No. 3).

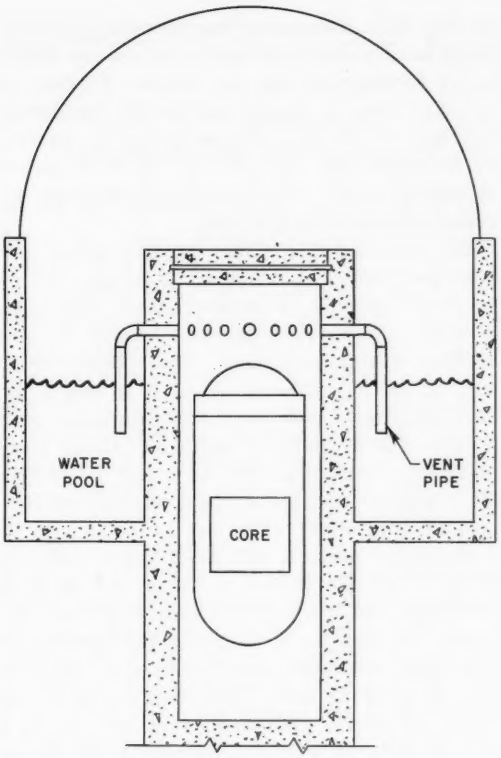

Figure 2—Simplified schematic of containment system.[3]

means of a blasting cap. The test parameters were varied as follows:

Reactor pressure before firing, psi	600, 1000
Fraction of reactor vessel filled with liquid before firing	0.66, 0.80
Diameter of reactor discharge orifice, in.	0.6, 1.2, 1.6
Dry-well volume, cu ft	17.5, 20.3, 26.0
Vent area, sq ft	0.5, 0.9, 2.1
Vent depth of submergence, ft	0.75, 1.0, 1.5

One of the purposes of the transient tests was to test the analytical calculations on peak dry-well pressures. Although some of the assumptions used in the derivations of the analytical equations are given in reference 1, considerably more information is contained in reference 2. Since the equations are of particular interest to the specialist, they will not be repeated here; in general, the experimental results reported indicated that the analytical method of predicting peak dry-well pressure is satisfactory and conservative. The following variables are listed in order of decreasing importance in determining the maximum dry-well pressure: orifice size, depth of submergence, dry-well volume, and vent area. Of these variables the most important one, orifice size, is, possibly, the variable over which the designer has the least control, since it is the size of the leak, hole, or rupture that occurs in the reactor primary system. Thus the design of the containment system hinges on the estimate of the maximum credible size of rupture. Figure 3 summarizes the calculations for the Humboldt Bay reactor. The maximum credible operating accident postulated for that reactor assumes the following:[2]

1. Near-instantaneous main steam or feedwater pipe break.
2. Broken parts or other failed parts become missiles.
3. Blast effects and reactor-vessel reaction occur from the escaping steam and water.
4. Imperfections in the containment permit some leakage.

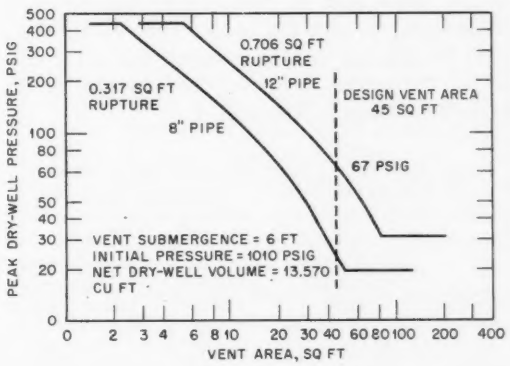

Figure 3—The effect of peak dry-well pressure on vent area.

On the other hand, a rupture of the reactor vessel, a large nuclear excursion, and an explosive chemical reaction are deemed incredible.

The feed-water line to the Humboldt Bay reactor is an 8-in. line. The main steam line is a 12-in. pipe; the calculations presented in Fig. 3 assume that water, rather than a steam-water mixture, is flowing through the break. The upper left-hand portion of the curve, a horizontal line,

results when the vent area is so small that the peak dry-well pressure is attained before a significant amount of steam can escape through the vents into the pool water; for this condition the dry-well pressure depends only on the volume of the dry well. The horizontal line at the lower right-hand end of the curve represents the condition in which the vent area is large enough that it contributes little to the resistance to flow, and the dry-well pressure depends on the break size and the depth of submergence of the vent. The intervening portion of the curve is an area wherein the peak dry-well pressure depends primarily on the flow resistance of the vents, and the effect of dry-well volume and vent submergence is minimized. It is the region in which the Humboldt Bay containment will "operate." If steam condensation in the dry well should tend to reduce the pressure below atmospheric, vacuum breakers are provided to equalize the pressure between the dry well and the pool air space.

Simulated fission products were added to the model reactor vessel for some of the transient test facility operations. The specific objective of these tests was to determine the effectiveness of the water pool in retaining fission products introduced through the vents. The results were said to indicate that, in general, the water pool is an "effective barrier." The results of the tests are shown in Table III-1.

Table III-1 RESULTS OF TESTS ON ENTRAINMENT OF SIMULATED FISSION PRODUCTS IN WATER[1]

Element	Initial amount in pressure vessel	Per cent released to containment volume	Concentration in containment volume, mole %
		−50%	−50%
Krypton	250 cc (std.)	25 + 100%	0.003 + 100%
Xenon	250 cc (std.)	Less than 45	Less than 0.005
Iodine	1 lb	5.8×10^{-5}	1.83×10^{-8}
		7.2×10^{-4} at 5 hr	2.3×10^{-7} at 5 hr
Sodium iodide	100 g	1.7×10^{-4}	1.4×10^{-6}
Zinc sulfide	110 g	2.1×10^{-6}	2.7×10^{-10}

Note: containment volume, after firing, 78.5 cu ft (air); pool volume, 129 cu ft; pressure-vessel volume, 3.12 cu ft.

This type of containment does have some complicating features. For a bottom-driven control-rod system, the rods are located within the dry well. Hence the Humboldt Bay plant provides for access to the bottom of the dry well in order to maintain the rod drives. Further, all primary system pipes that could conceivably fail must be either contained within the dry well or provided with fast-acting valves to prevent discharge of the reactor water in the event of a rupture outside the dry well.

Experiments of a rather similar nature have been performed by Sargent & Lundy. In tests recently reported,[3] a pressure drum, simulating a water-cooled reactor, was housed inside a vertical containment shell. The pressure drum was 42 in. in diameter by 23 ft in length, and the containment tank was 14 ft in diameter by 32 ft high. The drum had a number of 12-in. openings along its side as well as one at the bottom, all of which could discharge downward toward a pool of cold water covering the bottom of the containment tank. A 600-psi rupture disk was placed over one of the openings, and the drum was filled with a given amount of water and subjected to heat; the pressure in the containment tank was measured after rupture of the disk. For most of the tests, 8000 lb of hot water was contained in the pressure drum, and 17,000 lb of cold water was held in the pool at the bottom of the containment tank. As the height of the discharge nozzle was varied, in successive tests, from a few inches above the cold-water surface to about 20 ft above the surface, the maximum pressure recorded in the containment tank increased from about 5 to about 50 psig. The theoretical pressure rise, if there had been no cooling of the discharged water other than by mixing with the gas in the containment tank, was 153 psig. When 4800 lb of water was discharged with no cold water in the containment tank, a maximum pressure of 95 psig was observed, whereas the calculated "no cooling" maximum was 108 psig. In this test only, shock wave formation was reported.

References

1. C. C. Whelchel and C. H. Robbins, Pressure Suppression Containment for Nuclear Power Plants, ASME Paper 59-A-215, 1959.
2. Amendments 2 Through 5 to the Preliminary Hazards Summary Report, Humboldt Bay Power Plant, Unit No. 3, 1959.
3. A. Kolflat, Preliminary Report, 1959 Containment Test, Sargent and Lundy, October 1959.

Reactivity Lifetimes with Plutonium and U^{235} Enrichments

Under the plutonium recycle program at Hanford,* a study has been made of the relative reactivity worths of U^{235} and plutonium (of various isotopic compositions) as feed for a uniformly graded irradiation fuel cycle.[1] The uniformly graded cycle is one in which the reactor fuel composition consists of a uniform mixture of fuels having all degrees of radiation exposure, from zero (feed fuel) to the maximum (discharge fuel). Strictly speaking, the uniformly graded cycle can be achieved in an actual reactor only by discharging and reloading fuel in infinitesimal amounts over the entire volume of the reactor. Practically, the cycle can be approximated by partial reloading schemes which reload perhaps 20 per cent of the reactor fuel at a time. (A discussion of fuel reloading programs was given in the section on Refueling Methods for Solid Fuel Reactors in the September 1959 issue of *Power Reactor Technology*, Vol. 2, No. 4.)

The study considered a single lattice but varied the neutron utilization by varying the fractional neutron leakage. The fractional leakage of neutrons from a reactor may be specified by giving the value of k_∞ required for criticality: higher values of k_∞ represent higher fractional neutron leakage. In the study it was convenient to vary k_∞/ϵ rather than k_∞. The fast-fission factor, ϵ, is not far from unity. In some respects the loss of neutrons by leakage may be considered as equivalent to loss by any other process. However, other losses will not vary in the same way with fuel composition. Other things being equal, only that portion of the leakage which is made up of thermal neutrons will vary importantly with fuel composition. It will vary inversely with the effective thermal-neutron-absorption cross section of the reactor (Σ_a). Neutron losses due to parasitic absorption by such materials as fission products and structural materials will vary inversely as the macroscopic absorption cross section of the fissionable isotope. However, since the study considers arbitrary values of the fractional neutron loss, these distinctions are not of great importance.

The lattice used for the investigation is characterized by a constant value of the resonance slowing-down ratio

$$\frac{V_f}{V_m\,(\xi\Sigma_S)}\,\mathrm{F} = 3.00$$

where V_f/V_m is the fuel-to-moderator volume ratio, $\xi\Sigma_S$ is the slowing-down power of the moderator in the resonance region, and F is the fuel disadvantage factor for resonance neutrons. This amounts to holding the U^{238} resonance-escape probability constant except for the small variation due to the slight change in U^{238} content as enrichment is varied. The lattice resonance-escape probability (p) is defined in the study as the ratio of the number of neutrons reaching thermal energy to the number of neutrons slowing down past the U^{238} fast-fission threshold in an infinite lattice. In this definition of p, the net neutron production by resonance fission is subtracted from the loss of neutrons by absorption in U^{238} and other resonance absorbers. The values of p ranged from 0.927 to 0.949 for the Pu^{239} cases considered and from 0.898 to 0.924 for the U^{235} cases. The values for mixtures of plutonium isotopes were lower (down to 0.824) because of resonance absorption in the higher plutonium isotopes. The value of 3.00 for the resonance slowing-down ratio was stated to correspond to a moderator-to-fuel volume ratio of about 1.0 for H_2O, 13 for D_2O, and 55 for graphite, when the fuel is UO_2 of density 10 g/cm^3. However, the value chosen for the thermal utilization eliminates H_2O as a moderator to which the results might apply. The resonance slowing-down ratio also specifies, along with the fuel composition, the neutron spectrum in the thermal and near-thermal ranges. In the study the formulation of Westcott[2] was followed

*For other activities in the plutonium recycle program, see the discussion of the Plutonium Recycle Reactor (Sec. IX) in this issue.

Table IV-1 RELATIVE PERFORMANCES OF Pu^{239} AND U^{235} AS FISSIONABLE FEED IN REACTORS HAVING DIFFERENT EFFICIENCIES OF NEUTRON UTILIZATION[1]

k_∞/ϵ	Enrichment, % fissionable isotope in feed	Reactivity life, Mwd/ton			Fissions per fissionable atom in feed			Mwd per net gram of fissionable isotope destroyed			Percentage of total fissions in U^{235} when U^{235} is the feed isotope
		Pu^{239}*	U^{235}*	U^{235}*/Pu^{239}	Pu^{239}	U^{235}	U^{235}/Pu^{239}	Pu^{239}	U^{235}	U^{235}/Pu^{239}	
1.05	0.71	6,896	4,927	0.715	1.145	0.805	0.703	2.18	2.67	1.225	63.4
	1.00	12,764	11,809	0.925	1.505	1.37	0.910	2.22	2.36	1.063	52.2
	1.50	21,895	20,947	0.958	1.721	1.62	0.955	2.13	2.14	1.005	49.2
1.15	1.00	5,251	4,180	0.796	0.872	0.683	0.734	1.05	1.30	1.238	71.6
	1.50	14,697	14,197	0.966	1.155	1.098	0.950	1.52	1.68	1.105	63.2
	2.00	21,496	20,958	0.976	1.267	1.235	0.975	1.51	1.57	1.040	61.5
1.30	1.50	7,163	6,439	0.620	0.563	0.498	0.884	1.05	1.36	1.295	81.7
	2.00	11,640	11,832	1.015	0.686	0.739	1.077	1.05	1.21	1.152	76.9
	3.00	21,222	24,153	1.138	0.834	0.934	1.120	1.05	1.23	1.170	74.6

*The top column subheading Pu^{239} signifies that the fissionable material in the feed is pure Pu^{239}; the subheading U^{235} signifies that the fissionable material in the feed is pure U^{235}; the subheading U^{235}/Pu^{239} signifies the ratio of the numbers in the two preceding columns.

in accounting for spectrum effects. The usual effective cross sections ($\hat{\sigma}$) were used

$$\hat{\sigma} = \sigma_0 (g + rs)$$

where σ_0 is the 2200 m/sec cross section; g and s are terms characteristic of the substance, which define the departure of the cross section from the $1/v$ law in the "thermal" and "resonance" regions, respectively; and r is the fraction of epithermal neutrons in the spectrum. In the study the values of r ranged from 0.0650 to 0.17 for the Pu^{239}-fed cases and from 0.0475 to 0.1010 for the U^{235}-fed cases. The moderator temperature was in all cases 200°C.

The value of the thermal utilization (f) was arbitrarily set at 0.9 for natural uranium, and the average macroscopic parasitic absorption cross section was held constant; thermal utilization was calculated for other fuel compositions by taking into account both the change in fuel absorption and a typical change for the disadvantage factor. At 3 per cent enrichment the thermal utilization for the feed fuel had increased to 0.954 for the U^{235} case and to 0.976 for the Pu^{239} case. Xenon and samarium losses are included among the neutron losses represented by k_∞/ϵ; other fission products are treated by a burnup equation.

Three values of k_∞/ϵ were considered, and three enrichments of the feed fuel were considered for each value of k_∞/ϵ. The results for the cases in which the feed is pure Pu^{239} and pure U^{235} are compared in Table IV-1. As would be expected, the reactivity life of the fuel increases rapidly with feed enrichment at a given value of neutron loss, and the reactivity lifetime at a given enrichment decreases rapidly as the neutron losses are increased. When the neutron loss is small or when the enrichment at a given neutron loss is sufficient only for a rather short reactivity life, the plutonium feed gives considerably longer reactivity life than does the U^{235} feed. As the enrichment is increased to give longer reactivity life, the reactivity life given by the U^{235} feed becomes relatively better and, in the highest neutron loss case, surpasses that for the Pu^{239} feed. The same trends are, of course, evident if the reactivity life of the fuel is expressed as the number of fissions occurring over the lifetime of the fuel per fissionable atom initially present in the fuel.

The rather good performance of Pu^{239} so far as reactivity lifetime is concerned is, at first glance, surprising, since the value of η (fission neutrons produced per neutron absorbed) for Pu^{239} is less than that for U^{235}. The behavior of the Pu^{239} would be easier to discuss if values for the cross sections and neutron yields of the uranium and plutonium isotopes had been tabulated in the report.* However, the trend of the results does seem reasonable.

Two types of effects must be recognized. First, the neutron balance for the U^{235} feed cases is not that which would result if all fissions were in U^{235} since, over the life of the fuel, a substantial fraction of the fission occurs in plutonium isotopes. The last column of Table IV-1 shows, for the U^{235}-fed case, the percentage

*The values used were those of reference 2.

of total fissions occurring in U^{235}. One would expect the neutron balance behavior to be a weighted average between that characteristic of the plutonium η and that characteristic of the U^{235} η and to approach the plutonium case as the fraction of fissions in U^{235} decreases.

The second effect is that Pu^{239}, although it has a lower η value, has a higher effective fission cross section. The higher fission cross section reduces the neutron losses represented by $(1 - f)$; it also yields a higher reactivity for the feed fuel. One would expect that these effects would be most pronounced at low enrichments that yield relatively short fuel lifetimes. Presumably when one tries to attain long reactivity lifetime, particularly in reactors with high neutron losses, the effect of the lower plutonium η on conversion ratio is overriding, and the fuel lifetime relative to that obtainable with U^{235} decreases.

Further light is shed on the relation between the Pu^{239} and the U^{235} feeds if the heat output per net gram of fissionable isotope destroyed is considered. This quantity can be determined from the isotopic compositions of the feed and discharge fuels as given in the reference report.[1] The quantity is closely related to the average conversion ratio of the reactor and is, of course, a quantity of primary importance for the effective utilization of nuclear fuel. It may be seen from Table IV-1 that this specific production is in all cases higher for the U^{235} feed and is highest, relative to the value for Pu^{239} feed, in those cases when most of the fissions occur in U^{235}. It is evident from these numbers that the U^{235}-fed reactors in all cases have higher conversion ratios than the Pu^{239} cases, and one would infer that the longer reactivity lifetimes exhibited by the plutonium-fed reactors are due to the higher reactivity of feed fuel at a given enrichment. Thus the U^{235}-fed reactors, in producing a given quantity of energy, burn less net fissionable isotope (U^{235} plus Pu^{239} plus Pu^{241}), but the fuel must be discharged, because of reactivity deficiency, at a relatively higher fissionable-isotope content.

The reference stresses the comparison of feed fuel composed of three additional mixtures of the plutonium isotopes. These mixtures are defined as mixtures which would be obtained if pure Pu^{239} (no U^{238} present) were exposed, in a reactor having a constant epithermal ratio (r) of 0.08, until 50 per cent, then 75 per cent, and then 90 per cent of the original Pu^{239} was burned. The compositions of the various plutonium mixtures are given in Table IV-2. Selected results of the reactivity lifetime calculations are listed in Table IV-3. In Table IV-3 the enrichment refers to the percentage of fissionable isotope (Pu^{239} plus Pu^{241}) in the fed fuel. It is to be noted that the "burned" plutonium mixtures show accentuated trends, relative to U^{235}, of the same type shown by Pu^{239}. This situation is a more complex one. Reference to Table IV-3 indicates that the number of fissions obtained per fissionable atom in the feed increases with the more highly burned plutonium in reactors with low neutron losses. Also, although not specifically calculated, the comparison with U^{235} in Table IV-1 based on megawatt-days per net gram of fissionable material destroyed should improve for highly burned plutonium since the η, or neutrons per absorption, for Pu^{241} exceeds that for Pu^{239}. Important factors contributing to the behavior are, no doubt, the high effective fission cross section of Pu^{241}, particularly in the low-enrichment case, and the important resonance absorption by Pu^{240}, particularly in the higher enrichment cases.

Table IV-2 ISOTOPIC COMPOSITION OF STOCK PLUTONIUM[1]

Per cent burnout of Pu^{239} atoms	Isotopic composition, wt.%			
	Pu^{239}	Pu^{240}	Pu^{241}	Pu^{242}
0	100.00	0	0	0
50	75.20	19.50	4.92	0.38
75	52.95	30.12	14.28	2.65
90	31.35	33.59	24.96	10.10

Table IV-3 COMPARISON OF U^{235} AND PLUTONIUM ISOTOPE MIXTURES[1]

k_∞/ϵ	Enrichment, % fissionable isotope	Type of enrichment	Maximum attainable exposure	
			Fissions per fissionable atom in feed	Mwd/ton
1.05	0.71	U^{235}	0.81	4,930
		Pu^{239}	1.15	6,900
		Pu, 50% burned	1.15	6,950
		Pu, 75% burned	1.22	7,300
		Pu, 90% burned	1.32	8,130
1.30	3.0	U^{235}	0.93	24,150
		Pu^{239}	0.83	21,200
		Pu, 50% burned	0.69	17,600
		Pu, 75% burned	0.63	15,900
		Pu, 90% burned	0.57	14,500

Self-sustaining Plutonium Recycle in Sodium Graphite Reactors

Reference 3 is a study of the use of plutonium recycle with natural-uranium feed in sodium graphite reactors. Existing designs of the sodium graphite reactor require enrichments which are too high for this kind of operation, but it is considered a possibility provided a calandria type design is used and low-cross-section materials are employed for fuel jackets and structural parts.

If the plutonium manufactured during fuel irradiation in a reactor is recycled as part of the feed for the reactor, it will supply some of the fissionable isotope needed for feed, and the proportion of U^{235} in the feed may be reduced. In order for the U^{235} feed requirement to be as low as the U^{235} content of natural uranium, the reactor must make rather effective use of the fission neutrons. This required high neutron economy may be manifest as a relatively low enrichment requirement (U^{235} plus fissionable plutonium isotopes) for operation, or as a high conversion ratio. Both of these characteristics are favored if the parasitic loss of neutrons is kept low and if the number of neutrons produced by the fissionable isotope per neutron it absorbs (η) is high. The parasitic neutron losses depend primarily on the reactor composition, whereas η, at least for Pu^{239}, depends rather strongly upon the neutron temperature in the reactor.

The study reported in the reference, which is an approximate study, approaches the problem by calculating the rate of plutonium production and the isotopic composition of the plutonium in reactors having various conversion ratios, after the recycle program has reached an equilibrium state. These same reactors, if fueled exclusively with U^{235} as the fissionable isotope, would exhibit somewhat different initial conversion ratios and would require, for operation, enrichments which may be specified. The relation between the average conversion ratio of the recycled reactor and the initial conversion ratio of the U^{235}-fed reactor involves only the η of Pu^{239}, if it is assumed that η for U^{235} and η for Pu^{241} are independent of neutron spectrum, as is done in the study. If one then chooses a value of η for Pu^{239}, one can specify a set of U^{235}-fed reactors, each characterized by a value of the initial conversion ratio and an enrichment requirement for operation, which would just operate with natural-uranium feed and plutonium recycle. Sets of reactors of this kind are specified, for various values of η of Pu^{239}, in Fig. 4,

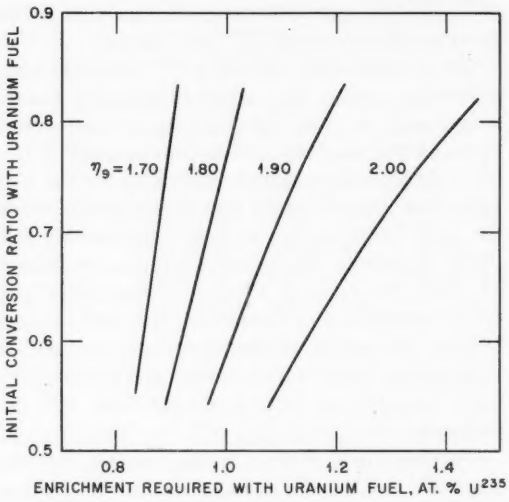

Figure 4—Conditions for self-sustaining plutonium recycle (equilibrium plutonium concentration corresponds to zero irradiation per cycle).

which is reproduced from the reference. For example, if the neutron temperature in the reactor is consistent with a value of 1.90 for η of Pu^{239} and if the reactor requires an enrichment of 1.1 per cent when operating on pure U^{235} and U^{238} fuel, and yields an initial conversion ratio under those conditions of about 0.7, then it will just operate with natural-uranium feed and equilibrium plutonium recycle. The attainable fuel exposure under these conditions would be infinitesimal. To obtain longer exposure at the η value of 1.90, one must move to the left of the 1.90 curve, choosing a reactor which, with U^{235} feed, either requires lower enrichment or yields a higher conversion ratio, or both. The farther to the left one moves, the higher will be the attainable fuel exposure.

In Fig. 5, curves of Maxwell-average η values for Pu^{239} as functions of neutron temperature are reproduced, as derived in the reference from three different sources. It is evident that the value of η is strongly affected by the thermal-neutron temperature; and if values from Fig. 5 are related to the curves of Fig. 4, it is also apparent that these changes represent quite important changes in the enrichment and conversion ratio requirements for self-

sustaining plutonium recycle. Since the neutron temperature will be at least as high as the moderator temperature, it appears probable that a sodium graphite reactor designed to operate on self-sustaining plutonium recycle must be one that can be made critical with uranium fuel of low enrichment, probably below 1 per cent U^{235}.

The basic design change, which is proposed for improving the neutron economy of the sodium graphite reactor, is from a core using individually canned hexagonal blocks of graphite to a calandria in which there is, in effect, a single block of graphite pierced by holes for the fuel elements. Each fuel element is located within a process tube through which the sodium flows, and the process tubes lie within the calandria tubes which constitute a barrier between the sodium and the graphite in the event of a process-tube leak. Uranium-metal fuel rods are used for maximum reactivity, in 7-rod clusters. The fuel jackets, process tubes, and calandria tubes are all of zirconium. The graphite is cooled by conduction to the sodium coolant, across the helium-filled gap between the calandria tube and the process tube. This results in a rather high graphite temperature, which is estimated as an average of 600° C.

The general characteristics of a reactor of this type are given in Table IV-4. The initial conversion ratio of the reactor, when fueled with U^{235}, is 0.70. If the reactor is operated with plutonium-recycle and natural-uranium

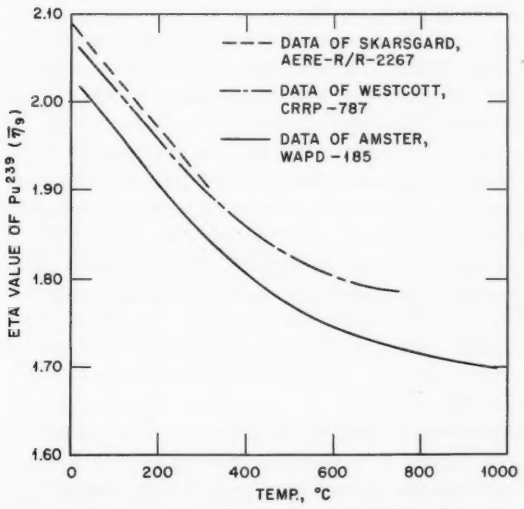

Figure 5 — Maxwell-average η values for Pu^{239}.

Table IV-4 GENERAL SPECIFICATIONS OF AN SGR DESIGNED FOR SELF-SUSTAINING PLUTONIUM RECYCLE

Power:	
Thermal power, Mw	630
Electrical power, Mw	250
Core:	
Diameter, ft	24
Height, ft	18
Lattice spacing, in.	14
Average reflector thickness, ft	2
Average moderator temp., °C	600
Fuel:	
Material	Uranium metal
Enrichment	0.9 at.% U^{235}
Fuel-element configuration	7-rod cluster
Rod diameter, in.	0.75
Number of fuel elements	378
Fuel specific power, Mw/ton	8.3
Cladding material	Zirconium alloy
Cladding thickness, in.	0.010
Process-tube inside diameter, in.	2.79
Process-tube thickness, in.	0.050
Primary coolant:	
Sodium inlet temp., °F	625
Sodium outlet temp., °F	1000
Sodium pressure drop in core, psi	15
Heat flux (average), Btu/(hr)(sq ft)	236,000

feed and with an approximation to uniformly graded irradiation in the radial direction, it is estimated that the average energy yield of the discharged fuel would be about 3750 Mwd/ton. At this exposure level, about 30 per cent of the initial U^{235} content of the feed would be burned. Thus the self-sustaining plutonium-recycle operation, in this reactor, although it would avoid the necessity for isotopic enrichment of the fuel, would be relatively wasteful of U^{235}.

The reference considers also the burning of recycled plutonium in fuel elements which are separate from the uranium fuel elements. It is thought that this scheme might yield somewhat higher U^{235} burnup if whatever plutonium discard occurs during the recycle program could be made up of the most exposed plutonium, thus preserving a somewhat higher ratio of fissionable isotopes in the recycled material.

The conclusion of the study is summarized in the following quotation:

> It appears technically feasible to design a SGR to operate on self-sustaining plutonium recycle. Such a reactor, however, would of necessity have a large core and low (for an SGR) volumetric power density and would require exclusive use of a low-cross-section material such as zirconium alloy for cladding and core structure. The fuel specific energy yield and U^{235} burnup attainable is uncertain but ap-

pears to be on the low side, perhaps 3000 to 5000 Mwd/ton and 25 to 40 per cent U^{235} burnup. Such a system would almost certainly compare unfavorably with a slightly enriched SGR if the fuel inventory annual rate and the unit costs for U^{235} enrichment and for fuel fabrication and reprocessing, currently prevailing in the United States, are applied. Expressed in a different way, it appears that an optimized plutonium-recycle case will require some enrichment of the uranium feed. These conclusions in large measure reflect the low reactivity of plutonium as a reactor fuel and, therefore, they apply in general to other thermal-reactor systems.

Presumably the final statement is intended to apply only in a qualitative sense, for there are certain reactor types, notably some employing D_2O moderation, which are expected to achieve relatively long fuel life with once-through natural-uranium feed. These reactors should show quite good economic performance with self-sustaining plutonium recycle, provided that the costs specifically attributable to the recycling process can be discounted.

General Studies

The results of an extensive fuel-cycle study, concerned primarily with the development of a computer code for calculating fuel cycles and fuel-cycle costs, has been reported in reference 4. The code, named FUELCYC, has been written for the IBM-704 computer. It computes the distribution of neutron flux with respect to energy and position in the reactor, derives effective cross sections for each nuclide at each point in the reactor, uses the effective cross sections to project the change of nuclide concentration at each point with time, determines the conditions under which the reactor is just critical, and evaluates fuel-cycle costs. Geometrically, the code solves the two-dimensional (radial and axial) diffusion equations in an axially symmetric cylinder. Four major energy groups are treated: fast fission, fast, resonance, and thermal, with the resonance group further divided into four subgroups. Leakage is assumed to occur in the fast and thermal groups, and each fuel nuclide is assumed to absorb neutrons in one of the resonance subgroups as well as in the thermal group. The neutron-energy spectrum in the thermal region (below 0.45 ev) is computed from the Wilkins equation, and effective thermal cross sections are derived by averaging over the spectrum.

Although the code is adaptable to the computation of fuel-cycle quantities for many fuel charging and discharging schemes, four such schemes have been specifically written into the code:

1. Batch irradiation of fuel fixed in place in the reactor, with criticality maintained by a uniform distribution of control poison.

2. In-out irradiation, in which there is a continuous replacement of fuel elements, the new elements being added at the axis of the core, partially irradiated elements being shifted radially outward, and fully exposed elements being removed from the periphery.

3. Out-in irradiation, in which fuel elements are fed continuously, in the reverse direction to the in-out scheme.

4. Graded irradiation, in which fuel elements, fixed in place in the reactor, are discharged individually and replaced by fresh elements on such a schedule that the average composition of fuel in each local radial region of the reactor remains time independent.

In all of the continuous reloading schemes (2, 3, and 4), the reactor remains critical without the addition of control elements or poison. In all cases studied, the fuel elements were assumed to be of full core length.

Although the main contribution of the study is the development of the FUELCYC code, some of the fuel-cycle calculations that have been made with the code are of general interest. The results of applying the four fuel reloading schemes to a pressurized-water reactor were studied in some detail. The reactor considered was similar in geometry and composition to the Yankee Atomic Electric Company reactor. It was, of course, necessary to vary the enrichment of the fuel to meet the demands of the different fuel cycles. The actual reactor is fueled with 51,420 lb of UO_2 at an enrichment of 3.4 wt.% U^{235}. It is cooled and moderated by light water at a pressure of 2000 psi and at a temperature of 516°F. The reflector consists of a ½-in. steel baffle with an effectively infinite amount of water beyond. The fuel elements consist of UO_2 pellets, 0.29 in. in diameter, loaded into 20-mil-thick stainless-steel tubes. The tubes are placed on a 0.42-in.-square pitch to form a cylindrical core having a 3.1-ft radius and 7.7-ft height. Other pertinent data are listed in Table IV-5.

Table IV-5 CHARACTERISTICS OF PRESSURIZED-WATER REACTOR USED FOR FUEL-CYCLE CALCULATIONS[4]

Core dimensions, in.:*	
Equivalent diameter	75.68
Total active length	92.257
Temp., mean (T_{md}), °F	516
Power, Mw:†	
Thermal	480
Net electric	134
Nuclear properties:	
Initial resonance-escape probability for U^{238} (p_8)	0.738*
Initial resonance-escape probability for structural materials and coolant (p_c)	0.942*
Fast-fission factor (ϵ)	1.0584*
Fermi age (τ), cm^2	51.5*
Thermal disadvantage factor (ψ)	1.141*
Reflector savings ($\delta_R = \delta_H$), cm	7.5*
Microscopic 2200 m/sec absorption cross section for H_2O, barns	0.575‡
Microscopic transport cross section for H_2O, barns	70‡
Microscopic slowing-down power for H_2O [$(\xi\sigma_s)_{H_2O}$], barns	41.2‡
Microscopic 2200 m/sec absorption cross section for type 348 stainless steel, barns	3.206§
Atomic weight of type 348 stainless steel	55.63§

Item	Volume, cu in.	Weight, lb
Inventories:*		
UO_2 (wt.% U^{235} = 3.4)	141,091	51,420
Stainless steel (type 348)	48,025	13,520
H_2O	208,330	5,881
Zirconium	12,137	2,850
Void	5,421	
Total	415,004	73,671

*W. H. Arnold, Jr., private communications of Mar. 23 and Feb. 26, 1959.

†Yankee Atomic Electric Company Research and Development Program, Reference Design, Report YAEC-1, 1957.

‡A. M. Weinberg and E. P. Wigner, "The Physical Theory of Neutron Chain Reactors," The University of Chicago Press, 1958.

§D. J. Hughes and R. B. Schwartz, Neutron Cross Sections, Second Edition, Report BNL-325, 1958.

Table IV-6 PERFORMANCE CHARACTERISTICS OF PRESSURIZED LIGHT-WATER REACTOR FOR VARIOUS FUEL SCHEDULING METHODS

Fuel scheduling method, max. local burnup, Mwd/ton	Batch	In-out	Graded	Out-in
	At.% U^{235} in Feed			
10,000	3.14	2.93	2.95	3.02
20,000	3.58	3.17	3.20	3.39
30,000	4.10	3.42	3.53	3.79
40,000	4.71	3.70	3.88	4.20
50,000	5.34	4.06	4.24	
60,000	6.09			
	Average Burnup, Mwd/ton			
10,000	4,200	7,900	7,900	7,900
20,000	10,000	16,300	16,300	16,300
30,000	16,800	25,100	25,100	25,100
40,000	24,200	34,400	34,400	34,400
50,000	32,200	44,000	44,000	
60,000	41,200			
	Maximum-to-Average Power Density Ratio			
10,000	1.90*	3.28	2.54	1.80
20,000	1.49*	4.20	2.39	1.47
30,000	1.37*	5.16	2.30	1.38
40,000	1.29*	6.17	2.23	1.35
50,000	1.25*	7.20	2.18	
60,000	1.23*			

*At end of batch cycle.

Table IV-6 lists the more important results of the fuel-cycle calculations. The independent variable (first column) is the maximum local burnup of fuel, that is, the burnup at the position of maximum exposure in the most highly exposed fuel element at the time of discharge. The three sections of the table show, as functions of this variable, the required enrichment of the feed fuel, the average fuel burnup, and the maximum-to-average power density ratio in the fuel. It is to be noted that the enrichment required for a given average burnup increases in the order: in-out, graded, out-in, batch; with the differences being relatively small except in the case of the batch reloading system. The average burnups for the continuous reloading schemes are less than the maximum local burnup because of the axial variation of burnup in a given element. The maximum-to-average burnup ratio decreases with increasing maximum burnup because of the axial flux flattening caused by the preferential burnup near the centers of the elements. The maximum-to-average burnup ratio for the batch case is considerably higher because it is determined by both the axial and the radial power distributions in the reactor. Again, the ratio decreases with increasing burnup. The ratio of maximum-to-average power density is given, for the batch

case, at the end of the batch lifetime. At the beginning of the lifetime, it has the value 2.70. Both the initial and final ratios are, of course, determined by the spatial distribution of control poison over the batch lifetime, and the initial ratio could be made somewhat lower, at the expense of a somewhat higher final value than that tabulated, by an initial concentration of poison near the center of the core to flatten the power distribution. It is apparent that the maximum-to-average power-density ratio is quite poor for the in-out refueling system and becomes worse with longer fuel burnup, whereas the ratio for the out-in system is quite good and becomes progressively better with increasing burnup, at least up to about 35,000 Mwd/ton average burnup. It is to be emphasized, of course, that these maximum-to-average ratios are the smooth ratios for uniform lattices and do not include local peaking effects such as those due to water channels.

The power-distribution patterns established in the reactor after long burnup of the fuel are particularly interesting. In Fig. 6 are reproduced the contours of constant power density — in one quadrant of a plane which bisects the core and contains the core axis — for three different fuel-burnup conditions: the initial condition of the batch-loaded core, the final condition (just before discharge) of the batch-loaded core, and the equilibrium condition of the out-in loaded core. It is to be noted that in both of the latter cases the maximum power density occurs at a considerable distance from the core axis but that for the out-in case the maximum power density lies on the central plane of the core, whereas in the batch case it lies above and below the central plane.

It is probable that, in choosing fuel reloading programs, considerations of maximum-to-average power density and maximum-to-average burnup will be more important in most cases than considerations of fuel enrichment.

Reference 5 reports a study of reactivity lifetimes of fuels composed of mixtures of U^{235}, U^{238}, and thorium. The objective of the study is to determine whether mixtures of U^{238} and thorium as fertile material would yield reactivity-exposure curves which are flatter than those obtained with either material separately and would, therefore, minimize the problems of reactivity change with fuel burnup. Space-independent calculations for many different mixtures were made by means of an analog

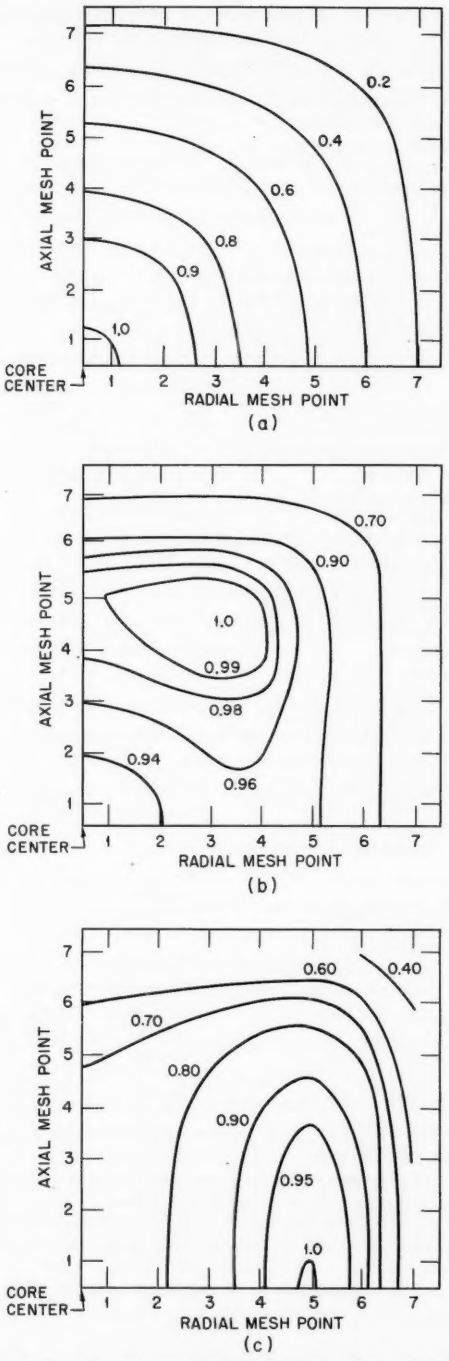

Figure 6 — Two-dimensional contour plot of power density in one quadrant of a vertical plant bisecting the reactor core. (*a*) Batch loaded, initial. (*b*) Batch loaded, final (23,000 Mwd/ton average). (*c*) Out-in loading cycle, equilibrium (23,000 Mwd/ton average discharge burnup).

computer, using a fixed set of nuclear constants, corresponding to a slightly hardened spectrum at 650°K. The results of the study are summarized in the quotation:

1. By varying the atom ratio of a fuel consisting of Th^{232}, U^{235}, and U^{238}, it is possible to attain, for a specific reactor, an efficient use of the original fuel.
2. Removal of fission products during the operation greatly increases the lifetime of a fuel.
3. For systems using Th^{232} as fertile material, very large reactivity lifetimes are possible for an initial conversion ratio significantly less than the theoretical maximum $(\eta - 1)$ as compared with systems using U^{238} only as fertile material.
4. The characteristics of the η variations in a Th^{232}-U^{235} fuel are almost a mirror image of the η variations in U^{238}-U^{235} fuel. Therefore it is concluded that a reactor which is loaded with a mixture of natural uranium and thorium can have a flat curve of reactivity versus irradiation time over its lifetime. The lifetime would then be determined theoretically by irradiation damage.
5. It is desirable to have as low an enrichment and as high a value of $[\mu = \epsilon(1 - p)L]$ as is consistent with good design, where L is the neutron-leakage probability.

Since, in this type of general study, questions of criticality must be ignored, the results must be studied in reference to a particular reactor type to determine whether the values of μ which give favorable reactivity lifetime curves are practically attainable. In considering the practical aspects of uranium-thorium mixtures, it must be recognized that whatever U^{235} is present in the discharged fuel will probably have its value degraded because of the alpha and gamma activities due to U^{233} and U^{232}. [The buildup of radioactivity in isotopes produced by neutron irradiation of thorium is described briefly in *Power Reactor Technology*, 1(4): 19 (September 1958), and 2(2): 42–43 (March 1959).]

References

1. D. P. Granquist, A Calculation of the Reactivity Worth of Plutonium and U^{235} as Enrichment in Thermal Reactors, USAEC Report HW-59758(Rev.), Hanford Atomic Products Operation, Aug. 8, 1959.
2. C. H. Westcott, Effective Cross Section Values for Well-moderated Thermal Reactor Spectra, Canadian Report CRRP-787(AECL-670), Aug. 1, 1958.
3. T. J. Connolly, Self-sustaining Plutonium Recycle in Sodium Graphite Reactors, USAEC Report NAA-SR-3912, Atomics International, Sept. 1, 1959.
4. R. T. Shanstrom, M. Benedict, and C. T. McDaniel, Fuel Cycles in Nuclear Reactors (Thesis), USAEC Report NYO-2131, Massachusetts Institute of Technology, Aug. 24, 1959.
5. J. C. Carter and R. C. Howard, Isotopic Abundance and the Variation of η in Irradiated Nuclear Fuels Consisting Initially of Combinations of Th^{232}, U^{238}, and U^{235}, USAEC Report ANL-6067, Argonne National Laboratory, October 1959.

In conventional reactor fuel elements, the fuel material is canned in some kind of nonfissionable jacket to prevent contamination of the reactor coolant system, and for other reasons. If the outside of the jacket becomes contaminated with fissionable material before the element is placed in the reactor, this function of the jacket will be partially negated. The contamination may or may not be a hazard, depending upon its level, upon the degree to which it can escape the reactor coolant system, and upon the ventilation and disposal systems in the reactor room. For example, in submarine applications, where ventilating air is recirculated, a relatively small amount of contamination may prove troublesome. In any case the presence of fission products originating in surface contamination can mask the effects of fuel-element failures, and for this reason surface contamination is quite undesirable.

The avoidance of important surface contamination can in some cases be difficult because exceedingly minute amounts of uranium suffice to give appreciable effects: in contamination studies, the quantity of fissionable isotope present on a surface is usually measured in units of 10^{-9} g per square decimeter of surface.

Reference 1 contains the results of a number of studies which were made at KAPL to trace down the sources of surface contamination that had been observed on some industrially fabricated zirconium-uranium alloy fuel specimens. The reference states that Zircaloy-2 will normally contain a small amount of natural uranium and that a limit of 5 ppm has been proposed for the permissible natural-uranium content of Zircaloy-2 used for fuel-cladding material. With this natural-uranium content, there would be approximately 18×10^{-9} g of U^{235} per square decimeter of surface within a layer of 0.3-mil thickness, the approximate thickness through which fission products could be released. This surface density of U^{235} may be considered to define the quantity of surface contamination which would be considered important. The reference states that some of the specimens examined had surface quantities of U^{235} in excess of 100×10^{-9} g/dm^2. A systematic study of the fuel-element fabrication and assembly steps was made to determine the source of the contamination. Initially, this was done by withdrawing sample elements from the fabrication process and analyzing them for contamination. The tests indicated:[1]

1. Minor contamination was present on the fuel elements after form rolling.
2. Major contamination was produced in vacuum annealing.
3. Pickling in HNO_3-HF (45 HNO_3, 5 HF, 50 H_2O) to a depth of 0.002 in. removed substantially all contamination.
4. Finished elements were uncontaminated.

A second series of tests was made by passing clean finished elements through single fabrication operations. These operations included the autoclave corrosion testing which was normally done on all finished fuel elements. The tests showed:

1. Major contamination was again produced by vacuum annealing.
2. No contamination was produced by pickling, even in highly contaminated acid.
3. Minor contamination was produced in welding.
4. Major contamination was produced in autoclave corrosion testing. The level of contamination varied widely from autoclave to autoclave.

Tests of the furnace and accessory surfaces used in the annealing revealed substantial U^{235} contamination on retort walls and annealing fixtures. Examination of the autoclave pressure vessels revealed no loose contamination, but the fixed contamination level on the interior walls, measured by alpha-particle counting, was in some cases as high as 19,500 dis/min/dm^2. These measurements, along with controlled laboratory tests on small specimens, showed that, during autoclave testing, contamination could be transferred from autoclave walls to Zircaloy surfaces and that, after its transfer, it

was apparently fixed in place by the oxide film formed on the Zircaloy during the autoclave testing. Such contamination could not be removed to any appreciable extent by successive washes with 50-50 nitric acid at room temperature.

The findings of the investigation emphasize the necessity for a high degree of cleanliness in those pieces of fabrication and testing equipment which contain the fuel elements at high temperatures and particularly in the autoclaves, whose function is to test the elements and to form a stabilized oxide coating on them.

Reference

1. W. M. Cashin, ed., Uranium Surface Contamination on Nuclear Reactor Fuel Elements, USAEC Report KAPL-2061, Knolls Atomic Power Laboratory, Oct. 23, 1959.

The General Electric Company, in its Atomic Power Equipment Department, is conducting a research and development project for the AEC on the use of solid neutron-absorbing materials for reactor control. The first topical report on this project[1] has recently been issued. It includes summary descriptions of what is known and what has been done previously in this field and of the nature of current programs and gives subjects and recommendations for future investigation. The document is a good general review of the control-rod materials field and contains extensive bibliographies which will be useful to the reactor designer.

Since the document itself is a review, the following discussion will attempt only to cover the points of most general interest to reactor designers and to add enough introductory material to point up the reasons for the various requirements imposed on control-rod materials.

Reactivity Requirements and Control-rod Effects

The basic purpose of control rods, beyond the adjustment of reactor power level, is to compensate the excess reactivity which must be built into the reactor to make it operable over its projected lifetime. Although the control rods may perform additional functions such as flux flattening or control of spatial oscillations of xenon content, the total reactivity worth required of all the control rods in the reactor is usually determined by the maximum excess reactivity which the reactor may have during its lifetime. Often there is a strong desire to provide this reactivity worth by using the smallest possible number of control rods; for the cost associated with each rod (the cost of the rod itself, its drive mechanism, and its installation) is fairly high, and each additional control rod adds to the complexity of the plant. In these cases the designer desires a control-rod material of the greatest possible nuclear effectiveness. In other cases, other considerations, such as the use of control rods for power flattening, may dictate that the total reactivity holddown capacity be distributed among a larger number of rods. The desire for materials of high nuclear effectiveness may then be reduced, although the designer may still wish to use effective materials in order to keep the size of the rods small.

In any case the nuclear effectiveness of a control-rod material is its key property, and the number of control rods necessary to compensate all the excess reactivity available is a key question in the design of a reactor.

The major reactivity changes in power reactors usually result from temperature and density changes in the reactor materials, the effect of fission products, and the burnup of fissionable isotope. Characteristic magnitudes of these changes vary from reactor type to reactor type, and each reactor within a type has its own characteristic reactivity changes. The H_2O-moderated reactors usually experience large reactivity changes over their lifetimes, partly because of the large volume coefficient of thermal expansion of the moderator, H_2O, which may cause a reactivity change of several per cent between room temperature and reactor operating temperature. Some H_2O reactors experience total reactivity changes of 25 per cent or more over the lifetime of a fuel charge. Other reactors may experience considerably smaller variations, but it is doubtful that many enriched solid-fuel power reactors of present types will experience reactivity changes less than 6 or 7 per cent k_{eff}. If it is required that the normal control-rod installation be capable of making the reactor subcritical by, for example, 5 per cent under all conditions, then most enriched reactors will have control-rod installations worth some amount in the range from about 12 to 30 per cent k_{eff}, whereas the natural-uranium reactors, with less available reactivity, may fall below this range.

To translate the control-rod "holddown" requirement into a specification of the number of control rods is usually a difficult problem in

reactor physics. Reference 1 gives a comprehensive bibliography of control-rod calculation methods as well as a brief review of the present status of control-rod theory. (A brief review of control-rod physics was given in the June 1958 issue of *Power Reactor Technology*, Vol. 1, No. 3. Papers which have appeared on control-rod theory since the review in reference 1 are listed as references 2 to 8.) Calculations are sometimes rather badly in error, not so much because of any inadequacy of reactor theory but because many practical control-rod installations present complex physical situations which are not described well by the approximations the calculator is tempted to use. In commenting on the many pitfalls of control-rod calculation methods that employ currently popular approximations, reference 1 states: "However, using methods of this type, an experienced reactor physicist can usually compute worth of a given control system with an error of less than 50 per cent in spite of the fact that using an inappropriate recipe can easily result in errors of a factor of 2."

This comment should suffice as a warning that the following discussion of control-rod worth, which is based on even more simplified concepts, is useful only for illustrating the relation between reactor physics and the problems of control-rod materials.

The absorber control rod produces a reduction of reactivity by absorbing some of the neutrons which otherwise would cause fission. The reactivity change produced by the absorption of a given fraction of neutrons in a reactor depends upon where in the reactor they are absorbed and upon the energy at which they are absorbed. However, in "thermal" reactors most of the neutron absorption (both in control rods and in other materials) occurs in the thermal energy range, and in most power reactors the complement of control rods is sprinkled fairly uniformly over the reactor volume. Consequently some insight can be gained by considering the case of pure thermal-neutron-absorbing rods in a pure thermal-neutron reactor, with the rods distributed evenly over the reactor volume. In such a case, if the control rods absorb a fraction C of all neutrons absorbed in the reactor, then the reactivity worth of all the rods is very nearly equal to this fraction C. In this simplified case the estimation of total control-rod worth reduces to the estimation of the fractional absorption of thermal neutrons by a regular array of absorbers in a reactor core medium which can, to a reasonably good approximation, be considered infinite in extent.

Ordinarily, control rods are desired to be nearly "black" to thermal neutrons. A rod is black to neutrons if all neutrons that cross its surface boundary are absorbed. Approximate blackness to thermal neutrons requires two characteristics: (1) the thermal-neutron-absorption cross section must be many times larger than the scattering cross section, and (2) the absorber material must have a thickness of several absorption mean free paths.

Figure 7 illustrates the changes in neutron absorption when a black, thermally absorbing, infinite slab is inserted in a slot, previously empty, in an infinite thermally absorbing medium which is fed by a thermal-neutron source distributed uniformly over the volume of the medium. Prior to the insertion of the slab, the neutron flux has a uniform value, ϕ_0, over the medium, the value being determined by the source strength and by the macroscopic absorption cross section in the medium (see Fig. 7(a). When the black slab is present, it absorbs some of the neutrons, and its absorption is compensated by an equal reduction of absorption in the medium adjacent to the slab. The neutron flux near the slab drops in such a manner as to produce just the proper reduction of absorption in the medium. The resulting thermal-flux distribution, $\phi(x)$, is shown in Fig. 7(b). The fractional difference between ϕ_0 and $\phi(x)$ at any point x (shown as a shaded area in the figure) may be regarded as the fractional absorption of neutrons from that point by the slab. A little way from the slab surface the curve $\phi_0 - \phi(x)$ takes the form of an exponential, decaying as $e^{-x/L}$, where L is the diffusion length of thermal neutrons in the medium surrounding the slab. If this behavior persisted right up to the surface of the slab and if the thermal-neutron flux reached zero at the surface, the area of the shaded region in Fig. 7(a) would be just $\phi_0 L$ on each side of the slab. Thus each side of the slab would absorb a number of neutrons equal to the number produced by the source in that volume of the medium which lies within one diffusion length of the rod surface. Actually the exponential behavior does not persist to the slab surface, and the actual number of neutrons absorbed is somewhat less than this. The actual number can be computed

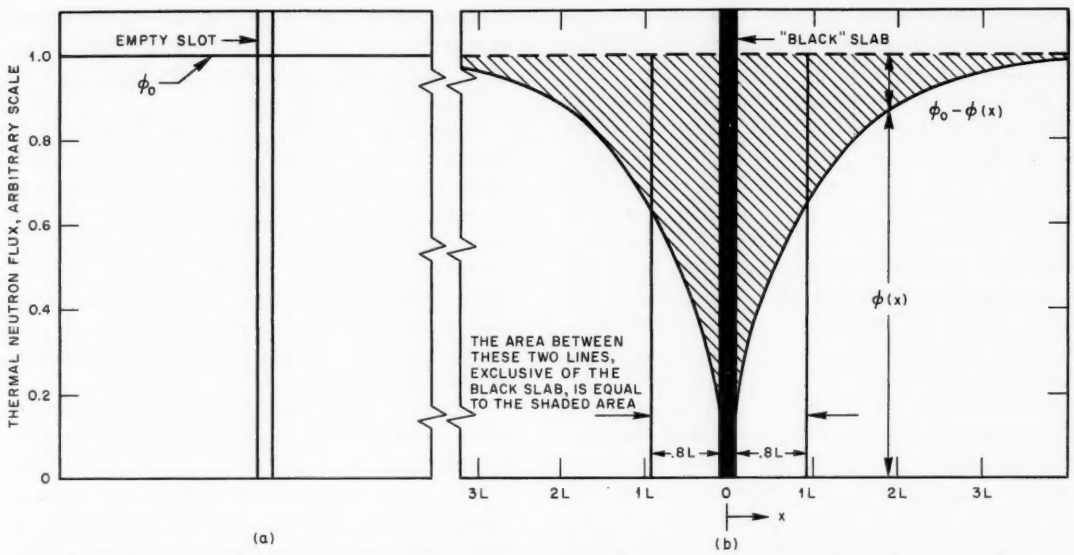

Figure 7 — Typical change of thermal-neutron flux distribution when a black thermal-neutron absorber (*b*) is inserted in an empty slot (*a*) in an infinite medium having a uniform source of thermal neutrons.

by taking into account the extrapolation length at the rod surface, which is determined by the transport mean free path in the surrounding medium. If, for example, the surrounding medium had the same thermal-neutron absorption and transport properties as the average core composition of the Experimental Boiling Water Reactor (EBWR),[9] the actual absorption in the slab would be equal to those neutrons produced within a distance of about $0.8L$ of the surface.

If other absorber shapes are considered, the results are rather similar in that the black absorber captures a quantity of neutrons equal to those produced within some characteristic fraction of a diffusion length. The exact value of the fraction will depend upon the shape of the absorber and upon the transport mean free path in the surrounding medium, but the variation in size of the fraction is unlikely to be large over the range of practical situations.

In the reactor core the situation is more complex than that considered above, because the thermal neutrons are not supplied by a uniformly distributed source but by the slowing down of fission neutrons which were generated at each point in the core at a rate proportional to the thermal-neutron flux at that point. Consequently the production of thermal neutrons near the control rod will be somewhat lower than in regions far from the rod. This is usually not an extremely large effect, however, because the diffusion of the neutrons during the slowing-down process makes the rate of production of thermal neutrons a good deal more uniform than the distribution of fission density.

The net effect of these considerations is that, for most control installations involving a fairly uniform lattice of control rods, a rough idea of the fractional absorption of thermal neutrons can be obtained by assuming that it is equal to the fractional core volume which lies within a distance αL of the control-rod surfaces. The α is a fraction which depends on rod shape and on the transport mean free path in the core; it will seldom be less than 0.5 or greater than 0.8; a value of 0.7 might be representative for most reactors.

This approach might be used to examine, for example, the control-rod absorption in the EBWR. In the region of the core occupied by control rods, each rod can be considered to be located at the center of a "cell" having a square cross section with a side length of $12\frac{3}{4}$ in. (see Fig. 8). The rod itself is a 10-in.-span cross. If one draws along the rod a line which is everywhere about $0.7L$ from the rod surface ($L = 1.8$ cm), the area enclosed between this line and the surface of the rod is 135 cm^2,

whereas the cross-sectional area of the cell, exclusive of the rod, is 1030 cm^2. This rough approximation indicates that the rod absorbs about 13 per cent of the neutrons, and the reactivity change corresponding to this fractional absorption should be 13 per cent k_{eff}. The quoted value of all the control rods in the EBWR is 12 to 14 per cent k_{eff}.* Little importance can be attached to the quantitative agreement or lack of it; for, actually, rods are not distributed uniformly over the volume of the EBWR, no allowance has been made for epithermal effects, the core composition is not really uniform up to the surface of the rod, and the rod is not inserted into a nonabsorbing slot, but actually displaces water. Nevertheless the estimate does illustrate some of the factors affecting control-rod worth. The method of estimating can be used to correlate roughly the rod requirements for specified reactivity worths in thermal reactors of widely varying properties. Table VI-1 compares the estimated worths with reported worths for four quite different reactors. The worth estimates are made simply by examining a cross section of the core with control rods inserted and taking the ratio of the area within $0.7L$ of the rod surfaces to the area of core external to rod surfaces.

The factors affecting rod reactivity worth can be further illustrated by considering the absorption by cylindrical rods in reactors of widely different compositions. Figure 9 illustrates the absorption by rods in a reactor having a low macroscopic absorption cross section in the core and a correspondingly long diffusion length. The medium to which the figure applies has average properties similar to those in the core of the original Calder Hall reactor.[13] The moderator is graphite, and the diffusion length in the core is 19.8 cm. If a black rod 2 in. in diameter is installed in such a medium, it absorbs a number of thermal neutrons equal to those formed within a distance of about 13.4 cm of the rod surface. If the rod diameter is increased to 3 in., the effective distance from which neutrons are drawn increases only slightly, to 14.4 cm. In considering these diagrams, three points are obvious:

1. The volume of the core from which neutrons are drawn by the rod is large compared with the volume of the rod. In this respect the rod is quite effective in influencing reactivity, and only a relatively small fraction of the core volume would have to be occupied by control rods in order to achieve a high degree of control-rod worth.

2. The number of neutrons absorbed by the rod does not increase in proportion to the size of the rod. The reason for this is obvious. Because of this effect, most low-cross-section reactors employ rods which are quite small relative to the size of the reactor.

3. Evidently it would not be profitable to install control rods very close together in a low-cross-section reactor, for then adjacent rods would have zones of effective absorption which would overlap and the total number of neutrons absorbed per rod would decrease. Actually the space necessary to avoid important mutual "shadowing" of the rods is somewhat greater than the distance indicated by the circles surrounding the rods in the figure. It would be unusual to find rods closer together than two or three diffusion lengths in any reactor.

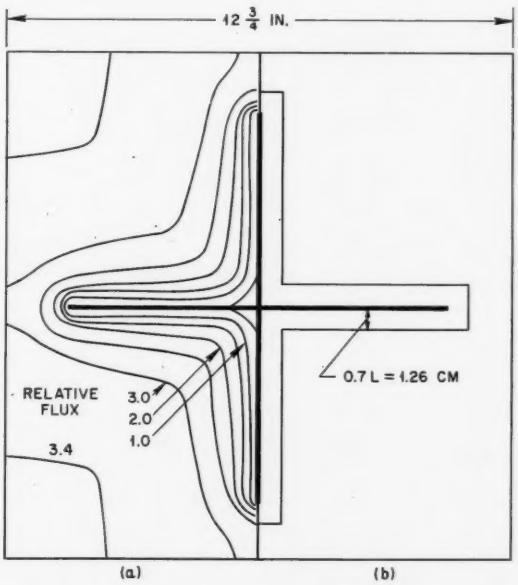

Figure 8—Typical control-rod cell in EBWR. (*a*) Contours of constant thermal-neutron flux (adapted from reference 9). (*b*) Approximate area of effective absorption.

* Reference 9. The worth listed in the reference (calculated) is given as the value of k_{eff} which the rods will hold just critical. The rod worth used here is $(k_{eff} - 1)/k_{eff}$.

Table VI-1 REACTIVITY WORTH OF CONTROL-ROD INSTALLATIONS IN SEVERAL REACTORS

Core diam., ft	Control-rod shape	Control-rod size	No. of control rods	Core diffusion length, cm	A (cross-sectional area of core), cm^2	B (cross-sectional area within distance $0.7L$ of rod surfaces), cm^2	Estimated rod worth, B/A	Reported worth of control rods ($\Delta k_{eff}/k_{eff}$)
EBWR[9] (Experimental Boiling Water Reactor), Boiling H_2O Type								
4	Cross	10-in. span	9	1.8	11,700	1,240	0.11*	0.12–0.14†
Adam[10] (Swedish Reactor for Heating), Natural Uranium Oxide–D_2O Type								
11.1	Cylindrical	90-mm diam.	32	14.8	91,000	20,200	0.22	0.15
SRE[11] (Sodium Reactor Experiment), Sodium Graphite Type								
6	Cylindrical	2.484-in. diam.	8	12.9	26,300	3,480	0.13	0.135
Calder Hall,[12] Natural Uranium–Graphite Type								
31	Cylindrical	1.75-in. diam. in 3.25-in. channel	48	19.8‡	703,000	36,500	0.052	0.068

* This value differs from the value estimated in the text because there is some core area which is not included in the nine "typical cells" surrounding the control rods.

† In reference 9 the (calculated) worths of the rods are given as the value of k_{eff} which the rods will hold just critical. To get the rod worth, as used here, take $k_{eff} - 1/k_{eff}$.

‡ Intermediate core region. See reference 13.

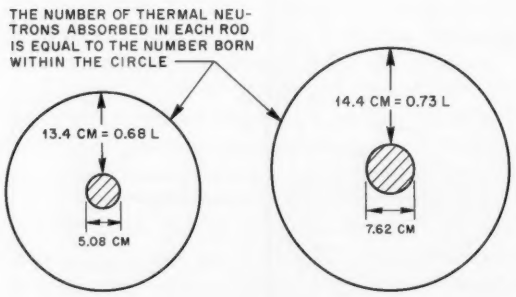

Figure 9—Relative numbers of thermal neutrons absorbed by 2- and 3-in. cylindrical black rods when placed in identical infinite media supplied by uniformly distributed sources of equal strength. Neutron transport and absorption properties are the same as in region B of Calder Hall, homogenized.

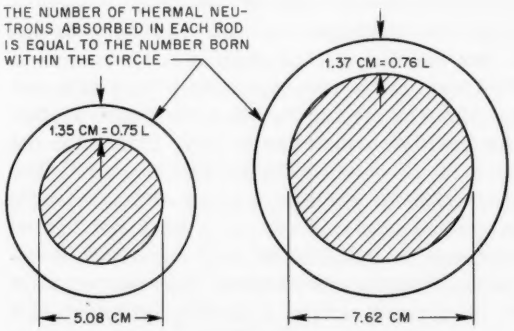

Figure 10—Relative numbers of thermal neutrons absorbed by 2- and 3-in. cylindrical black rods when placed in identical infinite media supplied by uniformly distributed sources of equal strength. Neutron transport and absorption properties are the same as in a uniform, cold EBWR core.[2]

Figure 10, which is necessarily drawn to a quite different scale, illustrates the absorptions by the same two rods if they were installed in a highly absorbing reactor core. The actual medium considered has the average properties of the cold EBWR core.[9] The main characteristics, which are as follows, are quite different than in the previous case:

1. The volume of core from which neutrons are drawn by the rod is not large relative to the rod itself.
2. The increase of absorption with rod size is more nearly proportional to the increase in surface area of the rod.
3. Since the area of effective absorption of the rods is small, rods may be installed relatively close together without important mutual shadowing.

Figure 10 illustrates some of the difficulties of devising efficient rod installations for water-moderated reactors. Quite evidently the thermally absorbing cylindrical rod is an inefficient means of compensating excess reactivity, for it occupies a rather large amount of core volume per neutron absorbed. Furthermore, when the rod is withdrawn from the core, the empty channel which it leaves poses a problem. If the channel is allowed to fill with water, the fast neutrons slowed down in the water will produce a peak in the thermal-neutron flux which will tend to overheat the adjacent fuel elements; and, in addition, the thermal-neutron absorption of the water, enhanced by the peaking of the thermal flux, may reduce the net reactivity gain resulting from withdrawal of the control rod. These are the reasons that rod shapes giving high surface-to-volume ratios, such as crosses, are used in water-moderated reactors. In the water reactor the diffusion length is so small that the rod surface must be brought into proximity to a substantial fraction of the uranium in the core in order to absorb a substantial fraction of the neutrons. Even when such extended surface rods are used, it is frequently difficult to arrive at a mechanical design of the core which will place this surface adjacent to a sufficiently large fraction of the uranium. For that reason it is desirable in water reactors to increase the basic nuclear effectiveness of the control-rod material. Once the macroscopic absorption cross section of the material has been made sufficiently high that the rod is black to thermal neutrons, further increases do not cause additional absorption of thermal neutrons. The only remaining way that the effectiveness of the material can be increased is by causing it to absorb the neutrons whose energies are higher than thermal.

It is difficult to absorb a large fraction of the epithermal neutrons, and there is no great incentive to absorb epithermal neutrons unless the number of epithermal neutrons normally present in the reactor core is important relative to the number of thermal neutrons. Ordinarily those reactors which have highly absorbing cores, notably the water (H_2O) reactors, will have high ratios of epithermal-to-thermal neutron flux. Consequently the use of epithermal control-rod absorption in water reactors is favored for two reasons: it is needed to attain adequate rod worth; epithermal absorption in such reactors can be reasonably effective in reducing reactivity.

There is a scheme which will make a control rod effectively an epithermal absorber even if the absorbing material of the rod has a high cross section only in the thermal energy range. This scheme is to use a relatively thick rod and to incorporate effective moderator in the rod so that some of the neutrons which enter the rod as epithermal neutrons will be slowed down to thermal energy within the rod and will be absorbed. This scheme can be illustrated by Fig. 10 if it is assumed that the rod consists of a cylindrical shell of absorbing material, just thick enough to be thermally black, and that the volume inside the shell is allowed to fill with water. Reasonably large control rods of this type can be very effective, for the pure water inside the shell is even more effective in thermalizing neutrons than the mixture of water and other materials which makes up the core proper. The scheme poses the difficulty of the water-filled channel which exists when the rod is withdrawn. This difficulty can be circumvented by providing a follower for the rod made of fuel elements similar to those in the rest of the core. These elements must, of course, be adequately cooled, and this may cause engineering complications. However, the rod type has been used in the Materials Testing Reactor (MTR) and the Army Package Power Reactor (APPR).* It is sometimes referred to as the neutron rectifier control rod.

* It is also used in the Argonne conceptual design of a prototype for an advanced boiling reactor, reviewed elsewhere in this issue.

If the scheme of incorporating moderator in the control rod is not used, absorption of epithermal neutrons can still be accomplished by the use of control-rod materials which have high epithermal absorption cross sections as well as high thermal absorption cross sections. Most materials considered for control rods have sufficiently high thermal cross sections that a reasonable thickness of the material is black or nearly black to thermal neutrons. Consequently the differences in effectiveness which different materials exhibit are principally due to differences in their epithermal cross sections, and these differences will show up with greater or lesser importance accordingly as the ratio of epithermal-to-thermal neutron flux in the reactor is higher or lower.

Effectiveness of Control-rod Materials

The thermal absorption cross section of a material determines how thick a layer of the material must be used in order to be black to thermal neutrons. For practical purposes a layer of thickness that is two absorption mean free paths or greater can be considered nearly black. Stevens[14] has shown that an absorbing layer of thickness equal to two absorption mean free paths absorbs something like 97 per cent as many neutrons as a completely black surface. Table VI-2 lists a number of elements and isotopes with high thermal-neutron-absorption cross sections and gives for each the surface density, or number of grams of absorber per

Table VI-2 AMOUNTS OF VARIOUS ABSORBERS REQUIRED FOR NOMINAL BLACKNESS TO THERMAL NEUTRONS[14]

(Two Absorption Mean Free Paths)

Element or nuclide	Average thermal cross section, barns	Abundance of important isotopes, %	Surface density for blackness, g/cm^2	Density, g/cm^3	Thickness for blackness, cm
Li	62		0.362	0.53	0.68
Li^6	818	7.52	0.024	0.53	0.045
B	651		0.054	2.3	0.023
B^{10}	3,470	18.8	0.0093	2.3	0.004
Rh	130		2.56	12.5	0.20
Ag	54		6.47	10.5	0.62
Ag^{107}	26	51.4			
Ag^{109}	71	48.6			
Cd	2,210		0.165	8.6	0.0192
Cd^{113}	18,000	12.3			
In	165		2.26	7.3	0.310
Sm	4,760		0.100	7.2*	0.0139
Sm^{149}	57,200	13.8			
Eu	3,980		0.128	7.3*	0.0175
Eu^{151}	7,800	47.8			
Gd	39,800		0.0128	7.6*	0.0017
Gd^{155}	60,000	14.7			
Gd^{157}	139,000	15.7			
Dy	950		0.55	8.1*	0.068
Dy^{164}	2,340	28.2			
Er	144		3.78	8.6*	0.44
Lu	96		6.05	?	~0.67
Lu^{176}	3,120	2.6			
Hf	91		6.38	13.4	0.471
Hf^{177}	320	18.4			
Re	73		8.28	20	0.414
Ir	372		1.68	22.4	0.075
Ir^{191}	820	38.5			
Ir^{193}	104	61.5			
Au	85		7.52	19.3	0.392
Hg	330		1.97	14.22	0.138
Hg^{199}	2,160	16.8			

* X-ray density for oxide.

square centimeter of surface, required to meet the blackness criterion of two absorption mean free paths.

It must be remembered that a further criterion for blackness is that the absorption cross section of the material be much larger than the scattering cross section. Thus large thicknesses of moderately absorbing materials do not make very effective control rods, and the effectiveness of a highly absorbing material may be impaired if it is diluted too strongly with a material which is a good scatterer. Stevens[14] cites the case of a B^{10} slab of thickness equal to two absorption mean free paths. This slab would fail to capture about 6 per cent of the neutrons crossing its surface because of its slight transparency. Such a slab would, of course, be quite thin. If it were diluted by steel sufficiently to form a slab 0.20 in. thick, the fraction of neutrons which avoided capture would increase to 8.3 per cent; some of these would pass through the slab, whereas others would be scattered out of the slab before absorption. This degree of dilution increases the scattering cross section to 20 per cent of the macroscopic absorption cross section. It appears that scattering cross sections of 10 to 20 per cent of the absorption cross section are tolerable, provided the absorbing and scattering nuclei are intimately mixed so that the competition between scattering and absorption is in proportion to the macroscopic absorption and scattering cross sections. If the scattering and absorbing materials are segregated, the scattering loss of neutrons may be considerably greater. The worst form of segregation is, of course, that in which the scattering material covers the surface of the absorbing material, as when the absorber is encased in a jacket or cladding of low absorption cross section. Stevens shows that a 0.040-in. jacket of steel reflects about 8 per cent of the neutrons incident upon the jacket, whereas a 0.10-in. thickness of steel reflects about 17 per cent. The actual reduction of rod effectiveness by the scattering effect of the jacket will be less than these percentages of reflection and will depend upon the surrounding medium, for some of the reflected neutrons will diffuse back into the rod. Further, any material which lies between the control rod and the fissionable material in the reactor core can produce a somewhat similar effect. If the material between the rod surface and the fissionable material is a moderator, then the net effect on rod effectiveness is the difference between the effect of the diffusion barrier which the material represents and the effect of additional neutron slowing down in the vicinity of the rod surface.

Since the contribution of epithermal-neutron absorption to control-rod worth depends upon the neutron energy spectrum of the reactor—principally upon the ratio of the epithermal-to-thermal neutron flux—it is difficult to generalize upon the desirable characteristics of epithermal absorbers other than to say that the best materials will be those having high cross sections over large ranges of the epithermal energy region. The three most widely used control-rod absorbers (boron, cadmium, and hafnium) illustrate the possible range of epithermal absorption behavior. Figure 11, reproduced from the data of Stevens,[14] shows the fractional absorptions by slabs containing these materials as functions of neutron energy. The figure gives the fraction of neutrons absorbed, of those striking the slab surface, for four different slabs: a $1/16$-in.-thick slab of cadmium, a 0.200-in.-thick slab of hafnium, a 0.200-in.-thick slab of steel containing 1.0 wt.% B^{10}, and a 0.200-in.-thick slab of steel containing 0.15 wt.% B^{10}. The latter case would correspond to about 0.9 per cent natural boron in the steel. Cadmium is the classic example of the thermal absorber. The $1/16$-in. thickness is black to neutrons up to an energy of about 0.4 ev. At this energy its cross section is decreasing very rapidly with neutron energy, and an increase in thickness of the slab is not very effective in increasing its neutron absorption: a doubling of the slab thickness would extend the range of blackness up to about 0.5 ev.

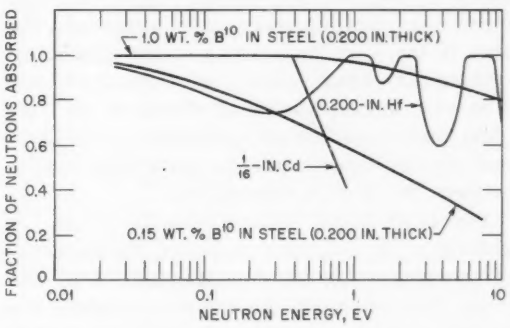

Figure 11—Fraction of neutrons absorbed by various slabs.[14]

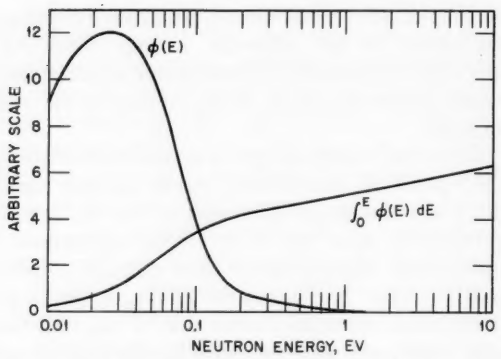

Figure 12—Neutron-flux spectrum in H_2O containing 2.9 barns of $1/v$ absorber per H atom.[15]

Since hafnium is not a very strong thermal absorber, the 0.2-in.-thick slab is not really black in the thermal energy region, although most of the thermal neutrons are absorbed. The slab is black in the vicinity of the absorption resonances which occur at 1.10, 2.38, and 7.80 ev. An increase in thickness of the hafnium would increase its absorption in the thermal energy range and in the epithermal ranges between the neutron resonances.

Boron-10 is the classic example of the $1/v$ absorber. An increase in either the thickness of the slab or in the concentration of B^{10} extends the range of blackness to higher and higher neutron energies. The 0.15 per cent B^{10} slab is about equivalent to the hafnium slab for neutrons of energies up to about 0.3 ev; at higher energies, it falls far below the hafnium curve. The 1 per cent B^{10} slab, however, is black up to about 0.7 ev and is about as good as the hafnium slab at higher energies.

Most epithermal absorbers are of the resonance type, like hafnium. Since these materials characteristically absorb in discrete energy regions, one of the methods of producing materials with high epithermal absorption efficiency is to mix absorbers in such a way that the resonances of one fall into the energy regions between the resonances of another. The mixture of cadmium, silver, and indium is one such combination of this type. Mixtures of the rare-earth elements have also been considered.

The importance of epithermal absorption in H_2O reactors can be inferred from Fig. 12, which shows the energy distribution of neutron flux in a typical water-moderated medium, after the calculations of Amster.[15] This flux spectrum, which was computed for water containing 2.9 barns of absorption cross section per hydrogen atom (boron absorption), is much like the spectrum that would be expected in a water-moderated reactor having an H_2O/UO_2 volume ratio of 2.0, with the uranium enriched to 2 per cent U^{235}. Since the importance of the epithermal energy range is distorted by the logarithmic energy scale, a better idea of the importance of the epithermal neutrons can be had from the integral, $\int \phi(E)\, dE$, which is also plotted in Fig. 12. [$\phi(E)$ and $\int \phi(E)\, dE$ are plotted to different arbitrary scales.] It is evident that a substantial portion of the neutron total flux lies above the cadmium cutoff at 0.4 ev.

The neutron energy spectrum and the absorption-cross-section curve are not the only quantities involved in determining the epithermal effectiveness of an absorbing material. Just as, in the case of purely thermal absorption, the control rod must compete against the absorption of the surrounding medium, so, in the epithermal case, the control rod must compete both against whatever epithermal absorption occurs in the surrounding medium and against

Table VI-3 CONTROL-ROD EFFECTIVENESS* FOR VARIOUS MATERIALS[1]

Material	Absorptiveness, $\Sigma_a t$ †	Effectiveness relative to hafnium
3.0 wt.% B^{10} in stainless steel (dispersion of minus 100-mesh particles of 90 per cent enriched boron)	27.2	1.12
Hafnium	2.40	1.00
0.97 wt.% B^{10} in stainless steel (alloy)	9.3	0.98
15 wt.% Eu_2O_3 in stainless steel (dispersion)	8.7	0.96
Indium	3.68	0.93
Silver	1.85	0.88
Cadmium	77.5	0.80
8.7 wt.% gadolinium in titanium	31.1	0.79
Tantalum	0.60	0.71
2.7 wt.% Sm_2O_3 in stainless steel (dispersion)	3.20	0.71
Haynes-25 alloy	0.96	0.68
Titanium	0.16	0.24
Zircaloy-2		0.05
2S aluminum		0.02

* Determined by R. R. Eggleston and a Critical Experiment Group of Bettis Laboratory on samples 2 by 2 by 0.2 in.

† Macroscopic thermal absorption cross section times thickness.

Table VI-4 MEASURED RELATIVE REACTIVITY WORTHS OF VARIOUS MATERIALS IN AN H_2O-MODERATED ASSEMBLY[18]

Material	Surface density, g/cm²	Thickness, in.	Relative worth,* bare	Relative worth,* Cd covered	Equivalent boron surface density, g/cm²	
					Bare	Cd covered
Cadmium	0.022	0.001	0.494	0.931	0.0090 ± 0.0005	
(Cd)	0.050	0.002	0.648	0.931	0.0192 ± 0.0010	
	0.101	0.005	0.728	0.928	0.0284 ± 0.0015	
	0.555	0.025	0.811	0.941	0.0440 ± 0.0026	0.0060 ± 0.0051
	1.104	0.051	0.838	0.948	0.0510 ± 0.0032	0.0100 ± 0.0053
	2.142	0.098	0.864	0.967	0.0593 ± 0.0040	0.0200 ± 0.0056
	4.389	0.201		1.000		0.0370 ± 0.0063
	6.585	0.305	0.928	1.020	0.0890 ± 0.0066	0.0500 ± 0.0071
Cobalt	5.601	0.252	0.855	1.046	0.0563 ± 0.0038	0.0810 ± 0.0105
(Co)	3.418	0.154	0.759	1.011	0.0345 ± 0.0018	0.0510 ± 0.0072
	2.187	0.098	0.663	0.988	0.0206 ± 0.0010	0.0323 ± 0.0061
Dysprosium	3.047	0.300	1.039	1.158	0.2050 ± 0.0190	0.2400 ± 0.0250
oxide	1.753	0.174	0.989	1.119	0.1380 ± 0.0120	0.1660 ± 0.0185
(Dy_2O_3)	0.505	0.050	0.801	1.034	0.0420 ± 0.0024	0.0710 ± 0.0087
Erbium	3.405	0.299	0.920	1.077	0.0840 ± 0.0061	0.1060 ± 0.0130
oxide	2.009	0.175	0.839	1.026	0.0520 ± 0.0033	0.0650 ± 0.0083
(Er_2O_3)	0.558	0.049	0.570	0.979	0.0137 ± 0.0007	0.0290 ± 0.0060
Europium	3.375	0.299	1.253	1.332	1.0900 ± 0.0710	1.0000 ± 0.1150
oxide	1.972	0.174	1.197	1.265	0.6850 ± 0.0570	0.6100 ± 0.0600
(Eu_2O_3)	0.561	0.050	1.032	1.130	0.1940 ± 0.0180	0.1850 ± 0.0200
Gadolinium	3.388	0.301	1.042	1.135	0.2100 ± 0.0190	0.1950 ± 0.0210
oxide	1.989	0.177	0.984	1.082	0.1330 ± 0.0110	0.1180 ± 0.0140
(Gd_2O_3)	0.567	0.050	0.885	1.011	0.0680 ± 0.0047	0.0510 ± 0.0072
Gold	14.531	0.297	1.038	1.164	0.2040 ± 0.0190	0.2540 ± 0.0260
(Au)	9.606	0.196	0.987	1.127	0.1360 ± 0.0110	0.1800 ± 0.0200
	4.926	0.101	0.868	1.076	0.0610 ± 0.0041	0.1100 ± 0.0135
	2.518	0.051	0.719	1.032	0.0273 ± 0.0014	0.0700 ± 0.0088
	1.318	0.027	0.564	1.004	0.0127 ± 0.0007	0.0460 ± 0.0068
Hafnium	0.175	0.276	1.106	1.217	0.3530 ± 0.0360	0.4050 ± 0.0390
(Hf)	6.833	0.206	1.051	1.189	0.2220 ± 0.0200	0.3200 ± 0.0310
	3.422	0.103	0.920	1.130	0.0840 ± 0.0062	0.1890 ± 0.0205
	1.476	0.045	0.726	1.072	0.0284 ± 0.0015	0.1050 ± 0.0130
	0.856	0.025	0.572	1.039	0.0133 ± 0.0007	0.0760 ± 0.0096
Holmium	3.365	0.302	0.745	1.087	0.0314 ± 0.0016	0.1280 ± 0.0150
oxide	1.955	0.176	0.602	1.038	0.0152 ± 0.0008	0.0740 ± 0.0094
(Ho_2O_3)	0.564	0.051	0.302	0.983	0.0036 ± 0.0003	0.0310 ± 0.0059
Indium	5.554	0.301	1.036	1.137	0.2000 ± 0.0190	0.2000 ± 0.0215
(In)	3.697	0.201	0.998	1.105	0.1470 ± 0.0120	0.1470 ± 0.0167
	1.858	0.100	0.908	1.058	0.0785 ± 0.0057	0.0940 ± 0.0120
	0.928	0.050	0.785	1.029	0.0386 ± 0.0021	0.0660 ± 0.0086
	0.468	0.025	0.632	1.003	0.0176 ± 0.0009	0.0450 ± 0.0068
Lutetium	2.244	0.175	0.772	1.059	0.0361 ± 0.0019	0.0930 ± 0.0120
oxide	1.605	0.125	0.693	1.041	0.0241 ± 0.0012	0.0780 ± 0.0099
(Lu_2O_3)	0.638	0.050	0.465	0.992	0.0078 ± 0.0004	0.0360 ± 0.0062
Samarium	3.357	0.302	1.063	1.155	0.2490 ± 0.0240	0.2340 ± 0.0240
oxide	1.966	0.175	1.018	1.113	0.1730 ± 0.0150	0.1580 ± 0.0173
(Sm_2O_3)	0.558	0.050	0.896	1.008	0.0730 ± 0.0052	0.0500 ± 0.0070
Silver	7.970	0.299	1.021	1.172	0.1760 ± 0.0155	0.2710 ± 0.0270
(Ag)	5.226	0.196	0.944	1.123	0.0995 ± 0.0076	0.1700 ± 0.0190
	2.746	0.103	0.798	1.065	0.0414 ± 0.0023	0.0990 ± 0.0125
	1.376	0.052	0.617	1.022	0.0167 ± 0.0009	0.0600 ± 0.0080
Tantalum	12.733	0.302	0.855	1.166	0.0680 ± 0.0047	0.2610 ± 0.0265
(Ta)	8.511	0.202	0.775	1.124	0.0370 ± 0.0020	0.1740 ± 0.0190
	4.214	0.100	0.572	1.059	0.0133 ± 0.0007	0.0980 ± 0.0120

(Table Continues)

Table VI-4 (Continued)

Material	Surface density, g/cm²	Thickness, in.	Relative worth,* bare	Relative worth,* Cd covered	Equivalent boron surface density, g/cm²	
					Bare	Cd covered
Terbium	2.287	0.175	0.829	1.067	0.0482 ± 0.0030	0.1010 ± 0.0135
oxide	1.624	0.125	0.765	1.040	0.0347 ± 0.0019	0.0730 ± 0.0090
(Tb_4O_7)						
Thulium	2.089	0.175	0.735	1.056	0.0292 ± 0.0015	0.0890 ± 0.0110
oxide	1.490	0.125	0.649	1.037	0.0193 ± 0.0010	0.0730 ± 0.0090
(Tm_2O_3)	0.580	0.049	0.418	0.992	0.0064 ± 0.0004	0.0370 ± 0.0063
Tungsten	9.900	0.204	0.693	1.077	0.0257 ± 0.0013	0.1120 ± 0.0136
(W)	9.581	0.197	0.675	1.053	0.0237 ± 0.0012	0.0890 ± 0.0110
Ytterbium	3.584	0.300	0.579	1.028	0.0138 ± 0.0007	0.0670 ± 0.0084
oxide	2.100	0.175	0.440	0.994	0.0070 ± 0.0004	0.0345 ± 0.0061
(Yb_2O_3)	0.581	0.050	0.194	0.957	0.0017 ± 0.0002	0.0150 ± 0.0054
Boron glass	0.0478†	0.101	0.8144	1.0051		
	0.1575	0.104	1.0062	1.1161		
	0.0335	0.152	0.7503	0.9903		
	0.0880	0.200	0.9282	1.0560		
	0.3026	0.206	1.0867	1.1806		
	0.1206	0.275	0.9728	1.0882		
	0.4241	0.290	1.1326	1.2232		
	0.0664	0.302	0.8756	1.0393		

* Edge corrected.
† Surface densities of boron.

the moderating neutron collisions which tend to slow the neutrons down past the control-rod absorption resonances. These effects can, of course, be evaluated theoretically, but experimental results are more convenient for surveying the approximate ranges of improvement of effectiveness that can be expected from the use of good epithermal absorbers.

Table VI-3 lists measured effectiveness for various control-rod materials relative to a 0.20-in.-thick hafnium sheet, as reported in reference 1. The measurements were made with small samples, 2 by 2 by 0.2 in. The spectrum in which the measurements were made is not specified, but it can probably be assumed that it is a typical water-moderated spectrum and that the relative values of effectiveness would be roughly the same for many water-moderated reactors.

Table VI-4 lists the results of relative worth measurements made in the Critical Experiment Facility at Vallecitos Atomic Laboratory.[16] The materials were used in the form of 3- by 6-in. plates having various thicknesses as recorded in the table. The critical assembly was H_2O moderated; it was fueled with UO_2 pellets, 0.491 in. in diameter, in 0.562-in.-O.D. aluminum tubes of 30-mil wall thickness. The fuel rods were located on a uniform-square lattice, with 0.8-in. spacing between centers; the enrichment was 1.6 wt.% U^{235}. Measurements were made of the reactivity worth of each absorbing plate, bare, and of each plate plus a constant cadmium box enclosing it. The relative worth is expressed, arbitrarily, as the ratio of the reactivity worth of the arrangement in question to the reactivity worth of a 0.201-in.-thick cadmium plate in the cadmium box. The results have been edge corrected to reduce the edge effect to that which would characterize a plate of zero thickness. The equivalent boron surface density is that surface density of natural boron which, if substituted for the sample (bare or in the cadmium box as the case might be), would yield the same reactivity worth. The epithermal effectivenesses of the materials are illustrated by their cadmium-covered relative worths and by the cadmium-covered equivalent boron surface densities.

Other measurements on rare-earth oxides and mixtures of rare-earth oxides may be found in reference 17.

Burnup of Control-rod Materials

Some control rods spend little time in the operating reactor; they may be used simply to

provide extra shutdown capacity or to compensate such reactivity excesses as the inverse temperature defect or the increase due to the decay of equilibrium xenon, which do not remain long in the operating reactor. Other rods are exposed to the reactor flux over long periods during their lifetime. They may be rods which compensate the excess reactivity provided for fuel burnup or for transient xenon override. These rods may suffer from radiation damage or from burnup of the absorbing isotope. Radiation damage is usually important only in those materials (boron and lithium) which undergo (n, α) reactions. The effects are discussed for boron in a later section. When appreciable burnup of the absorbing isotope is anticipated, extra material, beyond that needed for blackness, must be incorporated in the rod.

Whether deterioration of the rod is due to radiation damage or to burnup, its extent is determined by the number of neutron absorptions in the rod. A rough estimate of the number of absorptions can be made by recalling that the reactivity worth of the rod, at a position of average importance in the reactor, is just equal to the fraction of total neutron absorptions in the reactor which take place in the rod. For criticality reasons most of the absorptions in the reactor must take place in U^{235} or other fissionable isotopes. In almost all cases the fractional absorption in the fissionable isotopes will lie in the range 0.6 to 0.9. The destruction of 1 gram-atom of U^{235} yields a thermal energy output of about 186 Mwd. Consequently an estimate of the average number of gram-atoms of control-rod absorber destroyed is given by

$$\text{Gram-atoms of absorbing isotope destroyed} = \frac{\rho}{0.6} \times \frac{E}{186} = \frac{\rho E}{112}$$

where ρ is the worth of the control rod or control rods in question, E is the energy, in thermal megawatt-days, which the reactor produces while the rod is inserted, and the most pessimistic value of the fractional absorption in fissionable isotope has been used. Thus, if a B^{10} rod installed in a position of average importance in a reactor of 100 Mw(t) output is worth 0.25 per cent k_{eff}, the burnup of boron in the rod over a period of 10 years of equivalent full power is approximately

$$\text{Burnup} = \frac{(0.0025)\ (100)\ (10)\ (365)}{112}$$

$$= 8.2 \text{ gram-atoms}$$

or about 82 g of B^{10}. It must, of course, be remembered that a rod in a position of lesser importance will absorb more neutrons for a given rod worth. Further, the burnup in the rod will be distributed along the length of the rod in proportion to the power distribution in the reactor along the rod axis. If the rod is only partially inserted, there will be a further concentration of absorption near its tip. The latter effect may be very large if a number of strong rods are moved in unison as a bank.

When appreciable burnup in the rods must be anticipated, there is little benefit in the use of absorbing materials having extremely high microscopic thermal absorption cross sections; for, although quite small quantities of such materials may suffice for blackness, the burnup requirement may set the specification for the amount of absorber incorporated in the rod. If neutron absorption in the absorber yields a stable or long-half-life isotope which itself has a high absorption cross section, then, of course, the burnup requirement is reduced. Europium, for example, has two isotopes (151 and 153), both of which yield high-cross-section isotopes upon neutron absorption.

Other Requirements of Control-rod Materials

Of the remaining requirements for control-rod materials, the two most important, other than the obvious mechanical requirements, are compatibility with the environment within the reactor and susceptibility to adequate cooling. Little can be said in a general way on the first of these requirements; for a given reactor, the characteristics of the materials being considered must be checked in detail against the conditions imposed by the environment. The two materials that have been used fairly widely without protective claddings are hafnium and borated stainless steel. Both are compatible with water at the temperatures characteristic of boiling- and pressurized-water reactors. It is, of course, quite feasible to use materials which must be jacketed against the environment. However, jacketed rods sometimes in-

troduce problems in addition to that of maintaining the integrity of the jacket. They may increase the mechanical engineering problems, decrease somewhat the absorption effectiveness, and increase the problems of cooling. In H_2O reactors, where there is a strong desire to keep control-rod sections as thin as possible, a jacket may add an undesirable extra thickness.

There are three possible sources of control-rod heating: the energy produced by the neutron-absorption reaction in the rod, the energy deposited by fission gamma radiation from the surrounding fuel, and the energy deposited by gamma radiation generated in the inelastic collisions of neutrons. Of these sources, the latter is of the least consequence and the first is usually the most important, both because it usually produces the highest average energy deposition in the rod and because it may be more highly concentrated, particularly at the ends of partially inserted control rods. In (n,α) absorbers (boron) practically all of the energy of the absorption reaction is deposited in the control rod. In (n,γ) absorbers an appreciable fraction of the gamma-radiation energy escapes from the control rod. In either case the heat-generation rate in control rods in high-power-density H_2O-moderated reactors can be quite high. Adequate coolant flow must be provided for the rod, and, in the case of jacketed absorbers, adequate provision must be made for heat transfer from the absorber to the jacket.

Although it is important to assess the problem of control-rod heating adequately in high-power-density reactors and to provide for adequate cooling, it is also important to recognize that in some lower power-density applications the problem of control-rod cooling may be a trivial one. Whenever the problem of control-rod heating is not great, the incentive for control materials compatible with the reactor-core environment is considerably reduced, and it may be possible to produce adequate control rods quite inexpensively by simply canning an absorbing material in an appropriate jacket without great regard for the problems of heat removal.

Boron Steel[1]

The boron–stainless steel alloys are relatively cheap control materials which have been used for control rods in a number of applications, including applications in high-temperature water. The boron content used usually lies in the range between 1 and 2 wt.%; concentrations much above 2 per cent do not presently appear to be attractive for metallurgical reasons. The absorption mean free path of a 2 per cent alloy of natural boron is about 0.15 cm. Since the natural element contains about 18.8 per cent B^{10} (the highly absorbing isotope), this absorption mean free path can be reduced by about a factor of 5, at considerable expense, by the use of highly enriched B^{10}. The main disadvantages of boron–stainless steel as a control-rod material are the relatively low percentage of boron which can be incorporated in the alloy and the alloy's susceptibility to radiation damage which manifests itself as embrittlement of the alloy and some growth.

The alloys may be fabricated by conventional means. Austenitic alloys containing up to 3.2 wt.% boron have been cast by normal induction-melting methods in vacuum or inert atmospheres; alloy ingots containing up to 2.4 wt.% boron have been fabricated into strip by forging and rolling at temperatures near 1160°C; alloys containing up to 2.2 wt.% boron have been extruded after heating to 1150°C. Both the sigma and the Heliarc welding techniques are applicable to the alloys, the sigma welding being preferred.

The addition of boron to a stainless-steel alloy causes an increase in tensile strength and decreases in the ductility and impact strength. Neutron irradiation of the alloy causes further changes of the same kind. (Some irradiation tests on boron–stainless steel were reviewed in the September 1959 issue of *Power Reactor Technology*, Vol. 2, No. 4.) Boron-10, when it absorbs a neutron, disintegrates into Li^7 and an alpha particle. These products occupy more space than the original boron atom, and growth of the alloy occurs after sufficient irradiation. It is stated, however, that no growth appears to take place until nearly 0.7 per cent of the total atoms in the alloy have been transmuted by the (n,α) reaction and that, after the irradiation has reached this point, growth is rapid and proceeds at an increasing rate. Metallographic examination of boron–stainless steel alloys after irradiation has shown voids in the vicinity of boride particles; these voids were attributed to the helium gas (alpha particles) generated in the nuclear reaction. Other experiments which

Table VI-5 TENSILE-TEST RESULTS ON STAINLESS STEEL ALLOYED WITH NATURAL BORON (B^N) AND ENRICHED BORON (B^{10})[1]

Boron content, wt.%	Test temp., °C	Nonirradiated 0.2% yield strength, psi	Nonirradiated Ultimate tensile strength, psi	Nonirradiated Elongation, %	Irradiated 0.2% yield strength, psi	Irradiated Ultimate tensile strength, psi	Irradiated Elongation, %	Thermal nvt
0.0 (304 S.S.)	23	37,500	90,000	50.2	82,000	104,800		2.7×10^{20}
0.5 B^{10}	23	29,500	81,500	29.6	98,800	121,600	2.4	2.7×10^{20}
0.5 B^{10}	315	23,200	61,900	19.8	82,600	92,500	0.5	6.7×10^{20}
0.85 B^{10}	23	32,950	85,000	21.1	111,800	122,800	0.3	8.0×10^{20}
0.85 B^{10}	315	23,800	65,700	10.3		90,900	0.1	8.0×10^{20}
1.18 B^N	23	40,200	96,100	18.4	132,000	154,000		3.4×10^{20}
1.18 B^N	315				87,500	122,000		3.4×10^{20}
1.64 B^N	23	41,800	100,000	13.7	97,800	120,000		0.97×10^{20}
1.64 B^N	315				71,300	106,000		0.97×10^{20}
1.8 B^N	23	41,300	84,200	8.0	136,000	151,000		5.8×10^{20}
1.8 B^N	315				85,500	119,000		5.8×10^{20}
2.04 B^N	23	47,000	89,000	5.4	97,800	120,000		7.3×10^{20}
2.04 B^N	315				71,300	106,000		7.3×10^{20}

were carried to exposures of 1×10^{21} thermal nvt were reported to cause no gross dimensional changes or warping of the samples.

Tables VI-5 and VI-6 summarize some of the data on tensile strength and impact strength contained in the reference.[1] Other experiments are cited in which samples containing various amounts of natural boron up to 2 wt.% were irradiated to an exposure of 8×10^{20} nvt. It is stated that the yield strength increased by 250 per cent and the ultimate tensile strength increased by 80 per cent, whereas the elongation decreased to as low as 1 per cent of the original value. Since there appeared to be no difference in the irradiation behavior of the alloys which could be attributed to the different boron concentrations, it was postulated that the tensile strength reached a saturation value at a reasonably low level of neutron exposure. Marked embrittlement of alloys by irradiation was observed in other experiments at exposures as low as 8×10^{19} nvt.

The use of boron–stainless steel control rods in water-cooled power reactors has demonstrated that the corrosion resistance in high-temperature water is acceptable. Experimental measurements of corrosion rates are not entirely consistent. It appears, however, that additions of boron in the 1 to 2 wt.% range to stainless-steel alloys do not affect greatly the corrosion resistance in dynamic tests and that irradiation does not have an important effect on corrosion. Some static tests, however, have shown much greater weight gains for a

Table VI-6 RESULTS OF IMPACT TESTS ON NATURAL BORON (B^N) AND ENRICHED BORON (B^{10}) ALLOYED WITH STAINLESS STEEL[1]

Boron content, wt.%	Test temp., °C	Nonirradiated, Izod ft-lb	Irradiated, Izod ft-lb	Thermal nvt
347 S.S.	23	15.9	15.6	3.0×10^{20}
0.5 B^{10}	23	9.5	1.48	3.0×10^{20}
0.5 B^{10}	315	8.4	1.48	3.0×10^{20}
0.85 B^{10}	23	5.67	0.24	9.0×10^{20}
0.85 B^{10}	315	5.70	0.18	9.0×10^{20}
1.18 B^N	23	2.3	0.61	4.35×10^{20}
1.18 B^N	315	1.8	0.66	4.35×10^{20}
1.8 B^N	23	1.0	0.44	1.94×10^{20}
1.8 B^N	315	1.0	0.35	1.94×10^{20}
2.04 B^N	23	0.64	0.22	6.8×10^{20}
2.04 B^N	315	0.64	0.05	6.8×10^{20}

Table VI-7 CORROSION BEHAVIOR OF SOME STAINLESS STEEL–BORON ALLOYS IN 600°F WATER

Melt No.	Boron content, wt.%	Cumulative weight gain, mg/cm² 156 hr	514 hr	1203 hr	2013 hr	3000 hr	4008 hr	Descaled
SS-1	0.34	2.1	2.1	1.9	4.0	1.1	0.8	−2.6
SS-2	0.75	1.7	1.2	1.3	3.1	1.3	1.2	−3.7
SS-3	1.21	1.7	1.7	1.4	2.8	2.3	1.4	−6.7
SS-4	1.80	1.5	2.1	2.2	3.3	2.5	1.7	−8.6
N-272	2.32	2.6	2.8	2.1	4.4	3.4	2.0	−9
Water resistivity at end of test period, megohm-cm		0.8	0.3	0.3	0.2	0.2	0.2	

boron–304 stainless steel alloy than for an ordinary 304 stainless steel alloy and a much greater rate of weight gain after irradiation than before irradiation for the boron alloy. The latter difference was attributed to stress corrosion induced by the helium formed in the (n,α) reaction. The results of corrosion tests on unirradiated boron–stainless steel alloys at KAPL are given in Table VI-7. Presumably these were static tests.

Other Boron-containing Materials[1]

Alloys of boron with zirconium and titanium have also been made. The addition of boron to zirconium and titanium has effects qualitatively similar to those resulting from its addition to stainless steel: the tensile strength is increased and ductility is decreased; neutron irradiation produces a further very marked decrease in ductility. Boron contents between 1 and 2 wt.% appear to be practical. The unirradiated alloys with stainless steel, titanium, and zirconium show corrosion resistance to high-temperature water which decreases in the order named. The postirradiation corrosion-resistance trend is similar but more pronounced. Zirconium-base alloys irradiated to relatively high boron burnup appear to have poor corrosion resistance.

Of the boron compounds, boron carbide is the most widely used. It is a refractory material with a theoretical density of 2.51 g/cm^3; actual densities up to 2.4 g/cm^3 can be obtained in massive bodies. The material, although brittle, has relatively good thermal-shock resistance because of its high compressive strength (414,000 psi at room temperature), its relatively small value of thermal-expansion coefficient (45×10^{-7}/°C), and its reasonably high thermal conductivity (0.24 and 0.15 watts/(cm)(°C) for theoretically dense material at 200 and 800°C, respectively). The corrosion resistance of the material for high-temperature water is not considered good but is sufficiently good to prevent catastrophic corrosion rates if jacketed material is exposed to water through failure of the jacket. The corrosion resistance is much better for high-density material than for low-density material.

Neutron irradiation of boron carbide produces anisotropic dimensional changes in the boron carbide crystals. These effects appear to anneal out at 700 to 900°C. However, the deposition of helium in the lattice is a further cause of radiation damage. Samples irradiated to a burnup of 36 per cent of the B^{10} atoms were reduced to powder. The effects of elevated temperatures on radiation damage are not well known, and it is thought that high temperatures may be beneficial. At low temperatures, only a small fraction of the helium is released from the material even after the irradiation has proceeded to the point where the material breaks up into granules. Subsequent heating of such a sample to 800°C caused the release of about 19 per cent of the contained helium.

The borides of a number of metals, including titanium, hafnium, zirconium, niobium, and tantalum, have received some study, particularly with regard to aqueous corrosion, radiation damage, and helium retention. As yet, none of these materials has seen service as a control-rod material.*

Dispersions of boron or boron compounds in ductile metals may be used as alternatives to the boron alloys or to canned boron compounds. The helium problem is still present in the dispersion; it is usually the metal of the dispersion which is counted on to contain the helium. The most common material of this type is Boral, a dispersion of boron carbide in aluminum. This material is, of course, limited to low-temperature applications. The absorbing material for the first set of APPR control rods consisted of a dispersion of 3.23 wt.% boron (90 per cent enriched) in iron, clad with type 304 stainless steel. After approximately two years of service, this material has been replaced by a Eu_2O_3–stainless steel dispersion that is stainless-steel-clad. The B^{10}-Fe dispersion rods are being given postirradiation metallurgical examination.

Boron dispersions in stainless steel, titanium,† and Zircaloy have been investigated. The titanium-base dispersions exhibit excellent corrosion resistance in hot water when the boron content is relatively low, up to perhaps 3 per cent. Titanium-clad specimens of the titanium-boron matrix, purposely defected, appeared to be good up to boron contents of at least 12.9 wt.%. The corrosion does not appear

* Reference 18 discusses briefly some of the borides of interest.

† Two recent papers on boron-titanium dispersions are listed as references 19 and 20.

to be greatly increased by irradiation. The stainless steel–boron dispersions appear to be reasonably good when the boron content is low and rather poor when the boron content is high. A sample containing 1.6 wt.% boron lost 38 mg/dm^2 in 70 days at 345°C, whereas a 6 wt.% B^{10} dispersion lost 1250 mg/dm^2 under the same conditions.

The addition of boron in dispersion lowers the strength of the base material at room temperature, although at higher temperatures its effect may be small. Irradiation embrittles the dispersion, but the degree of embrittlement seems to vary with the base material. Titanium appears to be the least affected, whereas steel is quite sensitive in this respect. Long irradiation produces dimensional changes of a few per cent and may produce blistering, apparently as a result of the helium accumulation. Blistering has been observed in a titanium-B^{10} dispersion containing 1 per cent B^{10} after the exposure had reached 40 per cent burnup.

Dispersions of boron carbide in titanium and zirconium have shown the same pattern of aqueous corrosion behavior as have the boron dispersions. In general, the susceptibility to corrosion increases with the amount of boron carbide; the titanium dispersions can, on the whole, be described as having good corrosion resistance, but the zirconium and Zircaloy dispersions are rather poor.

The addition of boron carbide as a dispersion increases the brittleness. In the case of titanium-base dispersions, this increase was found to be greater than that produced by an equal quantity of pure boron in dispersion. The primary effects of neutron irradiation, again, are embrittlement and some increase of volume.

Some work has been done on dispersions of the diborides of zirconium, titanium, and hafnium, in zirconium and titanium matrices. The combination zirconium diboride in a titanium matrix presently appears to be most promising. Again the titanium base exhibits the best resistance to aqueous corrosion.

The effects of irradiation on a number of dispersions containing boron or boron compounds are summarized in Table VI-8.

Cadmium and Cadmium Alloys[1]

Metallic cadmium has been used rather widely as a control-rod material in low-temperature reactors. Its low melting point (321°C) precludes its use for high-temperature applications. It is a soft metal, of low tensile strength (2500 to 9000 psi ultimate tensile strength for as-cast specimens); it is ordinarily used with a jacket or cladding to provide mechanical strength. It does not have good corrosion resistance to water but does not react rapidly with water at temperatures up to the boiling point.

A ternary alloy of silver, indium, and cadmium has been developed, primarily at the Bettis Plant of the Westinghouse Electric Corporation, for use in pressurized-water reactors. Previous work had been done on alloys of silver and cadmium, but these binary alloys are inferior to the ternary alloy in both corrosion resistance and neutron absorption.

The alloy composition which appears to be nearly optimum for corrosion resistance is 81.5 Ag–13.6 In–4.9 Cd, where the composition is given in weight per cent. This alloy in water showed a corrosion rate of about 0.18 mil/year. The rate did not vary much with temperature over the range tested, up to 288°C, in degassed and hydrogenated water, nor was the rate affected much by a change from neutral to high *p*H water or by a change from static to dynamic test conditions. However, in oxygenated water (8 to 12 cm^3/kg) at 288°C and high *p*H, the corrosion rate was high, amounting to 6 mg/cm^2 at the end of 28 days.

The absorption of neutrons converts silver into cadmium, converts a little of the cadmium into indium, and converts indium into tin. Consequently, after long irradiation the composition of the alloy will change. An alloy 76.5 Ag–12.1 In–9.4 Cd–2.0 Sn, which simulated the one obtained by irradiation of the ternary alloy for 3000 hr in a flux of 1×10^{14} neutrons/(cm^2)(sec), was also corrosion tested and was found to have better corrosion resistance than the ternary alloy.

The neutron-absorption effectiveness of the ternary alloy approaches that of hafnium. The quaternary alloy corresponding to the irradiated material (alloy number 2115) is somewhat less effective. Table VI-9 shows the relative effectivenesses of various alloys as determined experimentally in a critical facility which was said to be designed to simulate the neutron-flux spectrum expected in full-scale pressurized-water reactors.

occur in approximately equal abundance, and each has an appreciable thermal-neutron cross section. The daughters produced by neutron capture also have high cross sections; consequently, europium is attractive for rods which must absorb many neutrons over their lifetime. Europium is one of the less abundant and more costly of the rare earths. Two of the gadolinium isotopes, comprising about 30 per cent of the natural material, have high cross sections. However, there is no continuous series of high-cross-section daughter decay products. Samarium has only one isotope of high cross section, of 13.84 per cent abundance. Consequently, samarium will burn out rapidly unless used in relatively high concentrations. Dysprosium has a lower cross section than the other three rare earths of interest and has been considered primarily for use as a burnable poison.

The rare earths, in the metallic form, are reactive chemically and must be protected from most reactor coolants. Work is under way to produce alloys with corrosion-resistant materials, but it is probable that such alloys will need protective cladding in most applications. Alloys with titanium and stainless steel have been made. In general, increasing amounts of the rare earths cause an increase in brittleness of the rolled alloy material. The corrosion behavior of these alloys appears very promising for rare-earth contents of a few per cent, but corrosion resistance deteriorates as the percentage of rare earth is increased. Little or no work has yet been done on the effects of irradiation on these alloys.

The rare-earth oxides hydrate rapidly when exposed to hot water; and, consequently, if the rare earths are used in oxide form, these too must be protected. Most of the present work is directed toward the use of dispersions of the rare-earth oxides in a metal matrix; this cermet is then clad with an appropriate material to eliminate corrosion. There is an economic incentive for using the rare earths in the oxide form rather than the metallic form since the cost of producing rare-earth metals is relatively high. Among the metals which have been used in rare-earth oxide dispersions are stainless steel, titanium, zirconium, and nickel. Much of the work has been done with samarium oxide rather than with the more expensive europium oxide, but the behavior is expected to be nearly the same for the two materials.

Stainless steel–Sm_2O_3 dispersions, which are stainless-steel-clad and which contain from 15 to 40 vol.% of the oxide, have been successfully fabricated. Since the rare earths capture neutrons by an (n,γ) reaction, no very strong irradiation-damage effects would be expected. However, bend tests on irradiated Eu_2O_3–stainless steel cermets showed some loss of ductility during irradiation. It is stated that examination of micrographs showed that the damage was adjacent to the Eu_2O_3 particles and that the cause of this damage was later shown to result from the reaction between the silicon in the stainless steel and the Eu_2O_3. Impact tests on 9.9 wt.% Eu_2O_3 dispersions in stainless steel after two cycles of MTR irradiation showed a decrease in impact strength by only 5 to 10 per cent in the temperature range 24 to 315°C. Bend tests on irradiated Gd_2O_3 cermets, irradiated for two cycles in the MTR, showed that the material retained 90 per cent of its preirradiation ductility. However, growth was noted of the order 0.3 per cent in all three dimensions.

Table VI-12 CONTROL MATERIAL COSTS[1]

Material	Cost per pound, dollars	Basis of cost
Boron (natural)	450 (99.6% purity) 15 (commercial grade)	Supplier
B^{10} (93% enriched)	1500	Private communication
B_4C	5–10	Supplier
Boral	8–18 (per square foot of 1/8- to 3/8-in.-thick sheet)	Supplier
Boron–stainless steels:		
2 wt.% B^N	6.35	Supplier
1 wt.% B^{10} (90% enriched)	52.40 (500-lb lot)	Supplier
Cadmium	2–3 (metal)	Supplier
Hafnium	50–100 (crystal bar)	AEC estimate
Dysprosium oxide	50* (99% purity)	Supplier
Europium oxide	790 (99% purity)	Supplier
Europium metal	1500	Supplier
Gadolinium oxide	35* (90% purity)	Supplier
Samarium oxide	25* (90% purity)	Supplier
Titanium sponge powder	6	Reference 23
Stainless-steel powder	20	Reference 23
Low-cobalt stainless steel equiv. to AISI 304 E/C (ingots)	5	Reference 23
Cd-In-Ag billets	20	Reference 23

* For lots of over 500 lb.

Material Costs and Applications[1]

Although the cost of a complete control rod involves many items besides the cost of the absorbing material in the rod and may be, in some cases, many times the cost of that material, some of the materials are rather expensive; their cost will, therefore, play a part in determining whether or not they will be attractive for a given application. The costs of some of the absorbing materials which have been discussed above are listed in Table VI-12, from reference 1.

Manufacturing experience sufficient to permit estimates of the relative costs of complete control rods of the various types has not yet been accumulated. In the EBWR, where some of the rods were of hafnium and some were of boron–stainless steel, a relatively clean comparison of manufacturing costs is possible. The total fabrication cost for a single hafnium cruciform rod, $\frac{1}{8}$-in. thick by 10-in. span by

Table VI-13 CONTROL-ROD TYPES IN VARIOUS POWER REACTORS[1]

Reactor	Control-rod environment	Control-rod type
Calder Hall	CO_2 outlet temperature 637°F	Number of rods adjustable, approximately 40; boron steel cylinders encased in low-cobalt stainless-steel sheaths
EBWR (Experimental Boiling-water Reactor)	Boiling H_2O outlet temperature 488°F	Nine cruciform rods, 10-in. span by 46 in. long (five rods are $\frac{1}{8}$-in. hafnium with Zircaloy followers; four rods are $\frac{1}{4}$-in., 2 per cent natural boron–stainless steel with Zircaloy followers)
VBWR (Vallecitos Boiling-water Reactor)	Boiling H_2O outlet temperature 545°F	Three central blades, 18 in. wide by $\frac{1}{4}$ in. thick, of 1 wt.% B^{10} stainless steel; four outer blades contain $\frac{1}{4}$-in.-OD cylindrical steel tubes filled with B_4C
ALPR (Argonne Low Power Reactor)	Boiling H_2O outlet temperature 420°F	Five cruciform rods, 14-in. span, 32 in. long, 0.220 in. thick, composed of 0.060-in.-thick cadmium canned in 0.080-in.-thick aluminum-nickel alloy; followers are of aluminum-nickel; four T-shaped rods of the same composition are provided for larger fuel loadings
Dresden Nuclear Power Station	Boiling H_2O outlet temperature 542°F	Eighty cruciform rods; 2 wt.% natural boron–stainless steel, 0.375 in. by $6\frac{1}{2}$-in. span by 102 in.
Enrico Fermi Atomic Power Plant (fast-neutron reactor)	Sodium outlet temperature 800°F	Ten cylindrical rods, enriched B_4C hollow cylinders encased in stainless-steel tubes; the stainless-steel tubes act as pressure vessels to contain the helium generated
OMRE (Organic Moderated Reactor Experiment)	Santowax OM cutlet temperature 530-710°F	Twelve cylindrical rods, composed of stainless-steel tubes, $1\frac{1}{4}$ in. OD by 36 in. long, containing compacted B_4C
APPR (Army Package Power Reactor)	Pressurized H_2O outlet temperature 450°F	Seven hollow square tubes, $2\frac{1}{2}$ in. square, with fueled followers; absorbing material is 3.23 per cent B^{10} in iron, clad with stainless steel; these original rods were replaced by others using Eu_2O_3–stainless steel dispersion in the spring of 1959
Shippingport Atomic Power Station	Pressurized H_2O outlet temperature 539°F	Thirty-two cruciform hafnium rods, 0.226 in. by $3\frac{3}{8}$-in. span by 71 in. long
Consolidated Edison (Indian Point) reactor	Pressurized H_2O outlet temperature 510°F	Twenty-one cruciform hafnium rods, $\frac{5}{16}$ in. by 7.5-in. span by $135\frac{5}{8}$ in. long
Yankee Atomic Electric Plant	Pressurized H_2O outlet temperature 514°F	Thirty-two extruded cruciform rods, of 80 wt.% silver, 15 wt.% indium, and 5 wt.% cadmium
STR (Submarine Thermal Reactor)	Pressurized water	Hafnium control rods
ARE (Aircraft Reactor Experiment)	Helium rod coolant, separated from the 1500°F molten-salt fuel mixture	One regulating rod of stainless steel; three shim rods of segmented cylindrical B_4C canned in stainless steel
SRE (Sodium Reactor Experiment)	Helium rod coolant, separated from the 960°F, outlet temperature, sodium reactor coolant	Eight cylindrical rods of 2.5 wt.% boron–nickel alloy rings encased in stainless-steel tubes; the shim rods use 18 rings, 2.5 in. OD by 1.75 in. ID by 4 in. long; the safety rods are slightly smaller

46 in. long, with a 39-in.-long Zircaloy-2 follower, has been given as $9500. The total fabrication cost for the boron–stainless steel rod, containing 2 wt.% natural boron, and similar to the hafnium rod in dimensions except for an increased thickness to ¼ in., has been stated as $2750. Of this cost, it is estimated that approximately $1900 is the cost of the Zircaloy-2 follower. The fabrication cost of control rods does not, of course, tell the complete story; for some rods, because of better burnout characteristics, better resistance to radiation damage, and better corrosion resistance, may last longer in the reactor than other rods. This consideration is reflected in the choice of the EBWR rods. The hafnium rods, which are superior with respect to burnout and radiation-damage resistance, are used to compensate the excess reactivity provided for fuel burnup; whereas the boron-steel rods are used primarily for shutdown and, on the average, receive considerably less neutron exposure. Thus the boron-steel rods, although much cheaper than the hafnium rods, do not do an equivalent job.

Current practice in the choice of absorbing materials for control rods is summarized in Table VI-13, which lists the materials for a number of power reactors which are either in operation or under construction. Reference 1, the source of the information in Table VI-13, contains a much more extensive list of the same kind.

References

1. Survey of the Physics, Metallurgy, and Engineering Aspects of Reactor Control Materials, USAEC Report GEAP-3183, General Electric Company, Vallecitos Atomic Laboratory, Atomic Power Equipment Department, San Jose, Calif., June 12, 1959.
2. A. F. Henry, A Theoretical Method for Determining the Worth of Control Rods, USAEC Report WAPD-218, Bettis Atomic Power Division, Westinghouse Electric Corporation, August 1959.
3. R. J. McWhorter, J. Russell, and B. Wolfe, The Use of Thermally Black Control Sheets, *Nuclear Sci. and Eng.*, 5(6): 382 (June 1959).
4. T. F. Ruane and M. L. Storm, Epithermal Hafnium Parameters for the Calculation of Control Rod Worth in Thermal Reactors, *Nuclear Sci. and Eng.*, 6(2): 119 (August 1959).
5. C. W. Maynard, Blackness Theory and Coefficients for Slab Geometry, *Nuclear Sci. and Eng.*, 6(3): 174 (September 1959).
6. L. Tonks, Uniformly Spaced Control Elements in a Reactor: Theoretical Basis of Application of "Absorption Area" to Reactor Control Evaluation, *Nuclear Sci. and Eng.*, 6(3): 202 (September 1959).
7. H. Uberall, Neutron Absorption by Control Rods of Varying Transparency, *Nuclear Sci. and Eng.*, 7(3): 228 (March 1960).
8. R. L. Murray, Theory of Asymmetric Arrays of Control Rods in Nuclear Reactors, USAEC Report APAE-48, Alco Products, Inc., Apr. 25, 1959.
9. The Experimental Boiling Water Reactor (EBWR), USAEC Report ANL-5607, Argonne National Laboratory, May 1957.*
10. I. Wivstad and C. Mileikowsky, Adam — A 75-Mw Nuclear Energy Plant for House Heating Purposes, A/CONF.15/P/136, Second United Nations International Conference on the Peaceful Uses of Atomic Energy, Geneva, 1958.
11. C. Starr and R. W. Dickinson, *Sodium Graphite Reactors*, Addison-Wesley Publishing Company, Inc., Reading, Mass., September 1958.
12. S. A. Ghalib and J. H. Bowen, Equipment for Control of the Reactor, *J. Brit. Nuclear Energy Conf.*, 2(2): 187 (April 1957).
13. G. Packman and B. Cutts, Basic Design of Reactor, *J. Brit. Nuclear Energy Conf.*, 2(2): 102 (April 1957).
14. H. E. Stevens, Nuclear Requirements for Control Materials, *Nuclear Sci. and Eng.*, 4(3): 373 (September 1958).
15. H. J. Amster, The Wigner-Wilkins Calculated Thermal Neutron Spectra Compared with Measurements in a Water Moderator, *Nuclear Sci. and Eng.*, 2(3): 394 (May 1957).
16. R. A. Becker and John L. Russell, Jr., Relative Effectiveness of Reactor Control Materials, USAEC Report GEAP-3201, General Electric Company, Vallecitos Atomic Laboratory, July 20, 1959.
17. H. F. Johnston, J. L. Russell, Jr., and W. L. Silvernail, Relative Control Rod Worths of Some Rare Earth Oxides, *Nuclear Sci. and Eng.*, 6(2): 93 (August 1959).
18. A. N. Holden, Borides of Interest for Control Materials, USAEC Report GEAP-3117, General Electric Company, Vallecitos Atomic Laboratory, Jan. 29, 1959.
19. L. B. Prus et al., Enriched Boron-Titanium Dispersions, *Nuclear Sci. and Eng.*, 6(3): 167 (September 1959).
20. E. S. Byron, F. O. VonPlinsky, and S. W. Porembka, Clad Titanium-base Dispersions Containing Boron, *Nuclear Sci. and Eng.*, 6(5): 361 (November 1959).

*This report is available from the Superintendent of Documents, U. S. Government Printing Office, Washington 25, D. C., for $2.25.

21. I. Cohen, Development and Properties of Silver-base Alloys as Control Rod Materials for Pressurized Water Reactors, USAEC Report WAPD-214, Bettis Atomic Power Division, Westinghouse Electric Corporation, December 1959.
22. J. G. Goodwin and F. R. Lorenz, A Study of Some Mechanical, Physical, and Corrosion Properties of Iodide Hafnium, *Nuclear Sci. and Eng.*, 6(1): 49 (July 1959).
23. W. K. Anderson, Broad Aspects of Absorber Materials Selection for Reactor Control, *Nuclear Sci. and Eng.*, 4(3): 357 (September 1958).

The operating principles and status of development of direct energy-conversion schemes were reviewed in a series of papers presented at the American Nuclear Society Symposium held in Pittsburgh on Mar. 19, 1960. The basic and practical limitations on obtaining increases in efficiency and power density were discussed. Conceptual methods of integrating direct-conversion devices with reactor heat sources, and some of the foreseeable major problem areas, were also presented.

The direct-conversion schemes described are: (1) thermionic emitter, (2) thermoelectric, (3) magnetohydrodynamic (MHD) generator, and (4) electrochemical energy converter or fuel cell.

To attain high efficiencies in the direct-conversion heat engines, it is necessary to reduce the irreversible heat losses. The heat losses are due to straight thermal conduction and radiation. The heat leak paths are generally the same as the electron flow paths. Hence it is difficult to reduce heat leaks without increasing the I^2R drop internally and/or in the lead wires.

Dr. C. E. Zener of the Westinghouse Electric Corporation gave a measure of the irreversible heat losses occurring in presently developed direct-conversion devices. He expressed this measure as follows:

$$\eta = \delta\eta_c$$

where η = over-all efficiency

$$= \frac{\text{electrical power output from device}}{\text{heat input into device}}$$

η_c is the Carnot efficiency, and δ is the degradation coefficient.

	δ
Regenerative H_2 fuel cell	0.10
Thermoelectric (bismuth telluride)	0.17
Thermionic emitter (2 mm spacing, cesium-coated anode)	0.30
MHD	>0.85

For the MHD generator, the lead losses result in only a small degradation of energy.

By proper design, it should be possible to improve the degradation coefficient δ. The goal is to uncouple the electron flow path from the heat leak path.

With the thermionic emitter, high power densities (about 30 watts per square centimeter of cathode surface) have already been produced. Laboratory models have been built and operated at 13 to 15 per cent efficiency. The process does require high-temperature operation (1500 to 2800°K) which presents materials problems. J. R. Reitz of Case Institute of Technology described the several regimes of operation of a thermionic emitter, namely, (1) vacuum, (2) low-density plasma, and (3) high-density plasma. For high current densities (of the order 100 amp/cm^2), it is necessary to operate in the high-density plasma regime. The Los Alamos plasma thermocouple operated in this regime to deliver about 60 amp/cm^2 at 2500°K cathode temperature.

S. J. Angello of the Westinghouse Electric Corporation presented a brief review of the thermoelectric effects. From an elementary derivation, he obtained

$$\delta = \frac{T_h}{4}\left(\frac{\alpha^2}{\rho k}\right)$$

where T_h = hot-junction temperature
α = thermoelectric power
ρ = electrical resistivity
k = thermal conductivity

Since α, ρ, and k are basic material properties, it is obvious that material development is crucial in increasing the efficiency of thermoelectric devices. The thermoelectric materials must withstand high temperatures and, when used in a reactor environment, must also withstand radiation damage. Present n type and p type materials are available which permit operation up to 1200°C to give an over-all theoretical efficiency of 16 per cent. Attention

must be paid to extraneous losses in the design of the thermoelectric device and in integration of the device with the heat source. Heat leak paths not directly through the elements themselves must be minimized. Care must be taken to minimize contact resistance to current flow between the elements and the heat-collector and heat-sink skins.

A great deal of material research work is required to develop thermoelectrics capable of higher temperature operation and having material properties leading to higher efficiencies. Between 1956 and 1960 the efficiency has been increased from 6 to 16 per cent. It is projected that with sustained effort on material development an efficiency of 30 per cent can be attained by the year 1970.

R. J. Rosa of Avco-Everett Research Laboratory described the MHD generator. The MHD generator extracts power directly from the motion of ionized gas through a magnetic field. It consists of a duct through which an ionized gas flows, coils which produce a magnetic field across the duct, and electrodes at the top and bottom of the duct. The ionized gas, by virtue of its motion through the magnetic field, has an electromotive force generated in it which drives a current through it, the electrodes, and the external load. The generator has no moving parts or close tolerances, and hence its cost is expected to be low compared to that of conventional conversion machinery for the same power output. Its efficiency is comparable to that of a gas turbine, i.e., it will have approximately the same enthalpy extraction from the gas for a given pressure drop through the device.

The most important quantity determining the feasibility and characteristics of MHD generators is the gas conductivity. For air seeded with 1 per cent potassium vapor, sufficient thermal ionization (~1 mho/meter gas conductivity) is obtained at temperatures in excess of 2000°K for a reasonably practical design. With this value of gas conductivity, a 100-Mw-output MHD generator would be about 30 ft in length and would require a 10,000-gauss magnetic field strength. It is evident that MHD generators tend to be quite large.

R. J. Rosa described an MHD device having a 10-kw power output which was successfully operated as a demonstration of the basic working principles of the device. The MHD generator extracted about 1½ to 2 per cent of the enthalpy of the gas.

Schemes for integrating the direct-conversion devices with a nuclear heat source were discussed conceptually, principally with a view of attempting to define the problems involved. The application of immediate interest is for space-satellite auxiliary power supplies wherein an important requirement is maintenance-free operation at full power for time periods of a year or more. The power requirements are quite modest, ranging from about 1 to 20 kw of net electrical power output. For this power range the reactor power density is low enough that it may prove practical to conduct the reactor heat to the surface of the reactor. Obviously, to keep the temperature at the center of the reactor within reasonable bounds and to minimize thermal stresses in core and reflector, structural material of high conductivity is required. The heat-collector skin of the thermoelectric device can be wrapped around the reactor to receive its heat by conduction and/or radiation from the reactor surface. The heat-sink skin radiates the waste heat to the space environment.

For the thermionic emitter application, the cathode surface is wrapped against the cylindrical surface of the reactor. The anode metal surface is also cylindrical and is concentric with the cathode surface; the intervening space is filled with cesium vapor. Again, the waste heat from the anode is rejected by radiation.

At the higher reactor power densities required for central power stations, the reactor heat could be removed in the conventional manner by forced circulation of a coolant (high-pressure gas or liquid metal) through the reactor. The high-temperature coolant would then be pumped past the heat-collector surface of the direct-conversion device. In this concept, the reactor heat source and the direct-conversion device are physically separated. The high temperatures required pose serious material problems and present a need for new reactor concepts.

Considerations are given to placing the thermoelectric material in contact with the fuel rods so as to receive the heat directly. A similar scheme for using the thermionic emitter as a topping device for nuclear reactors has been proposed and has been previously described. (See the section on Thermionic Energy Conversion in the December 1959 issue of *Power Reactor Technology*, Vol. 3, No. 1.) Another scheme is to place the thermionic emitter

and the thermoelectric device in series within the reactor. In this scheme the heat from the fuel rod first passes through the thermionic emitter. The cathode surface is the inner wall of a double-walled jacket for the fuel rod. The cathode is heated directly by fission in the fuel. The annular space within the double-walled jacket is filled with cesium vapor. The outer wall is the anode surface of the thermionic emitter and is also the heat collector for the thermoelectric elements. The heat rejected by the thermionic emitter passes through the thermoelectric elements to the heat-sink skin. The heat-sink skin is cooled in the conventional manner by the reactor coolant. With this scheme the thermoelectric device works as a topper in series with the conventional nuclear energy conversion system and, in turn, the thermionic emitter is a topper onto the thermoelectric device.

The problem of integrating the reactor heat source with the MHD generator appears to require development of unusual reactor concepts, such as the nuclear cavity reactor, in order to achieve the required gas temperatures without melting down the structures of the reactor.

J. C. Danko of Westinghouse Electric Corporation presented some results obtained on irradiation effects on thermoelectric materials. The prime subject for investigation was $Li_xNi_{1-x}O$. In-pile measurements of the Seebeck coefficient and electrical resistivity were made at reactor ambient temperatures and elevated temperatures. In addition, pre- and postirradiation measurements of the Seebeck coefficient, the electrical resistivity, and the thermal conductivity were performed.

Postirradiation measurements on samples of $Li_{0.013}Ni_{0.987}O$ after exposure to a total integrated thermal-neutron flux of 1.4×10^{19} revealed that the electrical resistivity had returned to the preirradiation value; the Seebeck coefficient had increased slightly; and the thermal conductivity had remained essentially unchanged. In-pile measurements of the Seebeck coefficient and electrical resistivity of $Li_{0.05}Ni_{0.95}O$ at 464°C and up to 8×10^{18} nvt (thermal) did not show much variation from the out-of-pile values.

PROGRESS ON SPECIFIC REACTOR TYPES

DESIGN STUDIES AND EVALUATIONS

A considerable volume of literature covering design and evaluation studies of specific reactor types, prepared by or sponsored by the Atomic Energy Commission, has been issued within the last several months. It is the purpose of this note to list these reports and to clarify their relations to one another.

In 1958 the AEC was authorized, under Public Law 85-590 (Sec. 101), to perform a series of design and engineering studies of four large power reactors. The results of those studies have been published as references 1 to 5. These reports were reviewed in the September 1959 issue of *Power Reactor Technology*, Vol. 2, No. 4, shortly after their publication. Since then, four more reports (references 6 to 9) have been issued which contain additional studies and information supplementing the original reports.

In June 1959 the Division of Reactor Development of the AEC undertook the task of defining a long-range program for civilian power-reactor development, generally referred to as the "Ten-year Program," and a further group of evaluation studies was made as part of that project. The large-power-reactor studies in references 1 to 9, although they undoubtedly contributed to the evaluations, did not constitute a formal part of the "Ten-year Program" study.

At the November meeting of the Atomic Industrial Forum, Frank K. Pittman, Director of the Division of Reactor Development, summarized the results of the studies to evaluate the potentials of the several reactor types. His paper was reviewed in the March 1960 issue of *Power Reactor Technology*, Vol. 3, No. 2. Since then, three reports covering the studies and the proposed development program (references 10 to 12) have been issued. A fourth report (reference 13) in several parts, covering the technical status studies for the individual reactor types, is yet to be published. The three reports issued to date have been summarized in reference 14.

References

1. Ebasco Services, Inc., and General Electric Company, Boiling Water Reactor Study, USAEC Report TID-8500 (Parts 1–3), April 1959. Part 1, 306 Mw Power Reactor Conceptual Design (previously available as Report IDO-24030, Vols. 1 and 2); Part 2, Separate Studies (previously available as Report IDO-24030, Separate Studies 1 Through 10); Part 3, 306 Mw Coal-fired Installation (previously available as Report IDO-24031).
2. Bechtel Corporation and Atomics International, Organic Cooled Reactor Study, USAEC Report TID-8501 (Parts 1–5), April 1959. Part 1, Summary of Study (previously available as Report BCPI-1, Vol. 1); Part 2, 300 Mw Power Plant Conceptual Design (previously available as Report BCPI-1, Vol. 2); Part 3, Reactor Concept Evaluation (previously available as Report BCPI-1, Vol. 3); Part 4, 75 Mw Power Plant Conceptual Design (previously available as Report BCIP-1, Vol. 4); Part 5, 300 Mw Coal-fired Power Plant Comparison Study (previously available as Report BCPI-1).
3. Stone and Webster Engineering Corporation and Combustion Engineering, Inc., Advanced Pressurized Water Reactor Study, USAEC Report TID-8502 (Parts 1–3), April 1959. Part 1, Phase I Report (previously available as Report SW-1, Vol. 1); Part 2, Appendices to Phase I Report (previously available as Report SW-1, Vol. 2); Part 3, 235 Mw Coal-fired Generating Plant (previously available as Report SW-1).
4. Sargent & Lundy Engineers and Nuclear Development Corporation of America, Heavy Water Moderated Power Reactor Plant, USAEC Report TID-8503 (Parts 1 and 2), April 1959. Part 1, Design Study (previously available as Report SL-1565, Vols. 1–3 and Addendum 1); Part 2, Preliminary

Design of the Prototype Plant (previously available as Report SL-1581, Vols. 1–3).

5. Division of Reactor Development, AEC Summary and Evaluation Report of Four Power Reactor Design Studies, USAEC Report TID-8504, August 1959.
6. Ebasco Services, Inc., and General Electric Company, Boiling Water Reactor Study, USAEC Report TID-8500, April 1959. Part 1 (Supplement), Refinements of 306 Mw Power Reactor Conceptual Design (previously available as Report IDO-24030, Appendix 1); Part 2 (Supplement), Separate Studies (previously available as Report IDO-24030, Separate Studies 1 R Through 6 R); Part 4, 100 Mw Boiling Water Reactor Conceptual Design (previously available as Report IDO-24032).
7. Bechtel Corporation and Atomics International, Organic Cooled Reactor Study, USAEC Report TID-8501, April 1959. Part 2 (Supplement), 300 Mw Power Plant Conceptual Design, Supplementary Studies (previously available as Report BCPI-1 Phase I Report, Supplement No. 2).
8. Stone and Webster Engineering Corporation and Combustion Engineering, Inc., Advanced Pressurized Water Reactor Study, USAEC Report TID-8502, April 1959. Part 1 (Supplement), Phase II-A Report (previously available as Report SW-1, Phase II-A Report, and Report SW-1, Phase II-A Report, Addendum 1).
9. Sargent & Lundy Engineers and Nuclear Development Corporation of America, Heavy Water Moderated Power Reactor Plant, USAEC Report TID-8503, June 1959. Part 3, Design Study (previously available as Report SL-1653, Part 3); Part 4, Design Study (previously available as Report SL-1661, Summary, Parts 1–3).
10. Civilian Power Reactor Program. Part I, Summary of Technical and Economic Status as of 1959, USAEC Report TID-8516, 1960.*
11. Civilian Power Reactor Program. Part II, Economic Potential and Development Program as of 1959, USAEC Report TID-8517, December 1959.
12. Civilian Power Reactor Program. Part IV, Plans for Development, USAEC Report TID-8519, February 1960.
13. Civilian Power Reactor Program. Part III, Technical Status (to be published as USAEC Report TID-8518). Book 1, Status Report on Fast Reactors as of 1959; Book 2, Status Report on Pressurized Water Reactors as of 1959; Book 3, Status Report on Aqueous Homogeneous Reactors as of 1959; Book 4, Status Report on Heavy Water Moderated Reactors as of 1959; Book 5, Status Report on Boiling Water Reactors as of 1959; Book 6, Status Report on Sodium Graphite Reactors as of 1959; Book 7, Status Report on Organic Cooled Power Reactors as of 1959; Book 8, Status Report on Gas Cooled Reactors as of 1959.
14. AEC Puts Together a Long-range Power Reactor Program, *Nucleonics*, 18(4): (April 1960).

*The reader may also consult USAEC Report SL-1674, Power Cost Normalization Studies, which contains supplementary information on this subject.

The Plutonium Recycle Test Reactor (PRTR) is an AEC facility, under construction at Hanford, which will be used to develop the technology required for the utilization of plutonium fuels in thermal heterogeneous power reactors. Specifically, the reactor provides facilities for the following:[1]

1. Irradiation testing of plutonium-bearing fuel elements.
2. Direct investigations of reactivity and exposure effects from isotope buildup on the uranium-plutonium fuel cycle.
3. Production of irradiated fuels for reprocessing and refabrication studies.
4. Investigation of reactor operating problems for plutonium-recycle operation.
5. Demonstration of the economics and practicability of various fuel cycles.

Operationally the facility will be utilized for research and development to test the feasibility of various plutonium-recycle concepts. Emphasis will be placed on obtaining physics data necessary to evaluate plutonium recycle, e.g., data pertaining to isotope cross sections and data on control characteristics.

The reactor is of the vertical pressure-tube type, moderated, cooled, and reflected with heavy water, and is designed to operate at a maximum of 70 Mw(t). The moderator is contained in an unpressurized aluminum calandria tank that has an 84-in. ID and is 115 in. in height. Eighty-five fuel channels, 18 shim control-rod channels, and 13 instrumentation channels are mounted vertically within the calandria with the fuel channels arranged on an 8-in. triangular pitch. To insulate the coolant from the moderator, a double-wall construction is utilized for the fuel channels. The outer aluminum tube is an integral part of the calandria; the inner process tube is fabricated of Zircaloy-2 and contains the fuel elements. Each process tube is connected to coolant manifolds by means of jumpers to allow maximum flexibility in monitoring and cooling individual assemblies. Heavy water flows vertically upward within the process tubes at a pressure of about 1000 psi. Heat generated in the reactor is used to make 425-psia steam in a primary heat exchanger, and this steam is condensed and disposed to the Columbia River. The heavy-water reflector is contained in an annular cylinder coaxial with the calandria.

The primary reactivity control system of the reactor is based on controlling the level of the heavy-water moderator within the calandria. A schematic of the primary control system is shown in Fig. 13. The moderator level in the calandria is maintained by means of a helium-gas-pressure balance system. Heavy water is continuously withdrawn from the storage tank and pumped into the calandria via a moderator heat exchanger. When the moderator level is in the normal operating range, heavy water is returned to the moderator storage tank from the calandria by flow through discharge ports at the top of the calandria and by flow over a weir at the bottom of the calandria. The pressure head required to maintain a given level is developed by means of a helium compressor; at steady-state operation most of the gas pumped through the helium compressor is returned to the compressor inlet through the control valves, but a small amount is sent to the helium purification system and is used to sweep the upper part of the calandria. The position of the control valves is determined by an automatic controller, a manual valve operator, or a safety interlock. This system is stated to be capable of maintaining the moderator within ± 0.05 in. over a range of moderator levels from 36 to 111 in. from the bottom of the calandria. Scram of the reactor is accomplished by rapid drainage of the moderator from the calandria. Upon receipt of the scram signal, the four 8-in. dump valves open, equalizing gas pressure between the top of calandria and the weir. The moderator then flows over the weir and into the dump chamber immediately surrounding the weir. Drainage from the dump chamber into the storage tank is through five 8-in. pipes; the dump chamber thus acts as a "receiver" for a significant part of the

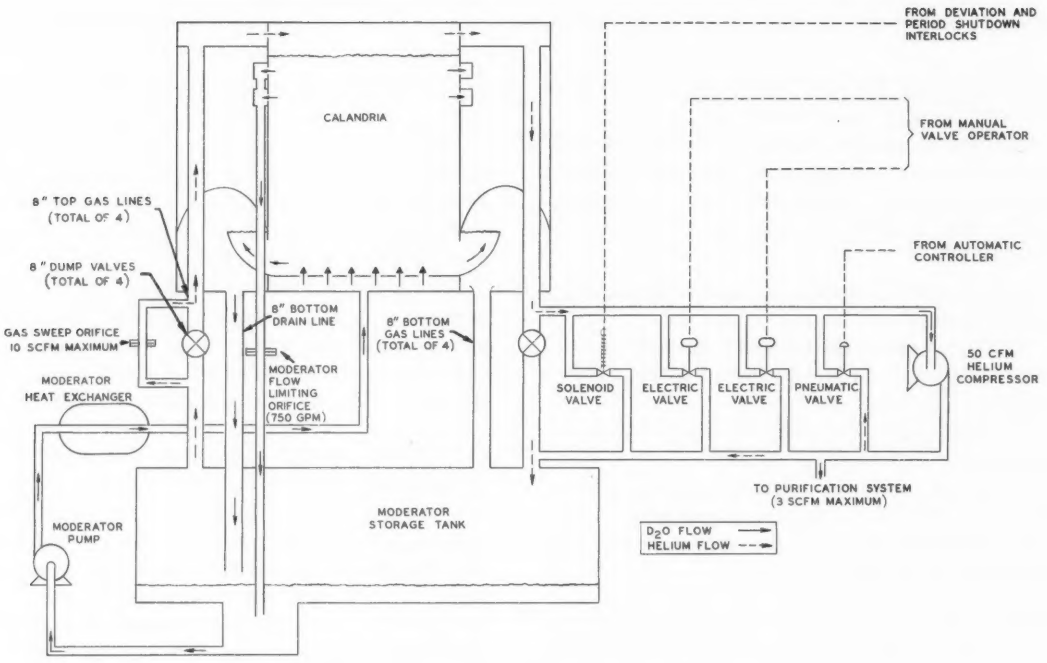

Figure 13—Primary-control-system flow diagram.

moderator during a scram, and this flow takes place rapidly. It is stated that, within 0.85 sec after receipt of a scram signal, the moderator level has fallen 2 ft, decreasing reactivity by no less than 0.018 k_{eff} (for the moderator level initially at its maximum).

Gross adjustments of reactivity are provided by the shim controls. Eighteen multiple-shim control units drive a total of 54 Inconel shim rods, worth a total of 0.115 k_{eff}. The rods are cooled by the heavy-water moderator and are top driven; when withdrawn from the core, they are stored in tubes extending down from the calandria into the bottom shield. The shim rods are operated manually by switches located within the control room. The shim rods are not intended as safety devices and are not actuated by scram signals.

The PRTR initial loading will contain two different types of fuel elements. The Mark-I element consists of a 19-rod cluster assembly employing a plutonium-aluminum fuel alloy or sintered UO_2 pellets. The fuel material is clad with Zircaloy-2 tubing, and 12 of the 19 rods are wrapped with a 72-mil Zircaloy-2 wire to maintain alignment of the tubes and thus provide for adequate flow of coolant. The Mark-II element is composed of a rod of UO_2 surrounded by two concentric annular rings of UO_2; Zircaloy-2 is also used as a cladding. The annular coolant-flow passages are maintained by means of ribs on the surface of the clads. Other plutonium fuel elements are also being considered, such as uranium dioxide–plutonium dioxide and elements wherein the active material is carried in a ceramic matrix.

The fuel-handling system provides for the charging and discharging of fuel elements when the reactor is shut down. The basic component of the system is the charge-discharge machine. This machine can be indexed over any process tube by means of rotating shield plugs, and a connection can be made to the process tube, after removing a shielding plug in the floor of the rotating shield. A hook is then lowered into the process tube to engage the fuel element, which is removed and stored in a shielded region of the charge-discharge machine. The machine is designed to handle the process tubes, should this ever be required. Underwater storage of irradiated elements is also provided in a pool exterior to the reactor containment building.

Table IX-1 PLUTONIUM RECYCLE TEST REACTOR (PRTR) ENGINEERING DATA[1]

General Reactor Data

Power level (nominal)	70 Mw
Heat to primary coolant loop	66.4 Mw
Heat to moderator coolant loop	2.2 Mw
Heat to reflector	0.6 Mw
Heat to shields	0.8 Mw
Primary coolant flow	8400 gal/min D_2O at 478°F
Primary coolant pressure	1025 psig at pressurizer
Reactor inlet temp.	478°F
Reactor outlet temp. (bulk)	530°F
No. of process tubes	85
Lattice	8-in. equilateral triangle
Fuel loading:	
No. of UO_2 tubes	42–75
No. of Pu tubes	10–43
No. of effective power tubes	60
No. of effective flow tubes	68
Maximum tube power	1200 kw
Maximum tube flow	123 gal/min
Maximum tube outlet temp.	542°F
Av. neutron flux (thermal)	8.3×10^{13} neutrons/(cm²)(sec) radial 7.7×10^{13} neutrons/(cm²)(sec) axial
Goal fuel exposure, U	5–8000 Mwd/ton
Xenon override time	Up to 2 hr
Time required for:	
Shutdown (normal)	10 Mw/min
Cool and depressurize primary coolant system (normal)	2 hr
Pressurize primary coolant system startup (from critical to full power)	Less than 5 min
Cold	2 hr (min.)
Hot	13 Mw/min (max.)
Power and neutron-flux distribution (unflattened):	
Radial flux distribution	0.72 av./max. (1.39 max./av.)
Vertical flux distribution (7.4-ft fuel)	0.833 av./max. (1.20 max./av.)

Reactor Piping: Process Tubes

Material	Zircaloy-2
Design stress	14,400 psi
Dimensions ID (active zone)	3.250 in. ± 0.010 in.
Wall thickness (active zone)	0.154 in. ± 0.008 in.
Length	17 ft 5 in.
Wall thickness (inlet end)	0.235 in.
OD (inlet end)	$2^1/_{16}$ in.
Weight	85 lb
D_2O flow area for empty tube (active zone)	8.3 sq in. (0.0576 sq ft)
D_2O flow area with cluster element, Mk-I, in tube	3.56 sq in. (0.0246 sq ft)
D_2O flow area with concentric element, Mk-II, in tube	2.27 sq in. (0.0158 sq ft)
D_2O flow/tube, maximum	123 gal/min
D_2O velocity, empty tube (123 gal/min)	4.75 ft/sec
D_2O velocity, 19-rod cluster element (123 gal/min)	11.1 ft/sec
D_2O velocity, concentric element (123 gal/min)	17.7 ft/sec (av.)
Flow split in concentric element:	
Inner channel	17%
Middle channel	49.4%
Outer channel	33.6%
D_2O inventory (85 tubes and nozzles)	450 gal with 19-rod Mk-I element
Pressure drop across cluster element	~7 psi
Pressure drop across concentric element	~15 psi

Fuel Elements

19-rod cluster elements:	
Length of active core in element	7 ft 4 in.
Length of element	8 ft 3 in.
Length of hanger	6 ft 2 in.
Length of fuel assembly (hanger and fuel-element assembly)	14 ft 5 in.
Bare rod diameter	0.504 in.
Sheath material	Zircaloy-2
Sheath thickness	0.030 in.
Core cross-sectional area (19 rods)	3.76 sq in.
Total cross-sectional area (19 rods) without wire wrap	4.76 sq in.
Core weight:	
UO_2	122 lb
Pu-Al	32.8 lb
Fuel-element assembly weight (19 elements)	
UO_2	160 lb
Pu-Al	70 lb
Hanger weight	40 lb
Fuel-assembly weight:	
UO_2	200 lb
Pu-Al	110 lb
Concentric elements:	
Length of UO_2 in element	7 ft 4 in.
Length of element	8 ft 7 in.
Length of hanger	5 ft 10 in.
Length of fuel assembly (hanger and fuel-element assembly)	14 ft 5 in.
UO_2 diameters:	
Rod OD (Mark-II C)	0.548 in.
Inner tube ID	1.082 in.
Inner tube OD	1.782 in.
Outer tube ID	2.328 in.
Outer tube OD	2.948 in.
Sheath material	Zircaloy-2
Sheath thickness	0.060 in.
UO_2 cross-sectional area (total)	4.34 sq in.
Total cross-sectional area	6.03 sq in.
UO_2 weight (10.2 g/cm³)	141 lb
Fuel-element assembly weight	195 lb
Hanger weight	40 lb
Fuel-assembly weight	235 lb
Maximum heat flux	400,000 Btu/(hr)(sq ft)

(Table Continues)

Table IX-1 (Continued)

Primary Coolant System	
Heating load	66.4 Mw
D_2O flow rate	8400 gal/min
D_2O inventory (exterior of ring headers)	2200 gal
Steam generator:	
Type and number	1, U tube and shell
Total surface area	6658 sq ft
Tube material	304 stainless steel
Total evaporation rate (full power)	214,000 lb/hr
D_2O velocity	12 ft/sec (max.)
D_2O pressure drop	14 psi
Pumps:	
Number and type	3, mech. seal
Spares in circuit	1
Operating head	110 psig
Capacity (each)	4200 gal/min
Electrical power (each)	350 hp
Material	316 stainless steel
Piping:	
Size	14 in. sch. 100
Material	304 stainless steel
D_2O velocity	24 ft/sec
Pressurizer:	
Pressurizing method	Helium bleed from hp tanks
Pressurizer size	109 cu ft D_2O
Control pressure	1025 psig
Steam system:	
H_2O flow	535 gal/min
Steam generator pressure	425 psia
Moderator Coolant System	
Heating load	2.2 Mw
D_2O flow rate	1086 gal/min
D_2O inventory	2544 gal
Temp. range	137–149°F
Heat exchangers:	
Type and number	1, countercurrent shell and tube
Total surface area	1000 sq ft
Pumps:	
Number and type	3, mech. seal
Electrical power (each)	60 hp
Spares	1
Operating head	110 psig
Capacity	600 gal/min
Secondary cooling water:	
H_2O flow rate	750 gal/min at 68°F inlet
Heavy Water (General)	
D_2O inventory, total	8210 gal
Purity specification	99.8%
D_2O density at 505°F	0.858 g/cm^3 (53.4 lb/cu ft)
D_2O heat capacity at 505°F	1.16 Btu/(lb)(°F)
Resin quantity (IX-1)	22 cu ft
Resin operating temp.	130°F
Total capacity, corrosion products	19.5 g equivalent/cu ft
Storage capacity (moderator storage tank and primary D_2O storage tank)	7000 gal
Reactor Core Components	
Calandria:	
Over-all length (top of vessel to bottom of vessel)	Outside 9 ft 10½ in.
ID of moderator shell	7 ft 0 in.
Wall thickness of shell	¼ in.
Over-all diameter of calandria, including dump chamber	11 ft 0 in.
Material of construction	Aluminum
Design pressure	5 psig minimum
Test pressure	6.25 psig
No. of process-channel shroud tubes	85
OD of process channel shroud tubes	4.25 in.*
Wall thickness of shroud tubes	0.065 in.*
Gas gap between shroud and process tubes	0.258 in. minimum
No. of flux-monitor channels	13
OD of monitor-channel tubes	1.5 in.
Wall thickness of monitor-channel tubes	0.049 in.
Material of monitor-channel tubes	Aluminum
No. of shim control channels	18
OD of shim control channels	2.5625 in.
Wall thickness of shim control-channel tubes	0.065 in.
Volume of heavy water in moderator	284 cu ft
Bottom drain line	8 in.
Top overflow line	8 to 4 in.
Reflector:	
Type of reflector used	Heavy-water tank type
Length of radial reflector (top to bottom)	6 ft 7¾ in.
Thickness of radial reflector	23⅜ in.
Over-all diameter of outer reflector tank	11 ft 0 in.
Total metal thickness between inner reflector and moderator	¼ in. of aluminum

*Center shroud tube: 6 in. OD; 0.085 in. thick.

The containment vessel houses all the PRTR process areas with the exception of the storage pool mentioned previously. The vessel is an all-welded steel cylinder with a hemispherical dome and ellipsoidal bottom head; the diameter is 80 ft, and the over-all height is about 120 ft. The top of the rotating shield plug is approximately at grade level, and the space inside the containment vessel below grade is divided into three cells by 5-ft-thick concrete shielding

walls. One of the cells contains the components necessary for reactor operation with the exception of the ion-exchange resins, which are housed in a vault exterior to the containment vessel. The second cell contains experimental equipment, and the third cell is an instrument and hot shop cell. Adjacent to the experimental equipment cell is an air-cooled pit used for the examination of irradiated fuel tubes and process tubes.

Additional engineering data on the PRTR can be found in Table IX-1.

Reference

1. N. G. Wittenbrock, P. C. Walkup, and J. K. Anderson, eds., Plutonium Recycle Test Reactor Final Safeguards Analysis, USAEC Report HW-61236, Hanford Atomic Products Operation, Oct. 1, 1959.

The Homogeneous Reactor Experiment No. 2 (or HRT) was discussed in the December 1959 issue of this journal, Vol. 3, No. 1. A detailed analysis of the power transients mentioned in that review has recently been published.[1] Table X-1 lists characteristics of a number of positive and one negative power excursion. Table X-2 summarizes the condition of the reactor during the runs. Additional information may be obtained from the December 1959 Review. During runs 14, 16, and 17, there were more than 800 positive excursions in which the power increased more than 7 per cent, and there were over 70 negative excursions in which the power fell by at least 7 per cent of normal power. The frequency of occurrence of the positive excursions over 7 per cent is shown in Fig. 14 as a function of power level. A plot of the frequency of occurrence of negative excursions is also shown in the reference, but there appeared to be little correlation to reactor power level. After the addition of acid for runs 17-B and C, the frequency of positive excursions decreased. In addition, for 2 hr during run 17-B, the core solution-circulating pump was operated in reverse, giving 40 per cent of normal forward fluid flow in the core. This point is also shown in Fig. 14. During run 17-B, the reactor was operated at average core temperatures from 243 to 272°C at two power levels, 1.9 and 3.6 Mw. At the lower power level, the excursion frequency was insensitive to temperature; whereas, at higher power level, the excursion rate increased with increasing temperature. The frequency numbers shown on the figure are averages taken over a relatively long period of time; the time between excursions was found to be quite irregular, ranging, for one run, from less than 1 min to as much as 141 min.

Table X-1 CHARACTERISTICS OF A NUMBER OF POWER EXCURSIONS[1]

Time	Date	Run No.	P_0, Mw	$\Delta P/P_0$, %	Time to peak, sec	Fastest period, sec	Peak reactivity addition, %	Rate of reactivity addition, %/sec	
								Maximum	Average
0149	8-15-58	17-A	3.3	−5.0	0.6	−7	−0.030	−0.070	−0.050
0450	8-15-58	17-A	3.3	5.4	10	40	0.060	0.011	0.006
0713	8-15-58	17-A	3.4	6.4	5	30	0.066	0.014	0.013
0627	8-15-58	17-A	3.4	6.6	3	16	0.058	0.024	0.019
0445	8-15-58	17-A	3.3	8.7	8	26	0.062	0.020	0.008
0600	8-15-58	17-A	3.4	11	4	16	0.066	0.026	0.016
0708	8-15-58	17-A	3.2	15	4	15	0.082	0.064	0.020
1700	9-4-58	17-B	2.2	31	3	6	0.13	0.079	0.043
1103	9-7-58	17-B	2.2	32	4	11	0.16	0.046	0.040
0135	9-6-58	17-B	1.7	47	5	9	0.19	0.094	0.038
0259	9-8-58	17-B	2.1	61	8	5	0.35	0.10	0.044
1838	9-4-58	17-B	2.4	150	7	7	0.58	0.15	0.083
1330	8-30-58	17-B	3.7	580	8	2	2.2	0.7	0.17

Table X-2 CONDITION OF REACTOR[1] DURING RUNS 13, 14, 16, AND 17

Run No.	Condition
13	D_2O reflector; powers up to 1.5 Mw
14	D_2O reflector; powers up to 6.3 Mw; terminated by occurrence of hole in core vessel
16	Blanket fuel concentration about 36 per cent of that in core; powers up to 5.8 Mw
17	Corrosion-sample assembly present in core; blanket fuel concentration about 32 per cent of that in core; powers up to 5.2 Mw
17-A	First 20 days of run 17
17-B	Twenty days following addition of 3.44 moles of acid on August 20
17-C	Two days following addition of 5.02 moles of acid on September 10

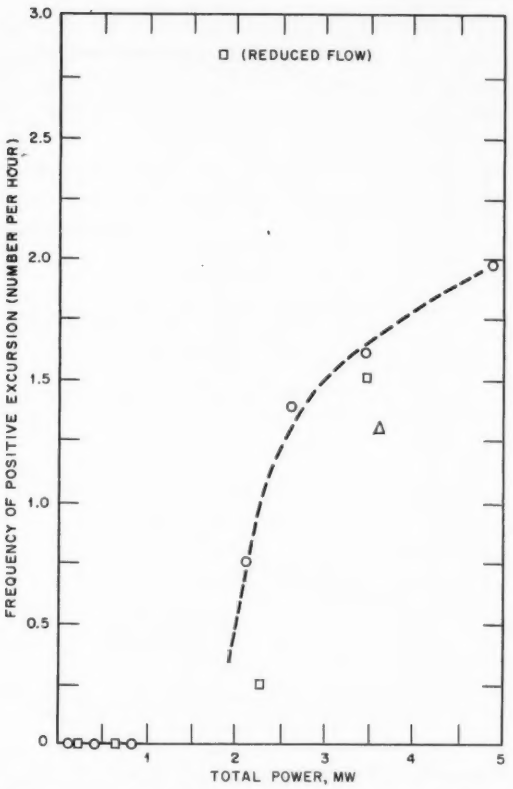

Figure 14 — The effect of total reactor power on frequency of positive excursions. ○, run 17-A (before acid addition). □, run 17-B (after acid addition). △, run 17-C (after second acid addition. Data represent 434 excursions with the average core temperature near 270°C.

A statistical analysis was made of the relation between the relative frequency of excursions and their size. It was found that Eq. 1 expressed this relation for all but five of the excursions.

$$f(x) = \theta\, e^{-\theta\,(x - x_0)} \qquad (1)$$

where $f(x)$ = relative frequency

x = power increase/initial power = $\Delta P/P_0$

θ, x_0 = constants for a given run*

The five excursions that were eliminated from the correlation by means of statistical "rules" are, however, the four largest excursions in run 17 and the largest in run 16; these are not statistically similar to the remainder of the excursions.

To analyze the excursion data, a program estimating the time variation of reactivity associated with a power excursion was coded for the IBM-704. It was stated that the reactivity obtained with the code is that reactivity associated with effects other than those produced by changes in delayed-neutron concentration and reactor temperature. Excursion histories were then analyzed using the computer program. The reactivities obtained were equivalent to moving several grams of uranium from outside the core into its center, or about 10 g from the upper screen to an average position in the core. The weights, of course, depend on which detailed excursion was analyzed; the numbers cited are for a peak reactivity addition of about 0.08 per cent. In general, the reactivity changes during the excursions could be satisfactorily explained by the movement of a relatively few grams of fuel of high density (solid) suddenly into the core where it would circulate and dissolve or pass out of the core. Repeated peaks in the excursion traces could be associated with the return of uranium to the core after passage through the external piping, since the time between peaks coincided closely with the transit time in the external flow loop.

A peculiar power trace that occurred during run 17 was analyzed. This trace exhibited nearly a step increase in reactor power followed by a rapid decrease to below the original power setting and a gradual ramp back to the setpoint; at least five such traces were observed in the power trace records. This behavior could be explained by uranium falling from the top of the core to the bottom of the core, and it is postulated that some, if not all, of these traces were caused by uranium-bearing corrosion specimens falling from their original position at the top of the core to the screen area. (See the December 1959 issue of *Power Reactor Technology*, Vol. 3, No. 1, for additional details on the corrosion specimens present during run 17.) The recovery of reactivity might then be caused by dissolution of the uranium from the specimens due to better flow patterns around the screens or some other mechanism. This might explain the four excursions in run 17 which would not fit the statistically determined frequency equation, Eq. 1; but the largest excursion in run 16, of course, could not be explained by a movement of corrosion specimens,

*For run 16, $\theta = 0.194$; $x_0 = 4.5$.

since presumably none were present in the reactor during run 16.

In addition to the excursions previously discussed, the HRT also exhibited a power variation termed "power fluctuations." These were small changes in power, usually less than 1 per cent dP/P_0. Shown in Fig. 15 is the parameter dP/P_0 versus reactor power for both the power fluctuations and power excursions. Figure 16 shows the frequency of positive peaks for the fluctuations and also a plot of Eq. 1. From the two curves it is evident that the fluctuations, although they occur more frequently (for "low" powers), have considerably lower amplitude. Data presented in the reference show that the fluctuations are apparently insensitive to core temperature. A hypothesis was advanced that the power fluctuations were due to slugs of "cold" fuel solution moving in convective flow within the core and/or blanket. The PDQ code was utilized to examine the reactivity changes associated with the movement of various amounts of cold fuel solution about the core, and, in general, the results appeared consistent with the behavior of the reactor. The operating experience with the HRT tends, however, to disprove this hypothesis. If convective flow were responsible, then the changed convective conditions, during the 2 hr in run 17-B when low flow was experienced, should have resulted in a change in frequency of the fluctuations. No such change was observed during the low-flow portion of run 17-B. A run was made on an analog machine to determine whether the small power fluctuations are a natural property of the circulating system of the HRT; however, the results showed none of the oscillatory character of the fluctuations, and stable behavior was observed. At the time of writing, the source of the fluctuations had not been identified.

The power-fluctuation traces shown in reference 1 bear a remarkable similarity to the power records of boiling-water reactors, shown in reference 2, page 89. Void formation in the HRT was studied using a one-dimensional, two-region diffusion code, but the application to the power fluctuations is not discussed in reference 1.

Since the discovery of the hole in the HRT in April 1958, the reactor has been operated as a one-region machine. The latest run, lasting for 105 days of continuous operation, was terminated when a second hole developed in the zirconium core tank.[3] The new opening measures

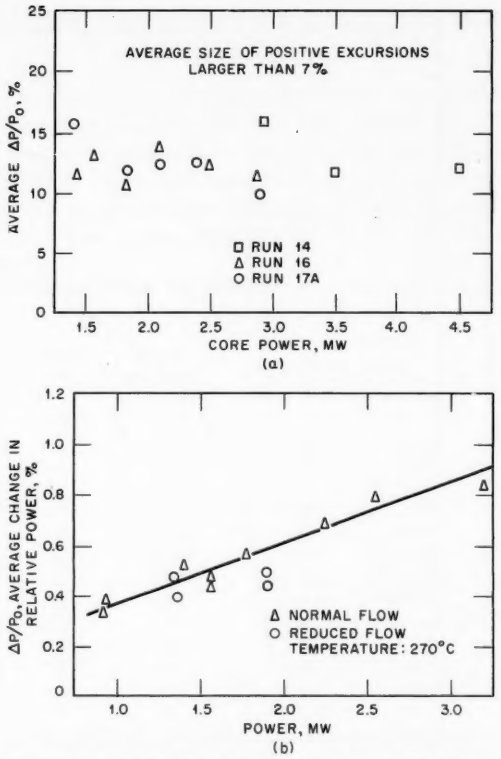

Figure 15 — The effect of core power level on (*a*) average size of positive excursions and on (*b*) power fluctuations.

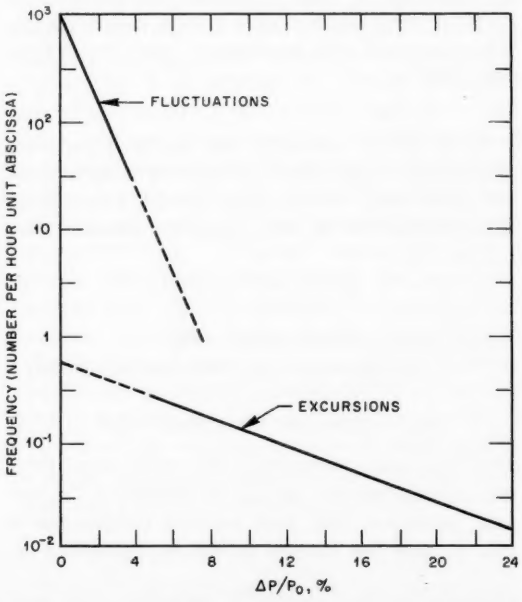

Figure 16 — The effect of power increase on frequency of excursions and fluctuations.

about ½ by 1½ in. and is located just below the equator of the spherical core tank. It is now planned to repair both holes in the core tank of the HRT and resume experimental operation with the flow in the core reversed, since it is thought that this will eliminate local stagnant areas which are believed responsible for both penetrations.

References

1. M. W. Rosenthal, S. Jaye, and M. Tobias, Power Excursions in the HRT, USAEC Report ORNL-2798, Oak Ridge National Laboratory, Feb. 29, 1960.
2. A. W. Kramer, *Boiling Water Reactors*, Addison-Wesley Publishing Company, Inc., Reading, Mass., 1958.
3. News Release No. NR-ORNL-8, Oak Ridge National Laboratory, February 1960.

Modifications of the EBWR

The EBWR, in its original form, has been adequately described in the literature.[1,2] A more recent publication deals with the modifications of the reactor to permit safe operation at 100 Mw(t) and evaluates the possible hazards associated with such operation.[3]

The EBWR has so far been successfully operated at a power of 61.7 Mw(t) with a core 4 ft in diameter by 4 ft in height. A combined analytical and experimental investigation of the stability of boiling-water reactors (see the December 1959 issue of *Power Reactor Technology* for additional details) has indicated that stable operation of the EBWR at 100 Mw(t) is probably feasible if the core diameter is increased to 5 ft; this size of core can be installed in the existing EBWR pressure vessel. The 5-ft-diameter core will be composed of the following set of fuel-element assemblies:

112	partially enriched (1.44 per cent) uranium (existing)
7	natural uranium (existing)
1	source element
28	highly enriched uranium (new)
148	total

The elements marked "existing" represent elements already fabricated for EBWR operation and are of two different types; some are of "thin plate" design and some are of "thick plate" design. These existing elements are composed of six fuel plates with an active length of 4 ft. The new fuel assemblies are of the rod type, wherein a 0.325-in.-OD fueled rod is clad with a $\frac{3}{8}$-in.-OD Zircaloy-2 tube. The fueled rod is a dispersion of highly enriched U_3O_8 in an X-8001 aluminum matrix; 49 such rods are contained in the fuel-element assembly. The active length of the new elements is 5 ft. Since the remainder of the core is only 4 ft in height, the new elements are of the reversible type, being symmetrical with respect to length. Removable upper and lower end fittings are provided to facilitate this reversible feature.

The core loading for 100-Mw operation employs the highly enriched elements as "spikes." The 28 spikes will be located in a square, surrounding 36 of the shorter, existing fuel elements. The location of the spikes in this position results in a considerable degree of radial power flattening. Control of the reactor is effected by nine cross type control rods with a 10-in. blade width. The rods are followed by a fueled plate follower of similar span; this is a departure, of course, from the old EBWR control-rod follower. The absorber section, 2 per cent boron in stainless steel, is 58 in. in length, whereas the fueled section, highly enriched uranium in a 304 matrix, clad with 304 stainless steel, has a length of about 36 in. Addition of 1 per cent boron–stainless steel strips to the sides of the spike elements is being considered should additional control be necessary. Since the old EBWR rod had an absorber section length of 46 in., redesign of the control-rod-drive mechanisms to accommodate this longer rod has been necessary.

Some changes to the pressure-vessel internals are necessary. To achieve a higher ratio of steam production rate to average steam void fraction in the core, increased recirculation of the water through the core is desired. To achieve this increased flow, it is proposed to put a core riser or chimney over the new core. This riser produces a greater head difference than was previously available between the mixture leaving the core and the water in the downcomer space. In order to accommodate the increased flow of steam from the pressure vessel, the outlet steam-collecting system is to be modified. This modification includes a larger steam outlet nozzle (increased from 6 to 10 in.) and a baffle system designed to permit operation with a higher water level in the reactor and still provide for steam-water separation. A larger feed-water inlet nozzle and distribution ring are also needed. The present turbogenerator will remain unchanged and is capable of absorbing

Table XI-1 PLANT PARAMETERS, MODIFIED EBWR[3]

General	
Type	Direct-cycle boiling reactor
Heat output, kw	20,000 kw for turbine; 80,000 kw for heating
Gross electrical output, kw	5000
Operating pressure, psig	600
Operating temp., °F	489
Coolant	H_2O
Moderator	H_2O
Fuel	U^{235}, U^{238}
Core	
Active diameter, ft	5
Active height, ft	5
Total uranium content, tons	6.4
Total U^{235} content, kg	65–90
Average water-to-uranium volume ratio	3.64
Structural material	Zircaloy-2 and aluminum
Fuel Assemblies	
Total number in core	147 (~20% of assemblies are spiked)
Cross-sectional dimensions, in.	3.75 × 3.75
No. of plates per assembly	6
No. of rods per spiked assembly	49
Side plates	0.060-in.-thick Zircaloy-2
Cladding	0.020-in.-thick Zircaloy-2
End fittings	Stainless steel
Composition of fuel "meat"	93.5% U, 5% Zr, 1.5% Nb (by weight)
Composition of spikes	Zr, Al structure with U_3O_8 (>90% enriched)
Thickness of meat in thin plates, in.	0.174
Thickness of meat in thick plates, in.	0.239
Thickness of meat in rods, in.	0.325 diameter
Width of water channels between thin plates, in.	0.428
Width of water channels between thick plates, in.	0.360
Power generation in average assembly, Mw	≤0.68
Nuclear Data	
Average thermal flux	3×10^{13} neutrons/(cm²)(sec)
Neutron lifetime, sec	6×10^{-5}
Reactivity to control, % k	~≤13
9 control rods with 8 fuel followers, % k	~15
Heat Transfer and Fluid Flow	
Average power density in core coolant:	
Spiked zone, kw/liter	135
Unspiked zone, kw/liter	115
Maximum power density in core coolant:	
Spiked zone, kw/liter	418
Unspiked zone, kw/liter	356
Steam flow (at 100 Mw), lb/hr	300,000
Average steam voids in heated channels, %	18.9
Average steam voids in total moderator, %	16.5
Average exit-steam quality, %	3.2
Pounds of water circulated per pound of steam	32
Subcooling at core inlet, °F	12
Nonboiling height of core, %	40 (av.)
Average coolant-inlet velocity, ft/sec	6.3
Average heat flux:	
Spiked zone, Btu/(hr)(sq ft)	136,000
Unspiked zone, Btu/(hr)(sq ft)	157,000
Maximum heat flux, Btu/(hr)(sq ft), based on maximum-to-average heat flux ratio of 3.1	485,000
Estimated burnout heat flux, Btu/(hr)(sq ft)	>1,000,000
Maximum surface temp., °F	514
Average fuel-centerline temp.:	
Thick plate (enriched), °F	579
Thin plate (enriched), °F	567
Rod (spike), °F	558
Maximum fuel-centerline temp.:	
Thick plate (enriched), °F	767
Thin plate (enriched), °F	724
Rod (spike), °F	694
Control Rods	
Total number	9
Spacing, in.	12.75 × 12.75
Shape	Cruciform: 10 by 10 in.
Material	Boron–stainless steel
Thickness, in.	0.250
Boron content, wt.%	2
Penetration of absorber into core, in.	60
56-in. travel time, sec	1.35
Maximum withdrawal rate:	
in./sec	0.4
% k/sec	~0.01
Strength of 9 rods, % k	~15
Pressure Vessel	
Diameter (inside), ft	7
Height, ft	23
Working pressure, psig	600
Design pressure, psig	800
Thickness of cylindrical portion, in.	2⅜
Material	SA-212 Grade B boiler plate
Cladding	0.1-in. type 304 stainless steel
Thermal shield	1-in. 18-8 stainless steel containing 1% boron

(Table Continues)

Table XI-1 (Continued)

Relief valve settings, psig	6, 50, 700, 725, 750, and 775
Total weight, tons	60
Weight of contained water, tons	14
Power Plant	
Condenser pressure, in. Hg abs.	2½
Flow rate to cooling tower, gal/min	13,650 (max.)
Feed-water flow rate, gal/min	600
Feed-water temp., °F	120
Generator output voltage, volts	4160
Steel Building	
Diameter, ft	80
Height, ft	119
Net volume, cu ft	~400,000
Design pressure (internal), psig	15
Design pressure (external), psig	0.5
Maximum leakage rate at 15 psig, cu ft/day	1000
Type steel	ASTM A-201 Grade B Firebox Quality
Sides of tank, inches thick	⅝ (cylindrical)
Bottom of tank, inches thick	⅝ (elliptical)
Top of tank, inches thick	⅜ (hemispherical)
Lining of tank below grade	2 ft (min.) concrete
Lining of tank above grade	1-ft-thick concrete
Capacity of water reservoir, gal	15,000
Flow rate of sprinkler system, gal/min	1000
Ventilation air flow rate, cu ft/min	3000
Personnel access	Air-lock doors
Freight access	Bolted and gasketed door

20 Mw(t); the remaining power will be either sent into the steam distribution system at Argonne or dumped to the air via air-cooled steam-condensing units. To prevent any possibility of contamination of outside steam lines, a secondary steam generator is postulated. Other design detail on the modified reactor is given in Table XI-1.

The capability of the modified reactor to supply 100 Mw of heat is not assured. Before modification, the reactor was operated at a maximum power of about 62 Mw, and extrapolation of oscillation tests indicated that the reactor might reach the limit of stability at about 68 Mw. If the naive assumption were made that average power density is the quantity which determines stability, then the limiting power output for the reactor would be nearly proportional to the number of fuel elements (neglecting the extra foot of length of the new elements). This assumption would indicate a maximum power of $68 \times 147/114 = 86$ Mw. The most important factors which will modify this estimate are (1) the extra circulating head provided by the chimney and (2) the changes in radial power distribution and in effective void coefficient of reactivity due to the changed fuel loading.

Aside from the question of stability, it is possible that a deterioration of the effectiveness of steam-water separation at high steaming rates might limit the maximum output.

If steam bubbles were entrained for a significant distance in the downcomer, the net driving head would be reduced. The resulting reduction in the recirculation flow rate would increase the core steam volume fraction and possibly hasten the onset of unstable operation. Equally as severe is the entrainment of water in the saturated steam flowing from the reactor. The use of the core riser decreases the volume available for disengagement, and the increased steam production rate increases the velocity in the steam dome to a superficial steam velocity of 1.89 ft/sec. The degree of steam separation that will take place under these rather adverse conditions is not amenable to calculation. It is true, however, that, even if the reactor were to deliver steam of too poor a quality to admit directly to the turbine, it is, in principle, possible to utilize external steam separation.

Since publication of reference 3, the modifications have been completed, and the EBWR has achieved criticality again. An extensive period of experimentation is planned to assess the effects of each of the structural modifications before very high power operation is attempted.

Advanced Boiling-water Design

A recent report[4] presents the results of a relatively brief conceptual design study by Argonne National Laboratory for the purpose of arriving at a design of a 50-Mw(e) prototype for a large boiling-water reactor of advanced design. An engineering study of essentially the same reactor has also been made by Sargent & Lundy.[5]

There has been rather general agreement that a profitable direction of development for the

Table XI-2 CORE DESIGN AND PERFORMANCE DATA, PROTOTYPE BOILING-WATER REACTOR[4]

Fuel Description

Fuel material	UO_2
Pellet diameter, in.	0.410
Gap material	He (2 atm. pressure)
Gap thickness, nominal (cold), in.	0.0015
Clad material	Zircaloy-2
Clad thickness, in.	0.025
Fuel-rod OD, in.	0.463
Fuel-section length, in.	40.5
Axial gap, in.	1.75
Active-zone length, in.	81
Triangular lattice pitch, in.	0.6

Core Description

Active-zone length, in.	82.75
Active diameter, ft	5.0
Fuel-assembly shape	Hexagon
Lattice pitch, in.	5.125
Rods per assembly	61
Assemblies per core (including control rods)	121
Rods per core	7381
No. of control rods	19
Power density, kw/liter	47

Core Materials

Weight of UO_2, lb	29,459
Volume Zircaloy-2/volume inside clad	0.312
Volume H_2O + steam/volume inside clad	1.52
Average density UO_2/unit volume inside clad, g/cm^3	10.0

Physics Data

Fuel enrichment (feed), at.%	2.65
Fuel enrichment (discharge), at.%	1.60
Pu^{239} and Pu^{241} content (discharge), at.%	0.64
ϵ	1.05
p	0.71
τ, cm^2	90
B^2, cm^{-2}	0.00104
k_{eff} (initial, hot, voided Xe + Sm poisoned)	1.046
δk (Xe, Sm), %	3.7
δk (initial to equilibrium), %	2.7
δk (voids), %	8.9
δk (between discharge points), %	4.8
δk (required, hot), %	18.5
δk in rods (hot), %	38
Burnup at discharge, Mwd/ton U	12,000
Total maximum-to-average flux	4.90

Hydraulic and Thermal Data

Total reactor power (design), Mw	165
Average power/assembly (design), Mw	1.36
Total heat-transfer area, sq ft	6,030
Total core flow area, sq ft	10.75
Average heat flux, Btu/(hr)(sq ft)	93,500
Maximum heat flux, Btu/(hr)(sq ft)	369,000
Fraction nonboiling length	0.25
Void fraction in boiling zone	0.267
Void fraction (uniform flux):	
Total	0.20
Exit	0.445
Steam exit quality	0.0575
Recirculation ratio	16.4 : 1
Slip ratio	1.57
Total flow rate (design), gal/min	30,000
Inlet subcooling, °F	9.5 (12.5 Btu/lb)
Steam rate (design), lb/hr	644,800
Average core inlet velocity, ft/sec	6.2
Core pressure drop (water), ft	11½
Average fuel-centerline temp., °F	1330
Maximum fuel-centerline temp., °F	4790

boiling-water reactor would be toward the achievement of higher power density in the core, provided this could be done without the addition of very expensive design features. It is, of course, probable that higher power density could be obtained in a straightforward way simply by increasing the subdivision of the fuel (smaller fuel-rod diameter) and by providing sufficient coolant flow velocity by forced circulation to keep the amount of reactivity invested in steam voids to something like a conventional level. Although this approach should require little or no further research and development, it has the disadvantage that the greater fuel subdivision increases the fuel fabrication costs per unit mass of fuel, and the provision of high circulation rates will be reflected in pump and piping costs. An alternate approach is to attempt to pack more fuel into a given core volume (i.e., increase the fuel-to-water ratio), to attempt to improve the spatial distribution of power, and to accept, if necessary, a high reactivity investment in steam void in order to avoid excessive coolant-circulation rates. The Argonne design lies in the direction of the second approach. It utilizes a high (for boiling reactors) UO_2-to-water ratio and accepts the accompanying high steam coefficient of reactivity, which, along with the coolant flow rate, results in a calculated investment of 8.9 per cent k_{eff} in steam voids at rated power. The power distribution achieved is not outstanding, partly because of the skewing of axial power distribution by the axial distribution of steam voids and partly because

Table XI-3 PRESSURE-VESSEL AND CONTROL-ROD-DRIVE DATA, PROTOTYPE BOILING-WATER REACTOR[4]

Pressure Vessel	
Inside diameter, ft	$8\frac{1}{2}$
Inside length, ft	$31\frac{1}{4}$
Main side-wall thickness, in.	3.25
Material:	
Shell plate	SA-212-B
Flanges	SA-105-II
Nozzles	SA-106-B
Shipping weight, lb	210,000
Operating pressure, psia	1000
Design pressure, psia	1100
Operating temp., °F	545
Design temp., °F	650
Vessel liner:	
Thickness, in.	0.187
Material	Type 304 stainless steel
Nozzles	
Coolant inlet:	
Inside diameter, in.	13.938
No. required	4
Flow velocity, ft/sec at 30,000 gal/min	16
Coolant outlet:	
Inside diameter, in.	20.938
No. required	4
Flow velocity, ft/sec	16
Control-rod Drive	
No. required	19
Type of operation	Gang-hydraulic-mechanical
No. of gangs	6
No. of drives per gang	3
Center rod drive	1
Normal driven speed, in./min	12
Fast shutdown time, sec	3
Control-rod weight (including fuel), lb	375

the fuel management program selected gives a relatively poor radial distribution.

Certain arbitrary goals affected some of the design decisions. In particular, a nominal value of 50 Mw/liter was selected as the average core power density, and the design was fitted to this specification. A length-to-diameter ratio of 1.30 was selected for the core in order to use rather long fuel elements which would be more nearly prototypes for the elements of a large reactor. The decision for a high fuel-to-water ratio led, directly or indirectly, to a number of other design decisions. A triangular fuel lattice was chosen because fuel-rod spacings become uncomfortably close in a "dry" square lattice. The triangular spacing led naturally to the selection of a hexagonal shape for the fuel-element assemblies. In a dry core the reactivity effectiveness of thermal-neutron absorption by blade type control rods is reduced, and the power peaks due to water channels are increased. These effects led to the selection of control rods in which the absorbing section consists of a hexagonal shell of absorbing material, filled with water. A fueled follower is provided to fill the water gap as the absorbing section is withdrawn. This construction is calculated to provide a negative reactivity capacity of 38 per cent k_{eff} in 19 control rods.

Other features of the design are: the upward direction of control-rod motion for reduction of reactivity (similar to Dresden) to improve the axial power distribution; the proposed fuel management program, which utilizes small batch reloading into the center of the reactor, with outward radial shift of the fuel elements as their exposure increases. Inversion of fuel elements is also employed to equalize the axial distribution of burnup. To accomplish the latter objective, fuel is handled in the form of hexagonal cartridges, each cartridge consisting of two half-core-length fuel assemblies placed end to end in a hexagonal holder. The holder consists of a hexagonal cage with end fittings to engage the top and bottom core grids. To invert fuel, the cartridge is removed from the reactor to the fuel storage pit. The two assemblies are removed from the holder and are replaced with their positions interchanged, the assembly initially in the top position being changed to the bottom position. This interchange, in effect, turns the fuel "inside out," placing the fuel which was originally near the ends of the core near the center of the core. After the inversion, the cartridges are placed in the reactor in a new radial position. The loading of new fuel into the center of the reactor minimizes the enrichment requirement for a given fuel lifetime but yields a relatively poor radial power distribution. The scheme does, however, fit in well with the axial inversion program, since the fuel cartridges, after the inversion which places the most reactive fuel near the center plane of the reactor, are occupying radial positions of reduced power density.

The characteristics of the reactor core are summarized in Table XI-2, and the pressure-vessel and control-rod-drive data are summarized in Table XI-3. The rated coolant flow at full power is 30,000 gal/min. This is supplied

by two pumps, each of 25,000 gal/min capacity, for experimental flexibility. Since the fuel-assembly holders are simply open cages, there is no partitioning of the coolant flow between assemblies, and the possibility of some lateral flow of coolant exists. It is stated that the resistance to lateral flow is about seven times the resistance to axial flow. The coolant pressure is 1000 psia, and the corresponding steam saturation temperature is 544°F. The reactor is designed for direct-cycle operation; steam-water separation is accomplished in external drums. The feed-water return temperature is 350°F. It was stated that a higher design pressure might be optimum for the prototype reactor but that the pressure of 1000 psi was selected as nearer the optimum for a very large plant.

Boiling Reactor Bibliography

A bibliography of selected literature on boiling-water reactors has been issued by the Technical Information Service Extension of the Atomic Energy Commission. It is listed as reference 6.

References

1. A. W. Kramer, *Boiling Water Reactors*, Addison-Wesley Publishing Company, Inc., Reading, Mass., 1958.
2. Experimental Boiling Water Reactor (EBWR), USAEC Report ANL-5607, Argonne National Laboratory, May 1957.*
3. E. A. Wimunc and J. M. Harrer, Hazards Evaluation Report Associated with the Operation of EBWR at 100 Mw, USAEC Report ANL-5781(Add.), Argonne National Laboratory, December 1959.
4. J. M. Harrer, ed., Prototype Boiling Water Reactor, USAEC Report ANL-6019, Argonne National Laboratory, October 1959.
5. Conceptual Design Prototype Boiling Water Reactor, 50 Mw(e), Report SL-1647, Sargent and Lundy, Aug. 21, 1959.
6. J. M. Jacobs, comp., Boiling Water Reactors, An Annotated Bibliography of Selected Literature, USAEC Report TID-3088, June 1959.

*This report is available from the Superintendent of Documents, U. S. Government Printing Office, Washington 25, D. C., for $2.25.

Design studies of various reactor types were made in connection with the formulation of the AEC Ten-year Program for Civilian Power Reactor Development. Reference 1 is such a study by Atomics International, covering an investigation of the effects of core design parameters on power costs for a 300-Mw(e) organic-moderated reactor. The approach used in the study is, first, to define a reference design for the reactor, which, although not optimized, is expected to be somewhere near the optimum design. The effects of variation of specific design parameters are then investigated by varying those parameters individually (along with any dependent parameters) around the reference design point. The effects of the variations are evaluated in terms of the change which they produce in the total power-generation cost.

An earlier design study of a large organic-moderated reactor had been made as one of the studies carried out under the authorization of Public Law 85-590 (Sec. 101) and was reviewed in the September 1959 issue of *Power Reactor Technology*, Vol. 2, No. 4. The later study[1] differs primarily in that it does not employ nucleate boiling of the organic coolant and in that it employs uranium–3.5 per cent molybdenum fuel clad with finned aluminum, rather than uranium dioxide jacketed in SAP (sintered aluminum powder). It is stated that the design is

Table XII-1 ORGANIC-MODERATED REACTOR[1]

Reference Design Data	
Reactor type	Organic moderated and cooled
Gross electrical power, Mw	314.4
Gross cycle efficiency, %	31.1
Thermal power to primary coolant, Mw	1010
Net electrical power, Mw	291.5
Net cycle efficiency, %	28.9
Thermal power leakage from core, Mw	10
Total thermal power, Mw	1020
Coolant	Santowax R
Coolant inlet temp., °F	524
Coolant outlet temp., °F	600
Total fuel elements	372
Type of fuel element	Finned plates
Fuel (aluminum clad)	Uranium–3.5% molybdenum alloy
Initial enrichment, at.%	2.1
Total lattice spaces in core	408
Core diameter, in.	164
Core height, in.	156
Core operating pressure, psi	90
Total weight of fuel in core, kg	120,400
Total weight of uranium in core, kg	115,600
Average burnup, Mwd/metric ton of uranium	7,000
Peak burnup, Mwd/metric ton of uranium	11,000
Initial reactivity (first core), %	9.5
Depleted enrichment	1.38
Plutonium in spent element, g/kg of uranium	3.67
Initial conversion ratio	0.6
Moderator-to-fuel ratio	3.42
Control-rod type	Cruciform
No. of control elements	73
Total worth of control rods, %	15
Peaking factors:	
Over-all	4.08
Axial	1.57
Radial	1.5
Element (adjacent to rod)	1.73
Hot-channel factors:	
F_ϕ	1.08
$F_{\Delta t}$	1.30
F_θ	1.43
Maximum coolant velocity, ft/sec	15
Average coolant velocity, ft/sec	10
Maximum permissible fuel temp., °F	1200
Maximum cladding surface temp., °F	750
Maximum fuel-element power, Mw	4.1
Core pressure drop, psi	80
Maximum heat flux, Btu/(hr)(sq ft)	94,000
Burnout heat flux, Btu/(hr)(sq ft)	500,000
Maximum specific power, kw(t)/kg of uranium	35.7
Average specific power, kw(t)/kg of uranium	8.8
Core power density, kw(t)/liter	18.8
Mode of heat transfer	Forced convection
Total coolant flow, lb/hr	95,000,000
No. of primary loops	4
Steam pressure, psig	550
Steam temp., °F	580
Containment	Totally enclosed primary system

based upon current technology and that it is capable of construction today with no additional research and development. The estimated power cost for a 300-Mw(e) plant is 9.02 mills/kw-hr, which is higher than that estimated in the original large-reactor design but lower than that cited for a 300-Mw(e) organic-moderated plant in the AEC summary[2] of technical and economic status as of 1959 (11.45 mills/kw-hr). Most of the latter difference appears to be due to the use of an average fuel exposure at discharge of 7000 Mwd/metric ton of uranium in reference 1 rather than a value of 4500 Mwd/metric ton of uranium as in the AEC report.

The main characteristics of the reference design are summarized in Table XII-1. The reactor core is 13.7 ft in diameter and 13 ft high. It is made up of 372 fuel elements arranged in a close-packed lattice. Each element, in cross section, consists of 10 metal fuel plates, of uranium–3.5 per cent molybdenum alloy, clad with a finned aluminum sheath. The 10 fuel plates are enclosed within a square stainless-steel box having a wall thickness of 0.060 in. and an outside dimension of 6.2 in. The elements are 180 in. long and have an active length of 156 in., made up of 20 subassemblies, each 15.6 in. long and consisting of 10 pairs of half-width plates. The fuel meat thickness is 0.117 in. The cladding has a minimum thickness of 0.02 in. and provides 51 fins, 0.20 in. high, on each plate. The inside of the cladding is coated with a 0.001-in. nickel diffusion barrier. The core is surrounded by a 6-in. organic reflector and two annular steel thermal shields, 6 and 1.5 in. in thickness. The core vessel is 17.2 ft in diameter and 60 ft high and has a wall thickness of $2\frac{3}{8}$ in.

The parameter perturbation study was limited to parameters affecting the reactor cost, primary heat-transfer equipment cost, net fuel cost, and organic-coolant makeup cost. These comprise about 65 per cent of the cost of nuclear power from the reference plant. The detailed parameters varied are as follows: core and fuel geometry; fuel-plate thickness; resonance escape probability; stable fission-product poisons; fuel exposure; fuel-element box thickness; gross axial and radial flux-peaking factors; element flux-peaking factor; hot-channel factors; fuel-element surface temperature; high boiler content in the coolant; core length-to-diameter ratio; coolant velocity; and average specific power. The results of the study are presented in graphical form, an example of which is given in Fig. 17, for the effect of variation of maximum fuel-element surface temperature.

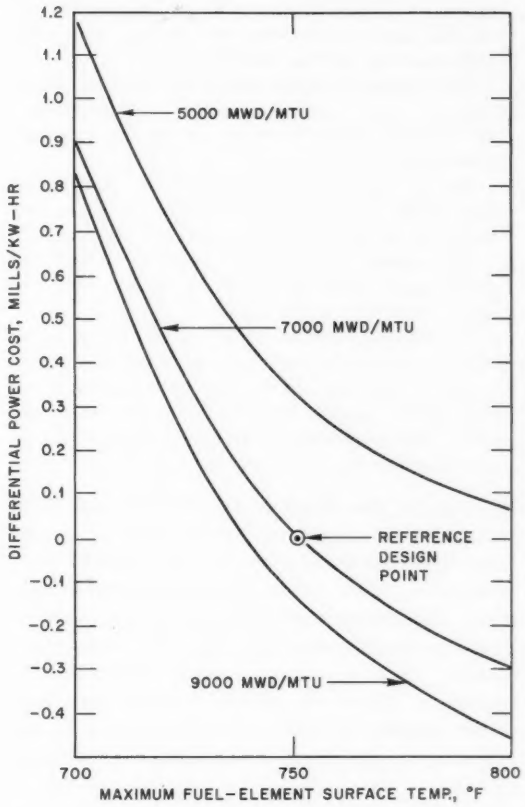

Figure 17 — Effect of maximum fuel-element surface temperature on differential power cost (adapted from reference 1).

The authors present the following conclusions:[1]

The most important cost determining factors among the parameters investigated are the thermal parameters of fuel-cladding surface temperature and hot-channel factors. Each of these variables increases in importance as the fuel exposure increases.

If the moderator-to-fuel ratio (M/F) is changed by varying the fuel-plate thickness while keeping the number of plates constant, there is an economic optimum M/F which is dependent on fuel exposure. For a fuel exposure of 5000 Mwd/metric ton of uranium, the economic optimum M/F is 4.5. For an exposure of 7000 Mwd/metric ton of uranium, the optimum M/F is around 5.0, while for 9000 Mwd/metric ton of uranium, the optimum is in excess of 5.0.

Considerable savings can be realized by flattening the radial and fuel-element neutron-flux distributions, with more savings accruing for higher fuel

exposures. Less savings can be realized by flattening the axial neutron-flux distribution, with little difference for various fuel exposures.

The resonance escape probability has little effect on power costs at low fuel exposures. This parameter becomes more important as the fuel exposure increases.

The average fuel exposure need not be extended beyond 8500 Mwd/metric ton of uranium for the type of metal-fueled reactor considered in this study.

The quantity of structural steel in the fuel elements has a pronounced effect upon fuel costs and should be kept to a minimum.

The optimum coolant velocity for a reactor of this type is 11.2 ft/sec for the hot channel.

Lattice spacing, core length-to-diameter ratio, high boiler content between 20 and 40 wt.%, and stable fission-product poisoning between 40 and 60 barns/fission have little effect on power costs.

In general, the effect of varying the individual parameters changed the power cost by something less than 1 mill/kw-hr, e.g., Fig. 17.

Several of the results deserve further comment. The power cost was surprisingly insensitive to moderator-to-fuel ratio. The moderator-to-fuel ratio in many reactor types has an important effect on power density, and high power density is often rather effective in decreasing capital cost. Presumably, this insensitivity in the case of the organic reactor is partly due to the relatively low pressure of the coolant and to the absence of stored mechanical energy in the coolant system. Thus the major effects of large reactor size, in increasing the costs of the reactor vessel and of the containment structure, are considerably tempered.

Although the possibility of decreasing power cost by extending fuel exposure may be an academic one in a reactor employing metallic fuel elements, the conclusion, that increases in fuel life beyond 8500 Mwd/metric ton of uranium do not decrease power cost, is at first glance surprising. Reference 1 points out that the minimum occurs at this relatively low value because the ground rules for computing fuel cost arbitrarily specify that inventory charges are to be based on 1.6 times the fuel in the reactor.

The rather low value for the optimum coolant velocity results partly from the circumstance that, as coolant velocity is increased, the thickness of the stainless-steel fuel-element box must be increased to withstand the flow pressure drop. The effect of the stainless-steel absorption on neutron physics produces an adverse effect on the power cost.

Although the effect of varying the high boiler residue content is investigated in the report, there is no discussion of the effect of variations in the basic rate of organic decomposition on power cost.

Reference 1 points out that the variations studied are primarily variations in design parameters and predicts that larger improvements can be achieved through extensions of the existing technology.

References

1. R. W. Hardy and B. L. Hoffman, Core Parameter Survey Report for Organic Cooled Reactors, USAEC Report NAA-SR-4510, Atomics International, December 1959.
2. Civilian Power Reactor Program. Part I, Summary of Technical and Economic Status as of 1959, USAEC Report TID-8516, 1960.

NUCLEAR SCIENCE ABSTRACTS

The U. S. Atomic Energy Commission, Technical Information Service, publishes *Nuclear Science Abstracts (NSA)*, a semimonthly journal containing abstracts of the literature of nuclear science and engineering.

NSA covers (1) research reports of the U. S. Atomic Energy Commission and its contractors; (2) research reports of government agencies, universities, and industrial research organizations on a world-wide basis; and (3) translations, patents, books, and articles appearing in technical and scientific journals.

Complete indexes covering subject, author, source, and report number are included in each issue. These are cumulated quarterly, semiannually, and annually providing a detailed and convenient key to the literature.

Availability of *NSA*

SALE *NSA* is available on subscription from the Superintendent of Documents, U. S. Government Printing Office, Washington 25, D. C., at $18.00 per year for the semimonthly abstract issues and $15.00 per year for the four cumulated-index issues. Subscriptions are postpaid within the United States, Canada, Mexico, and all Central and South American countries, except Argentina, Brazil, British and French Guiana, Surinam, and British Honduras. Subscribers in these Central and South American countries, and in all other countries throughout the world, should remit $22.50 per year for subscriptions to semimonthly abstract issues and $17.50 per year for the four cumulated-index issues.

EXCHANGE *NSA* is also available on an exchange basis to universities, research institutions, industrial firms, and publishers of scientific information. Inquiries should be directed to the Technical Information Service Extension, U. S. Atomic Energy Commission, P. O. Box 62, Oak Ridge, Tennessee.

TECHNICAL PROGRESS REVIEWS may be purchased from Superintendent of Documents, U. S. Government Printing Office, Washington 25, D. C. for $2.00 per year for each subscription or for $0.55 per issue. The use of the coupon below will facilitate the handling of your order.

POSTAGE AND REMITTANCE: Postpaid within the United States, Canada, Mexico, and all Central and South American countries except as hereinafter noted. Add $0.50 per year, or $0.15 per single issue, for postage to all other countries, including Argentina, Brazil, British and French Guiana, Surinam, and British Honduras. Payment should be by check, money order, or document coupons, and MUST accompany order. Remittances from foreign countries should be made by international money order, or draft on an American bank, payable to the Superintendent of Documents, or by UNESCO book coupons.

order form

SUPERINTENDENT OF DOCUMENTS
U. S. GOVERNMENT PRINTING OFFICE
WASHINGTON 25, D. C.

Enclosed:
document coupons ☐ check ☐ money order ☐

Charge to Superintendent of Documents No._____

Please send a one-year subscription to

☐ REACTOR CORE MATERIALS
☐ POWER REACTOR TECHNOLOGY
☐ NUCLEAR SAFETY
☐ REACTOR FUEL PROCESSING

(Each subscription $2.00 a year; $0.55 per issue.)

SUPERINTENDENT OF DOCUMENTS
U. S. GOVERNMENT PRINTING OFFICE
WASHINGTON 25, D. C.

(Print clearly)

Name_____

Street_____

City_____ Zone____ State_____